DISSERTATION

BIOPHYSICAL BEHAVIOR IN TROPICAL SOUTH AMERICA

Submitted by

Ian Timothy Baker

Graduate Degree Program in Ecology

In partial fulfillment of the requirements

for the Degree of Doctorate

Colorado State University

Fort Collins, Colorado

Summer 2011

COLORADO STATE UNIVERSITY

11 May 2011

WE HEREBY RECOMMEND THAT THE DISSERTATION PREPARED UNDER OUR SUPERVISION BY IAN TIMOTHY BAKER ENTITLED BIOPHYSICAL BEHAVIOR IN TROPICAL SOUTH AMERICA BE ACCEPTED AS FULFILLING IN PART REQUIREMENTS FOR THE DEGREE OF DOCTORATE.

Committee on Graduate Work

_____

_____

_____

_____

_____

Advisor

_____

Department Head

ABSTRACT OF DISSERTATION

BIOPHYSICAL BEHAVIOR IN TROPICAL SOUTH AMERICA

The concentration of CO_2 in the atmosphere is rising, in response to human activities such as consumption of fossil fuel, cement production, and land cover change. This increase is mitigated by the fact that currently, approximately one-half of the CO_2 of anthropogenic origin does not take up permanent residence in the atmosphere, but is absorbed by the oceans and terrestrial biosphere- the 'missing sink', which is partitioned almost equally between ocean and land. The increasing concentration of CO_2 is forecast to alter the radiative forcing at the planet's surface, resulting in increased global temperatures, although the exact spatiotemporal nature of the warming is uncertain. The missing sink has also eluded a quantitative description. We do not completely understand its spatial patterns, nor can we say with certainty how this sink will evolve under changing climatic conditions in the future. Furthermore, the atmospheric CO_2 growth rate is variable with time, and the dominant source of this variability has been traced back to terrestrial processes.

The land surface has significant influence over variability in the global atmospheric CO_2 growth rate and the tropics, especially tropical South America, has been identified as a region of particular import. The Amazon rainforest is the largest tropical forest in the world, and contains up to 10% of terrestrial biomass. Gross fluxes of CO_2 (photosynthesis and respiration) are massive, and slight variability in these large components can impose a net CO_2 flux that is felt globally. In the tropics, seasonality in day length and temperature are minimal. The dominant signal is annual wet and dry seasons, caused by the oscillation of the Intertropical Convergence Zone (ITCZ) northward and southward during the year. Interannual variability is imposed by the El Niño-Southern

Oscillation (ENSO), which can influence large-scale circulation patterns globally. During an El Niño, eastern Pacific sea surface temperatures are anomalously warm, which results in suppression of the ascending branches of the Hadley and Walker cells over South America, and subsequent decrease in precipitation. However, these patterns, while statistically significant on the continental scale, are spatially variable from event to event. Inverse behavior, in the form of increased South American precipitation is found during a La Niña, or anomalously cold eastern Pacific sea surface temperatures.

A positive correlation between El Niño and the atmospheric CO_2 growth rate has been noted, and a canonical explanation has evolved. In this canon, El Niño results in decreased precipitation over Amazonia, which results in decreased photosynthetic uptake, often at a lag of 6-12 months. Decreased precipitation results from less cloudiness, which can also increase solar forcing at the surface. This will result in warming, which can enhance respiratory processes that release carbon to the atmosphere. Therefore, there are two pathways (reduced photosynthesis and/or increased respiration) whereby an El Niño event can lead to a net release of CO_2 from the land to the atmosphere.

Some researchers predict that the Amazon forest is a fragile ecosystem, and that slight changes in temperature and/or precipitation patterns there will result in conversion of the forest to grassland or savanna, producing a massive release of stored carbon from vegetation into the atmosphere. This release will cause a significant increase in global atmospheric CO_2 concentration, initiating a positive feedback on radiative conditions that will cause further warming globally.

However, there is uncertainty in this conceptual model. There is no question that tropical forest function has decoupled, to some extent, from annual cycles of wet and dry. Were this not the case, the forest could not survive a dry season. But our physical understanding of this system, as represented by numerical models, has had difficulty reproducing observed behavior. Uncertainty also arises from a dispute surrounding what mechanisms drive variability in Amazonia. Some researchers have observed a 'greening-up' of the forest during annual and interannual drought, suggesting that the forest is light-limited. Others say that this observation is spurious, and

that Amazonian forests exhibit stress and mortality during or following periods of reduced rainfall. Studies using CO_2 flask observations and atmospheric circulation simulations have also indicated that large-scale response to ENSO forcing is inconsistent.

The Large Scale Biosphere-Atmosphere Experiment in Amazonia (LBA) is an international research collaboration that ran officially from 1995-2005, and has provided a wealth of observational data from a formerly data-poor region. We have been able to use this data to address some of the uncertainty in the canonical explanations of surface ecophysiology in tropical South America.

We begin at a single point. From observational studies, we are able to identify mechanisms that have been observed to facilitate forest function through seasonal drought. Using surface-atmosphere exchange data from a observation tower in the Tapajos River National Forest, Brazil, as an evaluation metric, we can incorporate these mechanisms, singly and combined, into numerical models. By doing so, we identify both a deep soil that provides a reservoir for storing water, as well as rooting systems that can access this stored water, as requirements for maintaining forest function in the model. When these are incorporated into a numerical model, we demonstrate an ability to capture annual cycles and interannual as well as diurnal variability in our simulations.

Next, we extend the analysis across vegetation and moisture gradients. Maintaining our comparison to surface observation sites, we show that physiological function and annual cycles of surface-atmosphere exchange of energy, water, and carbon are a function of both annual rainfall and the characteristics (length, severity) of annual drought. In the wettest regions, we find no annual cycles; variability is imposed by synoptic- to monthly-scale variability in forcing. Gross fluxes of carbon are always large, Bowen ratio is always low, and slight variations in precipitation, radiation, and temperature can impose net changes in flux. As annual precipitation decreases and dry season length increases seasonality emerges in carbon flux, with a phase shift between photosynthetic and respiratory processes. Forest function is maintained annually, indicated by no reduction in latent heat flux during the dry season. In many cases transpiration actually increases with increasing insolation. It appears that there there is either a) a reduction in respiration, as surface soil dries, b)

an increase in photosynthesis, as light levels increase when rain decreases, or c) a combination of these two processes that results in carbon uptake during seasonal drought. A net efflux of carbon is found during the rainy season. Moving further downgradient in precipitation, to the savanna (cerrrado), photosynthetic and respiratory process are in-phase, and tightly coupled to annual rains. Total ecophysiological function (photosynthesis and respiration) is greatly reduced during the dry season, but photosynthesis is impacted more severely than respiration, resulting in a net release of carbon during the annual drought. As vegetation shuts down, latent heat is reduced and the Bowen ratio rises. During seasonal rains, plant function is resumed, and net carbon uptake ensues. We demonstrate an ability to capture mean seasonal cycles across these gradients in our computer models.

Finally, having demonstrated an ability to capture mean behavior at multiple observation sites, we extend the analysis across a large spatial domain and over time that includes multiple ENSO cycles. We find that on the scale of tropical South America, there is a net efflux of carbon during the wet season and uptake during seasonal drought. Radiation explains the most variability in ecophysiological function over the wettest regions (implying light-limitation), with water playing a larger role in areas where annual precipitation is less. There is variability in the response to moisture and light in the forest nearer the forest-savanna boundary, suggesting an interdependence of processes. Regional response to ENSO is heterogenous. During the 1997-1998 El Niño, canonical behavior was observed; precipitation decreased, and there was a basin-wide efflux of CO_2 in a combination of photosynthetic and respiratory processes. In the 1987 El Niño, the response was more heterogenous, with regional patterns of both uptake and efflux. This suggests that variability around seasonal cycles of precipitation, as well as magnitude of the anomaly, combine in complex ways to determine large-scale carbon status.

We anticipate that this research will have implications for understanding of present climate, as well as predictions for the future. Tropical South America is critical to global carbon flux, and surface-atmosphere exchange has implications for atmospheric circulation and the development and

cessation of annual wet and dry cycles. We've developed numerical models that, when confronted with observations, behave consistently. We anticipate that improved understanding of present-day ecophysiology can only make predictions of future climate more robust.

Ian Timothy Baker
Graduate Degree Program in Ecology
Colorado State University
Fort Collins, Colorado 80523
Summer 2011

ACKNOWLEDGEMENTS

I've been fortunate to collaborate with many remarkable people during the compilation of this work. First and foremost, I'd like to acknowledge A. Scott Denning for giving me the opportunity to complete this degree. Scott hired me as a programmer in 1999, and I expressed to him my concern that I would not be professionally satisfied with programming alone. I told him that unless I was given some scientific 'meat' to chew on, I probably wouldn't stay in the position long. Scott responded by telling me that he'd give me the latitude to do as much science as I could handle. I've taken him at his word, and 12 years later I think I can say it's worked out pretty well for both of us.

The research topic in this dissertation has been gnawing at us for a while. One of Scott's students, Jun Liu, tackled it with indifferent results in 2002. The real breakthrough came when Lara Prihodko had the idea to break the problem down to component parts, and identify how and where our model simulations diverged from observations. When Lara left our group to do research on nutrient cycling in African savannas, I took the ball and ran with it.

In my position as staff scientist for Professor Scott Denning, I've had the opportunity to work closely with an exceptional group of students. I think I've learned as much from them as they have from me. I'd like to thank Ni Zhang, Tess Krebs, Erica McGrath-Spengler, Nick Parazoo, Jih-Wang Wang, Andrew Philpott, Joanne Skidmore, Parker Kraus, Isaac Medina, Kathy Corbin, and Biljana Orescanin for their collaboration. I'd especially like to thank Anna Harper, as we've worked together on Amazon research for a long time.

I sincerely value the collaboration and assistance of scientists and friends. There is something about scientific discussion that you can't get from reading papers alone. I've been fortunate to be

able to talk shop with Joe Berry, Neil Suits, Kevin Gurney, Jim Collatz, Kevin Schaefer, Reto Stöckli, Ken Davis, Bruce Cook, Ankur Desai, Steve Wofsy, Scott Saleska, Humberto da Rocha, Pedro and Maria Silva Dias, Gustavo de Goncalves, Natalia Restrepo-Coupe, Julio Tota, Ying-Ping Wang, Lixin Liu, John Knaff, Marcos Costa, Ravi and Erandi Lokupitya, Mark Branson, Kelley Wittmeyer, Don Dazlich, David Thompson, Amy Butler, Niall Hanan, Levi Silver, Chris Williams, Norm Wood, Brad Christofferson, Josh Fisher, Ben Poulter, Rafael Rosolem, David Baker, Hewlley Imbuziero, and Bill Gray.

Observational data in Brazil was made available as a direct result of the Large Scale Biosphere-Atmosphere Exchange in Amazonia Experiment (LBA), and was invaluable to this work. The Principle Investigators and collaborators at all of these data are too many to mention here, but I would like to acknowledge their collective contribution.

I'd like to recognize the assistance of my advising committee: Scott Denning, David Randall, Wei Gao, Mike Coughenour, and Don Estep. This whole endeavor was initiated (to some extent) by Dave Randall in 2003, when he told me "you're doing the work, why not get the credit?"

Finally, I'd like to thank the funding agencies that made this possible.This research was sponsored by the National Science Foundation Science and Technology Center for Multi-Scale Modeling of Atmospheric Processes, managed by Colorado State University under cooperative agreement No. ATM-0425247. This research was also funded by Department of Commerce/National Oceanic and Atmospheric Administration contract NA08AR4320893, NASA contracts NNX06AC75G and NNX08AM56G, Department of Energy contract DE-FG02-06ER64317, and NICCR contract MTU050516Z14.

DEDICATION

This dissertation is dedicated to my wife, Paige Ryan, for tolerating and supporting me through this process. At times, it's been tough on us both. I also dedicate this dissertation to my son Liam, as evidence that even an aging dog can pick up a new trick now and then. We all get older, but education doesn't ever have to stop. Try to learn something new every day.

"Decide what to be and go be it"-The Avett Brothers

CONTENTS

FIGURES

LIST OF TABLES

Chapter 1

INTRODUCTION

1.1 Overview

This dissertation addresses the topic of interaction between the land and atmosphere in tropical South America, and the chapters herein follow a logical progression of applying what we've learned, from small to large scales. I'll start with a brief introduction for context, to introduce reasons why we should care about the Amazon and study it. I'll give a brief summary of research efforts, from here at Colorado State University Atmospheric Science Department, as well as what has been published in the refereed literature. I do not include a formal literature review, as this is done in the introductory material in the individual chapters.

This story starts, as many studies of this kind do, with the rising level of CO_2 in the atmosphere. Human activity, in the form of fossil fuel consumption, cement production, and land cover/land use change, has resulted in an increase of atmospheric CO_2 concentration of approximately 140 parts per million [*Keeling et al.*, 1995] over the last 250 years. This increase in CO_2, a greenhouse gas, is predicted to increase the earth's temperature, although the exact spatiotemporal nature of this warming is not completely known [*Friedlingstein et al.*, 2006; *IPCC*, 2007]. There's also an added wrinkle: only about 50% of the CO_2 humans emit in a given year takes final residence in the atmosphere, while the rest is absorbed by the oceans and terrestrial biosphere [*Oeschger et al.*, 1975; *Tans et al.*, 1990; *IPCC*, 2007]. So global atmospheric CO_2 levels are rising, but at a rate of about half what we might expect them to if the 'missing sink' weren't extant. The CO_2 growth rate also shows variability on annual and interannual bases. Interannual variability in the growth rate is determined by seasonality and the spatial configuration of land and oceans [*Tans et*

al., 1990]. Interannual variability can be influenced by volcanic activity [*Roderick et al.*, 2001] as well as by variability in the meteorological forcing (i.e. temperature, precipitation) imposed at the land or ocean surface.

There is considerable interest in the missing sink: It's spatial configuration has relevance to political negotiations and agreements, and its temporal evolution will play a large role in determining atmospheric conditions in the future. So what do we know? We know that about half of the sink (one-quarter of CO_2 with human origin) is taken up by oceans, half by land [*Gurney et al.*, 2002; *Rödenbeck et al.*, 2003]. We also know that land uptake is highly variable, more so than ocean, and the interannual variability of flux is more well known than the net flux itself, which has considerable uncertainty [*Bousquet et al.*, 2000; *Peylin et al.*, 2005; *Baker et al.*, 2006; *Gurney et al.*, 2008]. It has also been determined that a large fraction of the land variability can be traced back to the tropics, especially tropical South America-the Amazon Basin [*Rödenbeck et al.*, 2003; *Gurney et al.*, 2008]. Finally, CO_2 flux in tropical South America has shown to have a negative correlation with El Niño [*Rayner and Law*, 1999; *Rödenbeck et al.*, 2003], although the relationship is not absolute [*Bousquet et al.*, 2000]. Finally, it is not known how the overall land sink will evolve over the next 100 years, whether it will remain as a sink, or if the sign will change and the land will become a net source of CO_2 to the atmosphere [*Friedlingstein et al.*, 2006].

It's easy to see where I'm going here. The land is an important and highly variable component of the 'missing sink', and, of the land areas, tropical South America has been implicated to play a significant role. Obviously, then, if we're trying to quantify global carbon flux as well as sources and sinks, we'd better have a good handle on South America. Do we?

The Amazon Basin contains the largest tropical forest in the world, and, by some estimates, up to 10% of global biomass [*Houghton et al.*, 2001]. This extensive forest ($5.8X10^6$ km^2 *Salati and Vose*, 1984) yields massive gross fluxes of CO_2 between the atmosphere and land. It is intuitive to think that small changes in these large gross fluxes can result in significant net flux, and

influence the global CO_2 growth rate. Tropical South America straddles the equator; there is seasonality in day length, especially to the south, but the overall temperature seasonality is small. In Amazonia, seasonality is defined by wet and dry seasons. As the Intertropical Convergence Zone (ITCZ) moves north and south throughout the year, associated large-scale precipitation oscillates along a northwest-to-southeast line connecting Central America and southeast Brazil [*Horel et al.*, 1989]. At the terminal points on this line, variability is mostly explained by the annual cycle; the difference between wet and dry season is extreme. Nearer the center of this line, seasonality is less, and the majority of variability is explained by interannual variability. Annual precipitation over these central forest areas is large (well over 2 meters), and seasonality is diminished. Overall, forest regions generally experience 1500 mm or more annually. Interannual variability in South American precipitation is influenced by El Niño-Southern Oscillation cycles, which influence the Hadley and Walker circulation patterns [*de Souza and Ambrizzi*, 2002] which is translated into changes in large-scale precipitation [*Rasmusson and Carpenter*, 1982; *Ropelewski and Halpert*, 1987; *Yoon and Zeng*, 2010].

With this brief introduction as a backdrop, I'd like to recount a little of my initiation to South American ecophysiology as motivation for this research. Around 2001 I was learning about land-atmosphere interaction in general, and the Simple Biosphere Model (SiB) in particular, when we were alerted to some troubling results in some Colorado State University (CSU) Atmospheric General Circulation Model (AGCM) results. SiB is the land surface module for the simulations. These results are shown in Figure 1.1, and show total soil moisture, on a per-meter basis, averaged over the entire Amazon Basin. The blue line shows soil moisture from an older run, and reflect the seasonal change in soil moisture as it oscillates through 10 years of wet and dry seasons. The red line shows the same quantity, but from a newer model run, one with new and ostensibly 'better' atmospheric and land surface treatment. What we see is a secular trend in soil moisture in the new runs-there is desiccation during seasonal drought, and no recovery during the wet season. The finger of guilt was originally pointed at SiB. Precipitation recycling, or the amount of precipitation with local evapotranspirational (ET) origin, is large in the Amazon; diminished ET may result in

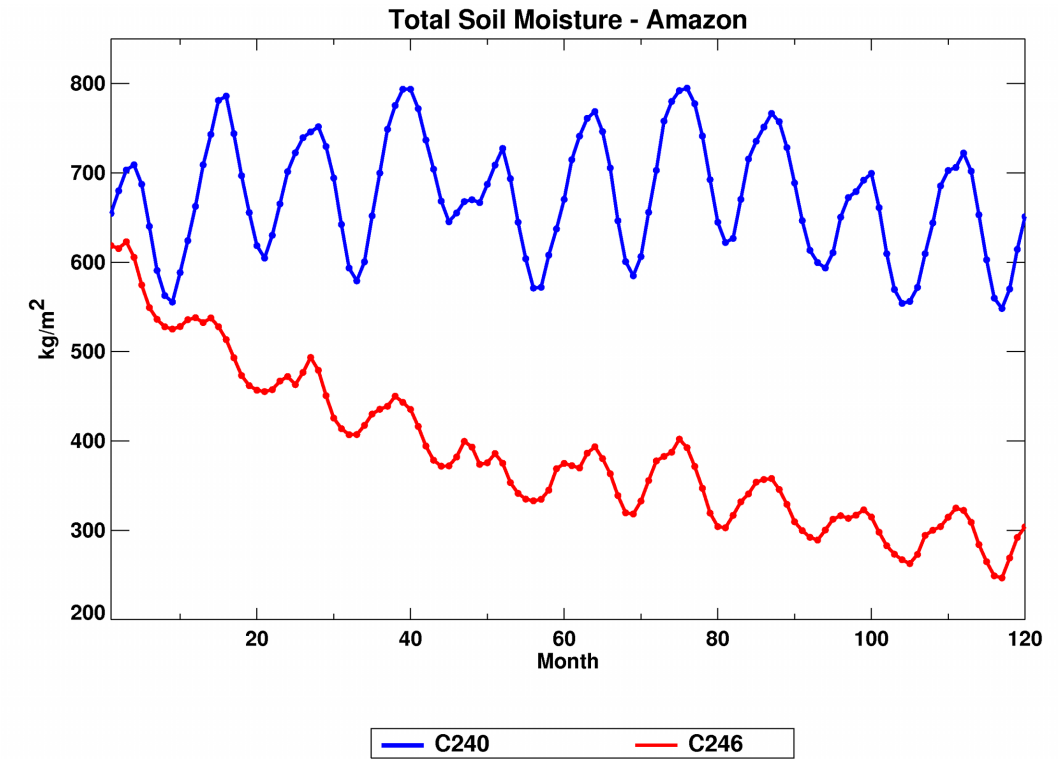

Figure 1.1: Regionally-averaged total soil moisture for the Amazon Basin. Blue line is from run C240, an AMIP simulation with older version of SiB and atmosphere. Run C246 is the 'new' run, with supposedly improved surface and atmospheric processes. Unpublished figure, courtesy of Mark Branson.

lowered wet season precipitation and insufficient recharge of soil moisture stores. This has been called 'stomatal suicide' [*Randall et al.*, 1996].

Ultimately, we were able to determine that in addition to reduced ET in SiB, there were issues with moisture convergence in the AGCM , but by then the die was cast. Jun Liu [*Liu*, 2004] looked into the issues with our treatment of the land, with somewhat unsatisfactory results. She found that using a deeper soil improved water storage capability, but did not materially improve simulations, either in stand-alone SiB simulations or in fully coupled AGCM runs.

At about the same time, *Saleska et al.* [2003] showed that simulated annual fluxes of carbon fluxes at a site in the Tapajos National Forest, near Santarem, Brazil, were almost exactly out-of-phase with observations (Figure 1.2). Simulations showed a robust forest during seasonal rains, and ecosystem stress and reduction of photosynthetic assimilation during annual drought. The observa-

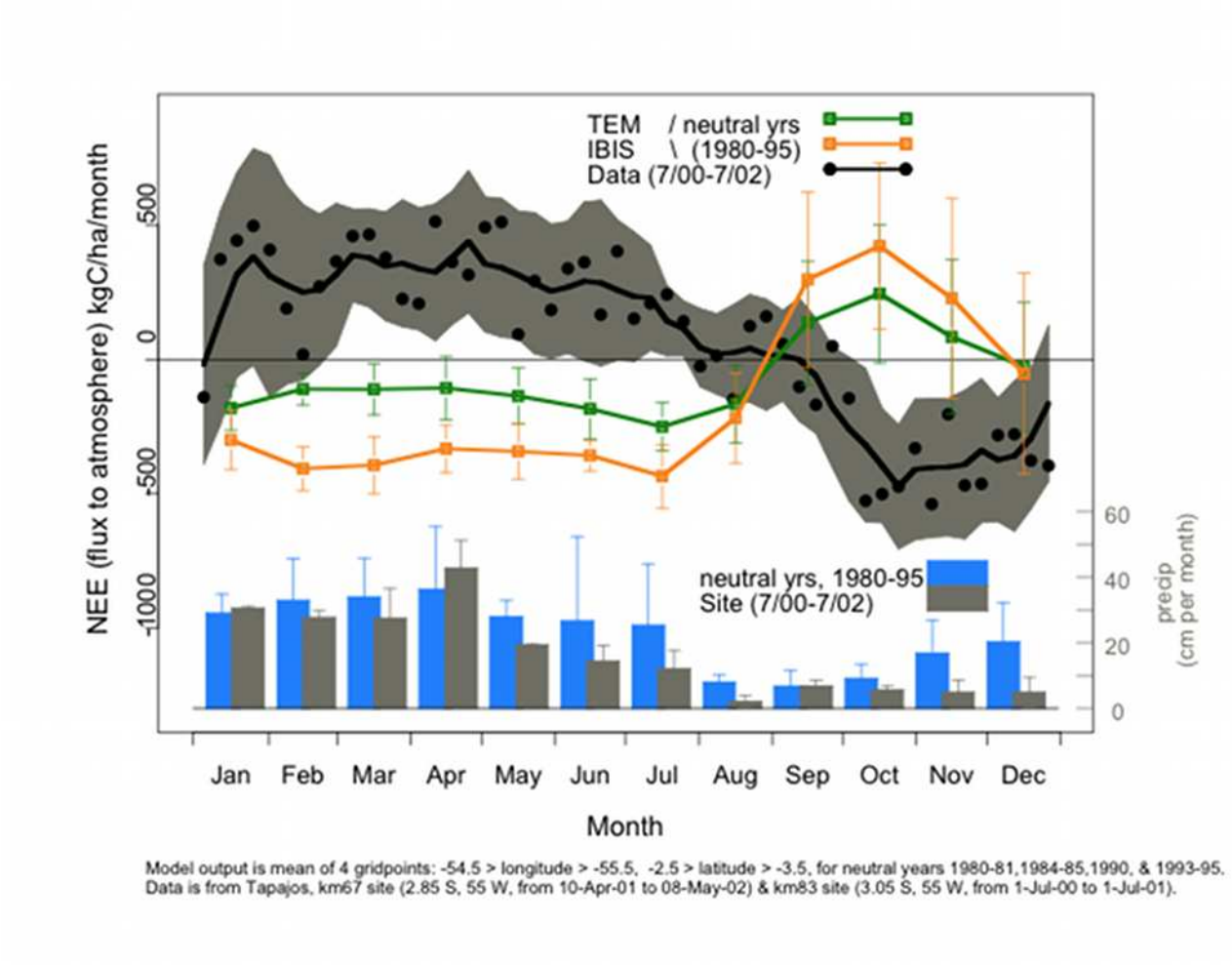

Figure 1.2: Comparison of observed and simulated annual-mean carbon flux for two sites in the Tapajos River National Forest, Brazil. From Saleska et al, *Science* [2003].

tions indicated carbon efflux during the wet season, and uptake once things dried out.

There have also been studies, from the Hadley Centre in England, over the last 10 years or so, that claim that tropical forests are in imminent danger [*Cox et al.*, 2000; *Cowlilng etal.*, 2004; *Huntingford et al.*, 2004; *Huntingford et al.*, 2008]. Minimal warming from current conditions has the potential to increase respiratory flux and decrease photosynthetic uptake, resulting in the release of a large amount of stored carbon. This will induce a positive feedback in radiative forcing, causing further warming. These are dramatic claims, and predict that wholesale conversion from forest to grassland or savanna will begin in the next 10-20 years.

But there's a fly in the ointment: The Hadley Centre model (HadCM3LC) uses, as a lower

boundary, the TRIFFID model [*Cox et al.*, 1999]. But TRIFFID is very similar in soil structure to the models shown in *Saleska et al.* [2003] and SiB. The latter were unable to capture seasonal cycles of carbon flux in the Amazon. Tight coupling of vegetation to energy and moisture fluxes in tropical forests implies that where carbon flux is erroneous, Bowen ratio will exhibit uncertainty as well, imparting a direct influence on weather and climate. If our understanding of ecophysiological behavior (and the models that represent that understanding) are unable to capture even the seasonality in the Amazon, what does this mean for our ability to capture interannual variability or predict the future?

That's where we stood at the outset. We did, however, identify an opportunity: The same datasets used by *Saleska et al.* [2003] were coming on-line to use for model evaluation. These datasets became available as a result of the Largescale Biosphere-Atmosphere Exchange in Amazonia Experiment (LBA; *Keller et al.*, 2004). Previously, surface data in Amazonia was sparse in coverage and limited and/or spotty in temporal coverage. LBA provided extensive and robust datasets that we could confront our models with.

So that's what we decided to do. This dissertation follows a progression from the point to regional or continental scale. In Chapter 2, we evaluate observed mechanisms that facilitate forest function through annual dry seasons at the Tapajos River National Forest site evaluated in *Saleska et al.* [2003]. We parameterize these mechanisms, and install them, singly and combined, into SiB, and confront the results with observations. With success at a single point, we expand the analysis to multiple sites, again evaluating model results against local-scale observations (Chapter 3). The multiple sites are located across vegetation and moisture gradients in Brazil, providing an opportunity to evaluate model response to heterogeneity in surface parameters (vegetation and soil) and meteorological forcing. Finally, having established model performance when directly compared to observations, we extend the analysis to a 'wall-to-wall' simulation across tropical South America over multiple years.This provides an opportunity to evaluate basin-scale biophysics on annual and interannual bases. We have an ability to evaluate large-scale response to ENSO cycles, and compare these results on a qualitative basis against 'top-down' inversion results. These results are generally

favorable. The appendix describes the latest version of SiB, which we call SiB3. No prior large-scale simulations of ecophysical behavior in Amazonia have the direct connection to observations that we utilize. We believe this gives our results an unprecedented level of realism, and provides firmer footing for predictions of future climate. Chapter 2 has been published in the peer-reviewed literature, and Chapters 3 and 4 as well as the appendix are in preparation for publication.

here are still many questions to be asked. The exact nature of the bidirectional coupling between surface and atmosphere in Amazonia has been postulated to play a critical role in wet season onset [*Fu and Li*, 2004; *Li and Fu*, 2004]. Furthermore, there is no question that a reduction in precipitation will, at some point, result in serious consequences for forest function. The exact nature of this 'tipping point' are not known. However, results from preliminary inclusion of our findings about surface function into atmospheric models has been encouraging [*Harper et al.*, 2010]. The research presented in this dissertation is a necessary first step to investigating these new questions.

Chapter 2

SINGLE SITE: TAPAJOS RIVER NATIONAL FOREST, KM83

This Chapter was originally published as "Seasonal drought stress in the Amazon: Reconciling models and observations" and is reproduced by permission of American Geophysical Union.

Baker, I.T., L. Prihodko, A.S. Denning, M. Goulden, S. Milller and H. da Rocha, 2008. Seasonal drought stress in the Amazon: Reconciling models and observations. *J. Geophys. Res.*, **113**, G00B01, doi:10.1029/2007JG000644.

2.1 Introduction

Changes in the biophysical state of the Amazon Rainforest exert a strong influence on global climate through associated changes in carbon and hydrological cycles [*Avissar et al.*, 2004; *Zeng et al.*, 2005; *Marengo and Nobre*, 2001; *Kleidon et al.*, 1999]. Perturbations to these cycles, for example from drought, deforestation, and ENSO events, have a strong influence because of the sheer geographical size of the region ($5.8X10^6$ km^2; Salati and Vose [1984]), the role it plays in regional meteorology [*Nobre et al.*, 1991] and the magnitude of the carbon stored there [*Houghton et al.*, 2001]. Inversion studies have shown Tropical America to be a small source of CO_2 to the atmosphere [*Gurney et al.*, 2002; *Stephens et al.*, 2007], although the interannual variability is large [*Bosquet et al.*, 2000]. However, there is much we still don't understand about carbon and hydrological cycles in the Amazon, and this ambiguity leads to uncertainty in projections of future climate change [*Magrin et al. 2007*; *Cox et al. 2000*; *Friedlingstein et al.*, 2001].

Observational campaigns and concerted modeling efforts assist in quantifying impacts of the

Amazon Rainforest on regional and global carbon and water cycles [*Andreae et al.*, 2002; *Avissar et al., 2002*; *Keller et al.*, 2004]. However, results are not always in agreement [i.e. *Huete et al.*, 2006; *Lee et al.*, 2005; *Ishii et al.*, 2007]. To accurately characterize the carbon dynamics across vegetation and moisture gradients in Amazonia will require cooperation between observational and modeling studies to achieve understanding of the biophysics that force fluxes in the region.

The driving climatic forcing in the region is precipitation amount and temporal distribution. Total annual precipitation and the length of dry season, usually defined as number of months with less than 100 mm precipitation, play a large role in vegetation distribution and fluxes of energy, water and carbon [*Keller et al.*, 2004; *Goulden et al.*, 2004; *Saleska et al.*, 2003; *Ichii et al.*, 2007]. The seasonality of surface-atmosphere fluxes are further controlled by topography, vegetation type, root depth, depth of soil and soil type. The carbon dynamics in the region are a function of carbon uptake by photosynthesis and release by respiration, with additional components of storage in soil and biomass and carbon export via runoff. Amazonia contains between 10-15% of the total global biomass [*Houghton et al.*, 2001]. A large fraction of the region consists of closed-canopy broadleaf evergreen forest, gradating to savanna (cerrado) in regions with less precipitation, although the cerrado is generally outside of the hydrogeographic basin of the Amazon River.

The interaction between the wet/dry seasons and the annual cycle of CO_2 uptake/efflux is not consistent across the Amazon Basin; *Keller et al.* [2004] report observations of carbon uptake during the wet season at locations in Jaru Reserve and Fazenda Maracai, while several sites in the Tapajos National Forest report uptake during the dry season [*Saleska et al.*, 2003; *Goulden et al.*, 2004].

Saleska et al. (2003) have shown that multiple ecosystem models are almost exactly out-of-phase with the observed annual NEE cycle in the seasonally dry Tapajos region. For example, Figure 2.1 shows observed and modeled average annual cycle of NEE for the years 2001-2003 using the Simple Biosphere Model, version 3 [SiB3; *Sellers et al.*, 1986; *Sellers et al.*, 1996a; *Baker et al.*, 2007]. Comparing our Figure 2.1 to Figure 3 in *Saleska et al.* [2003], the results are similar; SiB3 simulates CO_2 uptake during the wet season, and efflux during seasonal drought

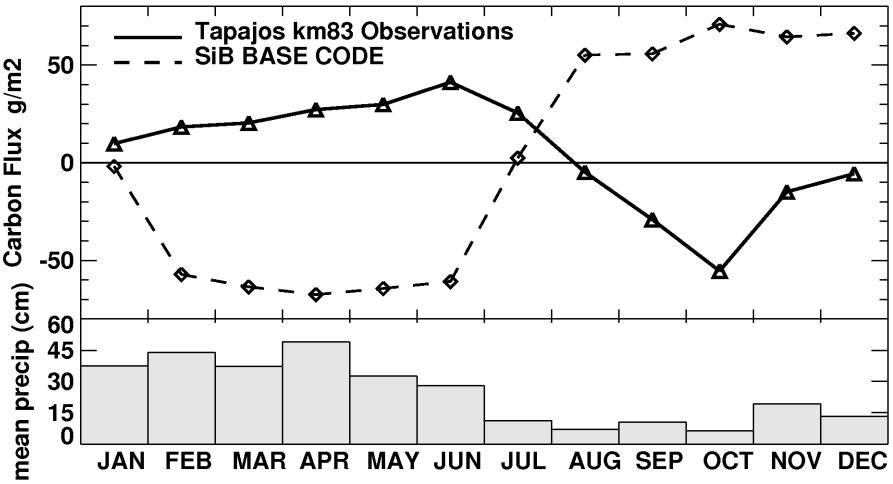

Figure 2.1: Average monthly Net Ecosystem Exchange (NEE) of carbon in g m^{-2} at Tapajos National Forest km 83 site, years 2001-2003. Observed flux is show as solid line, SiB3 simulation as dashed. Mean monthly precipitation in cm is shown below for reference. Positive values indicate efflux into the atmosphere, negative values indicate uptake by the biosphere.

as the model vegetation experiences stress due to declining soil moisture. The observations show exactly the opposite - efflux during the wet season, and uptake of carbon during the relative dry period of August-December. In SiB3, soil moisture and the ability of the roots to access water in the soil are the driving mechanisms that determine the annual cycle of NEE. When the soil is moist, carbon uptake is unstressed, and as the model soil desiccates in the dry season, the photosynthetic uptake is restricted. Model respiration is reasonably constant throughout the year, with the result that as photosynthesis wanes during the dry season, a net efflux of carbon to the atmosphere is produced. By identifying the mechanisms that operate in the real world and modifying model physics to incorporate them, we have an opportunity to improve model simulations and deepen our understanding of the system.

What responses has the local vegetation evolved to cope with seasonal drought? Up to half of the closed canopy forest in Brazilian Amazonia is able to access water in the soil at depths of 15 meters or more, with roots that extend deep into the soil [*Nepstad et al.*, 1994; *Jipp et al.*, 1998]. Using a water-balance approach, *Nepstad et al.* [1994] estimated that greater than 75% of the water extracted from the soil during the 1992 dry season at a forest in the Brazilian state of Para came from a depth greater than 2 meters. Roots were most abundant near the surface, but up to 10% of the total rooting mass was at depths between 4 and 10 meters. *Kleidon et al.* [1999] found that the inclusion of deep roots in climate models resulted in a better representation of seasonal air temperature. *Ichii et al.* [2007] found that rooting depth was critical for reconciling modeled Gross Primary Productivity (GPP) with satellite observations. Roots can act as conduits to move water within the soil as well: *Oliviera et al.* [2005] found that roots in three species of trees in the Tapajos National Forest had the ability to move water both upwards and downwards in the soil in response to moisture potential gradients. Briefly, when stomates are closed at night moisture can move through roots from moist regions of soil to areas of large saturation deficit . This is referred to as hydraulic redistribution (HR). During the dry season, near-surface soil layers are recharged with moisture from the deep soil, and during the wet season roots can supplement infiltration to make deep soil recharge more efficient. *Rocha et al.* [2004] observed apparent recharge of surface soil

layers at the KM83 site in the Tapajos region either through HR or the capillary action of the soil (observed at other Amazonian sites [*Romero-Saltos et al.*, 2005]). *Lee et al.* [2005] incorporated the HR mechanism into the Community Land Model (CLM) coupled to the Community Atmosphere Model, Version 2 (CAM2) and found that HR elevated soil moisture at all levels of the soil when compared to a control run. The control run had less photosynthesis than the HR simulation in all months, however the HR run still had 50% less photosynthesis during the dry season when compared to the wet season.

Studies using satellite-based observations of forest greenness have postulated that there is actually an increase in photosynthesis during the dry season, as forests respond to higher light levels in the absence of cloudiness. Using Enhanced Vegetation Index (EVI) data from the Moderate Resolution Imaging Spectroradiometer (MODIS), *Huete et al.* [2006] noted a 25% green-up across large portions of Amazon forest during the dry season. This result suggests that light response may play as large or larger role than phenology or rainfall variability in determining annual cycle of carbon flux. In grasslands, EVI was found to decrease during the dry season [*Huete et al.*, 2006; *Saleska et al.*, 2007] in contrast to the increase found in forests; this suggests that rooting depth or hydraulic redistribution associated with deep roots plays a significant role in the dry season green up, as grasses do not have the deep root density found in forests. The conceptual model that emerges, then, is one where soil depth and the ability of roots to utilize stored water is crucial to the ability of the forest to maintain function through annual drought that may last 6 months or more. The deep soil provides a reservoir to store rainfall from the wet season for use during the dry months of the year. Hydraulic redistribution by roots can enhance the ability of the soil to recharge moisture via infiltration, and can moisten near-surface layers by moving water upwards against gravity during the dry season. The soil hydraulics and root function provide a framework where photosynthesis does not experience large-scale annual stress, and more subtle mechanisms of photosynthetic response to light and of respiration response to slight changes in soil and litter moisture levels interact to provide the observed annual cycle of NEE.

This study focused on the CO_2 flux at the kilometer 83 tower in the Tapajos National Forest

[*Goulden et al.*, 2004; *Miller et al.*, 2004]. We simulated 3 years of fluxes between the atmosphere and terrestrial biosphere (emphasizing Net Ecosystem Exchange of Carbon, or NEE) using the Simple Biosphere Model [SiB3; *Sellers et al.*, 1986; *Sellers et al.*, 1996a; *Baker et al.*, 2003] and then, by identifying possible mechanisms not present in the model, we modify the model code and re-run the simulations, resulting in model carbon flux that is more realistic when compared to the observed flux. By confronting model simulations with observations, we can identify mechanisms that are incorrectly treated, and by noting the changes in model flux with inclusion of new mechanisms or modification of existing ones, we can make inferences about biophysical behavior in this region.

2.2 Methods

2.2.1 Site Description

The Tapajos National Forest km83 site is described in detail elsewhere [*Goulden et al.*, 2004; *Rocha et al.*, 2004; *Miller et al.*, 2004], however a brief description is given here to provide details specific to this paper. The vegetation is closed canopy, mostly evergreen, with a few deciduous species. The tower is located in a region of minimal topographic relief; within several kilometers, elevation change is on the order of 10 meters. The region was selectively logged in September 2001. However, the amount of total biomass removed was small (5%), and seasonal cycles of carbon flux as measured by the tower were not altered. Soil texture and carbon content varies across the site and are described in detail in *Silver et al.* [2000]. For the years 2001-2003, the average precipitation was 1658 mm, with a maximum of 1764 mm in 2003, and a minimum of 1559 mm in 2002. The dry season extended approximately from July through December, although there were individual months in this period with precipitation slightly in excess of 100 mm (December 2002, September 2003, November-December 2003) and over 200 mm of rain in November 2002. The precipitation recorded by the gauges for 2001-2003 is approximately 15% lower than what is reported in the region by the Global Precipitation Climatology Product (GPCP; *Adler et al.* [2003]). However, we believe that there is not a seasonal bias, and so have chosen not to artificially manipulate the precipitation data.

2.2.2 Model Description

The Simple Biosphere model (SiB) is a land-surface parameterization scheme originally used to simulate biophysical processes in climate models [*Sellers et al.*, 1986], but later adapted to include ecosystem metabolism [*Sellers et al.*, 1996a; *Denning et al.*, 1996a]. SiB is a model that is useful to meteorologists for its ability to simulate exchanges of mass, energy and momentum between the atmosphere and terrestrial biosphere, and useful to ecologists for its ability to do so in a process-based framework that allows for simulation of explicit biophysical mechanisms. The parameterization of photosynthetic carbon assimilation is based on enzyme kinetics originally developed by *Farquhar et al.* [1980], and is linked to stomatal conductance and thence to the surface energy budget and atmospheric climate [*Collatz et al.*, 1991, 1992; *Sellers et al.*, 1996a; *Randall et al.*, 1996]. The soil representation is similar to that of CLM [*Dai et al.* 2003], with 10 soil layers and an initial soil column depth of 3.5 meters. SiB has been updated to include prognostic calculation of temperature, moisture, and trace gases in the canopy air space, and the model has been evaluated against eddy covariance measurements at a number of sites [*Baker et al.*, 2003; *Hanan et al.*, 2005; *Vidale and Stöckli*, 2005]. We refer to this base version of the code as SiB3.

We used half-hourly, gap-filled observations of air temperature, pressure, humidity, wind speed, radiation and precipitation from the km83 site [*Miller et al.*, 2004; *Rocha et al.*, 2004; *Goulden et al.*, 2004] to drive the model for the years 2001 through 2003. Model parameters are determined using a combination of satellite data, literature values and standard SiB parameters [*Sellers et al.*, 1996b]. The annual cycle of Normalized Difference Vegetation Index (NDVI) collected over the km83 site is badly contaminated by clouds for all satellite products. Since there were no leaf area index measurements available for the site, it was not possible to determine whether there was a measurable phenological change (though one has been hypothesized by *Goulden et al.* [2004]). Thus a constant value of NDVI equal to 0.8, derived from the Global Inventory Monitoring and Modeling Study (GIMMSg) dataset [*Tucker et al.*, 2005], was used in the parameterization of the model. Soil texture, used by SiB3 to determine physical and hydrological characteristics of the soil, was set as sandy clay (52% sand and 46% clay) and was based on observations made in the area

[*Silver et al.*, 2000]. Root distribution follows *Jackson et al.* [1996] for broadleaf evergreen forest, and every soil layer, even at depth, has a non-zero root fraction.

The coupling between photosynthesis/transpiration and soil processes is achieved by an initial calculation of soil moisture stress on photosynthesis, followed by an algorithm for removing water from the soil once transpiration has been calculated. The calculation of water stress is commonly linked directly to root density as follows

$$waterstress = \sum_{i=1}^{nsoil} \left(\frac{1 - \frac{\theta_{wp}}{\theta_i}}{1 - \frac{\theta_{wp}}{\theta_{fc}}} \right) (rootf_i) \tag{2.1}$$

where $nsoil$ is the number of soil layers, θ_{wp} is volumetric soil water fraction at wilt point, θ_{fc} is volumetric soil water fraction at field capacitym, θ_i is volumetric soil water fraction of soil layer i, and $rootf_i$ is root fraction in soil layer i. Soil water stress on photosynthesis is calculated using the assumption that soil containing water at or above field capacity imposes no stress on photosynthesis, while soil at or below wilt point (defined as a moisture potential of -150 m) will result in almost complete loss of carboxylation capacity and attendant stomatal closure. The contribution of each model soil layer to overall stress is normalized by root fraction. Removal of water from the soil by transpiration follows the same process. The base SiB3 case, shown in Figure 2.1, shows the model NEE cycle obtained using this representation of soil water stress and water removal mechanisms.

2.3 Analysis

We implemented the evolutionary responses/biophysical mechanisms described in the introduction into SiB3 individually, to gauge model response. The primary metric for evaluation of model performance is Net Primary Production (NPP), defined as autotrophic respiration from canopy vegetation (not roots) less gross photosynthesis . On monthly timescales, Net Ecosystem Exchange (NEE) can be defined as R_{soil} – NPP, where R_{soil} is defined as heterotrophic respiration in the soil. We follow the convention that positive NEE implies flux into the atmosphere, while negative NEE depicts carbon flux into the terrestrial biosphere. The individual sensitivity studies

are:

(1) Soil Water Stress/Rooting Distribution (SiB3-SR): Total soil column depth (3.5 m) is unchanged, but soil water stress on photosynthesis is modified to relax the direct coupling to root fraction in each soil layer. Soil moisture deficit below field capacity for each layer is aggregated and a total-column stress amount is determined as follows:

$$waterstress = \frac{(1 + wssp)\frac{w_{column}}{w_{max}}}{wssp + \frac{w_{column}}{w_{max}}} \tag{2.2}$$

where w_{column} is water in the column in excess of wilt point (kg), w_{max} is maximum possible excess of water in the column (field capacity less wilt point; kg), and $wssp$ is a water stress curvature parameter (currently chosen as 0.2).

Stress on the whole ecosystem is thus parameterized as a function of plant available water within the total column, independent of root distribution. The new formulation provides a more gradual response to stress in the model, marked by a smooth transition between non-stressed and stressed regimes. For water removal by transpiration, an 'apparent' root fraction is determined for each soil layer depending on actual root fraction and moisture content of the layer.

$$rootr_i = \left(\frac{1 - \frac{\theta_{wp}}{\theta_i}}{1 - \frac{\theta_{wp}}{\theta_{fc}}} \right) \tag{2.3}$$

The apparent root fraction ($rootr_i$) is summed over the column, and each layer is normalized so that $rootr_{column}$ is unity. The apparent root fraction can be higher or lower than the initial root fraction ($rootf_i$) based on water content in the individual layer convolved with the moisture distribution within the column. This apparent root fraction is consistent with the observed ability of deep roots to carry large amount of water as reported by *Jipp et al.* [1998] or *Nepstad et al.* [1994], and is mentioned by *Lee et al.* [1995] as well.

(2) Hydraulic Redistribution (SiB3-HR): Following *Lee et al.* [2005] we incorporated a hydraulic redistribution term into the Darcy's Law equations used to calculate vertical move-

ment of soil water. Coding follows *Ryel et al.* [2002] and root conductivity values are taken directly from *Lee et al.* [2005]. The HR modifications allow soil water to move downwards more efficiently during periods of rain, and restore water to near-surface layers during dry periods. Total soil column depth remains 3.5 meters

(3) Soil Modification (SiB3-DS, or Deep Soil): Similar to case SiB3-SR, but we increase the total soil depth to 10 meters. The number of layers (10) in the model is unchanged, but each layer is increased in thickness. This treatment differs from the HR case both in the total depth of the 'reservoir' for water storage and because no water is redistributed between layers (other than basic infiltration or downgradient flow), therefore the storage dynamics are different. An additional modification to the soil in the DS case is the saturation fraction for maximum soil respiration. Following *Raich et al.* [1991], the relative rate of heterotrophic respiration is tied to soil moisture amount, dependent on type of soil. We found that the optimum soil moisture for respiration at km83 was too low in the model, so that there was almost no response of heterotrophic respiration to soil moisture. Soil respiration was dependent only upon soil temperature. However, observations showed that the annual average volumetric soil moisture at 10cm was 0.34 m^3m^{-3}, giving a percent of saturation of approximately 75 - 80%. By increasing the optimum soil moisture value for heterotrophic respiration to 75%, we were able to induce a respiration response to modeled annual cycles of soil moisture.

(4) Light Response (SiB3-SS, or Sunlit/Shaded): Increased sensitivity in model response to seasonal and diurnal variation in radiative forcing has been accomplished by explicitly resolving sunlit and shaded canopy fractions for energetics and photosynthetic processes [i.e. *de Pury and Farquhar*, 1997; *Wang and Leuning*, 1998; *Dai et al.*, 2004]. We modified the SiB two-stream canopy radiative transfer submodel [*Sellers*, 1985; *Sellers et al.*, 1996a] and canopy photosynthesis treatment [*Sellers et al.*, 1992] to accommodate sunlit and shaded canopy fractions, and coupled these treatments to the prognostic canopy air space utilized in SiB as outlined in *Baker et al.* [2003] and *Vidale and Stöckli* [2005].

The model was spun up from saturated soil conditions for 15 model years using the above four formulations and three years of observed meteorological forcing (2001-2003).

2.4 Results and Discussion

These four treatments were simulated individually and their performance was analyzed against observed fluxes of carbon, energy and moisture, although CO_2 flux is emphasized. All of these mechanisms were included in SiB3's model physics for a final simulation. These runs are shown in Figure 2.2. Monthly mean carbon flux from the SS run is similar to the results from the HR simulation. The effect of the sunlit/shaded (SS) run is seen in the short-term temporal response of CO_2 flux; these results will be addressed later, and are not shown in Figure 2.2.

In the control simulation (Figure 2.1) with the unmodified code, respiration is almost constant throughout the year, while NPP decreases during the dry season (not shown). As mentioned previously, there is little response in heterotrophic respiration to drying soil, most likely due to the inappropriate value for optimum soil moisture for respiration. Any moisture response in respiration appears to be compensated for by a temperature response to slightly warming soils during the seasonal drought. The main driver of the annual NEE cycle is the dramatic decrease in NPP with decreasing soil moisture. Moisture storage in the soil is adequate to maintain photosynthesis through June, but by August NPP has shut down to less than half the value at maximum productivity in May and June. Photosynthesis does not recover completely until March or April, when the soil moisture has been recharged by rain. It is interesting to note that increasing the soil depth of the base case from 3.5 to 10 meters has almost no effect on simulated fluxes. Near-surface soil layers, which contain the most roots, continue to dominate ecosystem behavior. These surface layers still dessicate quickly after rainfall ceases, so that the annual NEE cycle is almost indiguishable from that shown in Figure 2.1.

Relaxing the linkage between root distribution and stress postpones the change from uptake to efflux by 3 months (September vs. July), but the general behavior of SiB3-SR (Figure 2.2, panel A) is the same as the base case. Photosynthesis decreases as the soil desiccates and respiration is

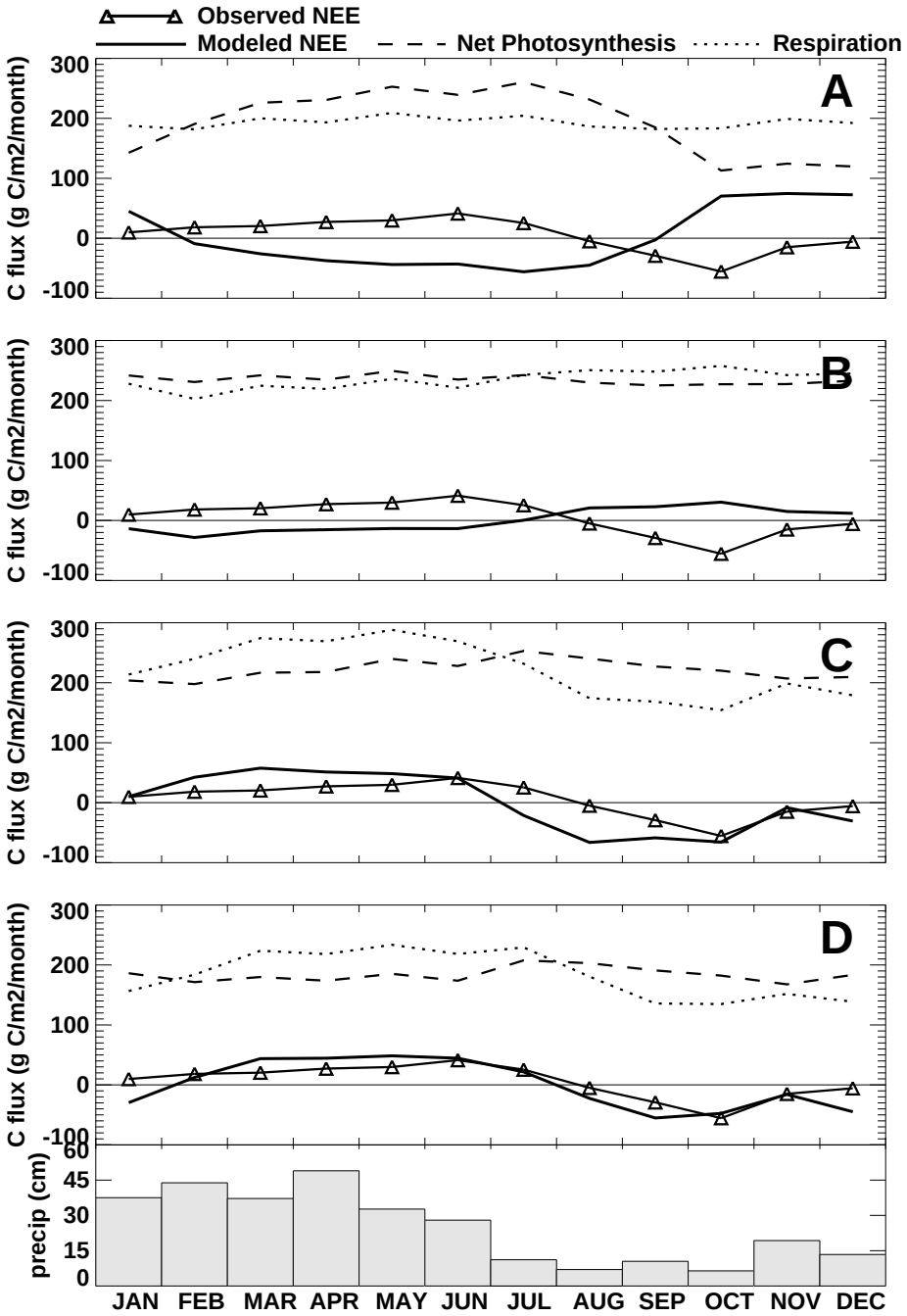

Figure 2.2: Average Monthly Photosynthesis, (dashed), Respiration (dotted), and NEE (solid) for four SiB3 simulations. A) Relaxed root stress calculation (SiB3-SR), B) Hydraulic Redistribution (SiB3-HR, C) Soil Depth/Respiration modification (SiB3-DS, 4) combination of the 4 mechanism runs. Mean monthly precipitation in cm is shown at the bottom for reference. Positive NEE values indicate efflux into the atmosphere, negative values indicate uptake by the biosphere.

nearly constant through the entire year. In this case, the reservoir of available water in a 3.5 meter deep soil is simply not sufficient to maintain ecosystem function through seasonal drought.

In the hydraulic redistribution case (Figure 2.2, panel B), the annual cycle of photosynthesis is almost uniform. Dry season stress, while still present, is minimal. However, heterotrophic respiration is also nearly constant in time, as opposed to observations that show a respiration decrease during seasonal drought [*Goulden et al.*, 2004]. The modeled respiration actually increases in the dry season in response to slightly warmer surface soil temperature as radiation increases with decreasing cloudiness. The annual NEE cycle, while much smaller in magnitude than in the control case, maintains the sign relationship between wet and dry seasons, which is inverted from the observed.

The deep soil case, where we increase soil depth from 3.5 to 10 meters and alter the respiration response to soil moisture, shows dramatic improvement over the control, SR and HR cases (Figure 2.2, panel C). We have also included the relaxed dependence on soil in this case, to distinguish it from the base case with deep soil. SiB3-DS is the SiB3-RS case with deeper soil and adjusted respiration response. NPP shows a maximum during the early stages of the dry season, in response to favorable light and soil moisture conditions. Heterotrophic respiration decreases as surface soil dries out. The surface soil has the largest root density, so under optimum conditions transpiration will remove water from the surface layers first. Radiative forcing at the ground surface is minimal beneath the closed canopy, but soil surface evaporation plays a small role. Without hydraulic redistribution to recharge the surface layers, the shallow soil becomes increasingly desiccated through the dry season, and transpiration load is transferred to the deeper layers in the soil. This combination of photosynthetic and respiration behavior has the effect of reversing the previously modeled NEE cycle, to the point where the sign of the annual cycle is now consistent with observations. There is efflux during the wet season, and uptake during seasonal drought. The modeled NEE now has monthly-mean magnitude comparable to observed for both segments of the cycle. Mean uptake of carbon begins early in SiB3-DS (July vs. August), but the sign of all other months are consistent with observed. This represents a large positive departure from previous model results.

The differences between the deep soil (SiB3-DS) and final simulation (Figure 2.2, panel D, representing a combination of the SiB3-HR, SiB3-SS and SiB3-DS runs) are subtle on the monthly-mean scale. The annual cycle remains consistent with observed, with the difference that July is now a month of efflux and January a month of uptake in the model results. The amplitude of the annual cycle of NEE is decreased by approximately 15% from the SiB3-DS to the SiB3-final run, while the amplitudes of the NPP and respiration annual cycles are both decreased by approximately 25%. This result is not inconsistent, since the timing of the variability is not temporally uniform. In the SiB3-DS run, the temporal peaks of respiration and photosynthesis are more pronounced, while in the final run the simulation produces a more stable or uniform behavior between wet and dry seasons. The end result, monthly mean NEE, is similar between the SiB3-DS and final runs, but the mechanisms have been modified.

The sensitivity of SiB3 to the various mechanisms is shown in a Taylor plot [*Taylor*, 2001] in Figure 2.3. Correlation coefficient is improved when compared to the control run in all simulations, but the largest correlation occurs in the SiB3-SS and final runs - which are virtually identical at a correlation coefficient of 0.85. It is interesting to note that although the correlation to the observations is high for SiB3-SS, the annual cycle was still inverted. In SiB3, adjusting the light response had a large impact on the diurnal scale, but not on monthly mean NEE. By increasing SiB3 response to light, we improve the correlation to the high-frequency observations. The variability of all simulations that did not include light response was smaller than observed, while the variability of the two simulations that included light response (SiB3-SS and final) were significantly larger than observed. By including sunlit and shaded canopy fractions in SiB3, GPP was increased by 25-30%. To maintain annual carbon balance there was an attendant increase in heterotrophic respiration [*Denning et al.*, 1996]. Therefore, adjusting the light response increased the amplitude of the diurnal cycle of NEE, but decreased the annual cycle of monthly mean NEE. Figure 2.4 shows monthly mean diurnal composites of NEE for April and October, aggregated over all years. For both wet and dry seasons the final run has a larger amplitude than the control run. However, the final run also simulates uptake during October (dry season) where the control run canopy is almost

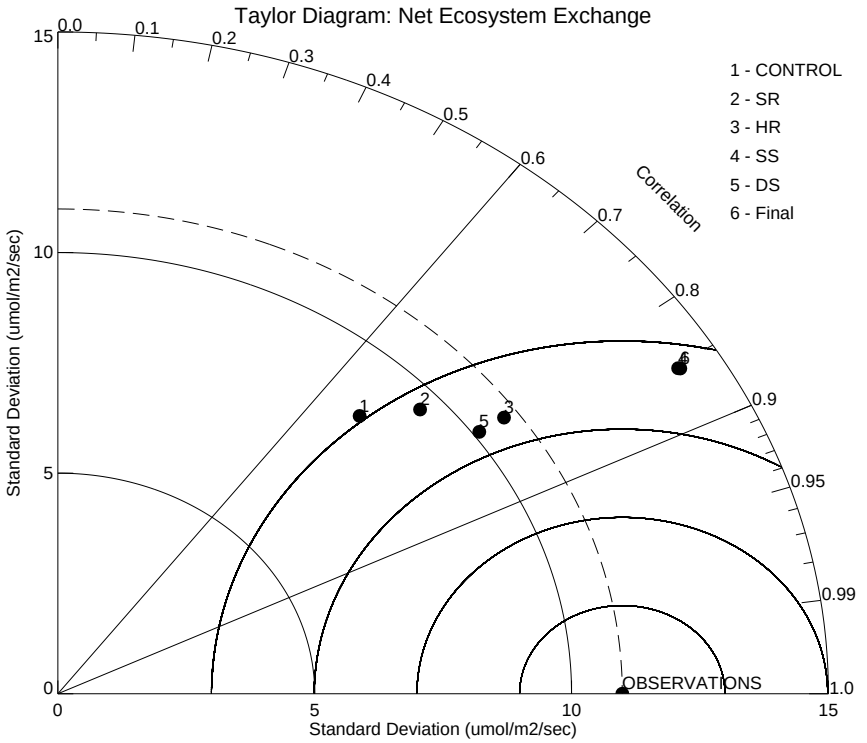

Figure 2.3: Taylor Plot of 30-minute modeled NEE against observed for years 2001-2003. Runs are identified as follows: 1) control run, 2) SiB3-SR, 3) SiB3-HR, 4) SiB3-SS, 5) SiB3-DS, 6) combination

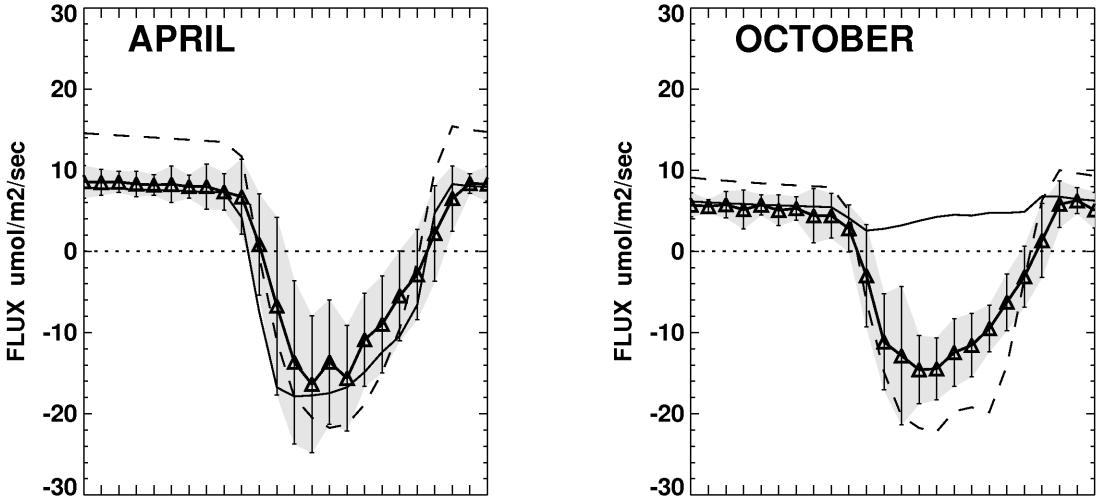

Figure 2.4: Monthly mean diurnal composited NEE for wet (April) and dry (October) months. Solid line with triangles is observed NEE, and shaded area represents +/- 1 standard deviation about the mean. Control run is shown as thin solid line, final simulation combining all mechanisms is shown as dashed line.

completely inactive. The shape of the diurnal cycle is closer to observed in the final run. This can be seen both in the larger correlation in the Taylor plot, and visually in Figure 2.4 as well.

However, SiB3 model physics do not include all details of local phenology, such as the genetically induced cycles of litterfall and wood increment as noted by *Goulden et al.* [2004]. SiB3 also maintains a constant annual Leaf Area Index (LAI) for broadleaf evergreen forests. LAI and, more importantly, fraction of Photosynthetically Active Radiation (fPAR) are obtained from satellite observations; water vapor and cloud contamination of satellite observations can induce errors in surface fluxes in SiB3 [*Los et al.*, 2000]. *Huete et al.* [2006] and *Saleska et al.* [2007] attribute part of the green-up in the Amazon Basin during the dry season to increased LAI. This feature will not be reflected in SiB3 simulations, and suggests that we may not currently have the ability to capture completely all mechanisms that effect biophysical function in the region.

It is well-known that eddy covariance instruments do not close energy budgets [i.e. *Mahrt*, 1998; *Wilson et al.*, 2002]. The sum of latent, sensible, and ground heat fluxes has a deficit generally on the order of 10-30% less than incoming radiation [*Twine et al.*, 2000]. This closure problem exists with carbon flux as well [*Aranibar et al.*, 2006], and there are additional issues of under representation of nocturnal CO_2 efflux [*Eugster and Siegrist*, 2000; *Lee*, 1998] though the site researchers at km83 made a strong effort to correct for this [*Miller et al.*, 2004]. Therefore, it is reasonable to assume that the magnitude of the observed NEE is smaller than reality. For this reason, a model simulation that has variability smaller than or equal to the observed, as in the case of the control, SiB3-HR and SiB3-DS runs (Figure 2.3) almost surely has magnitude that is too small. Following this line of reasoning, we might expect that a model simulation with variability exceeding the observed is reasonable, but determining the optimum excess is difficult due to multiple processes affecting both observations and model results. In this case, we see standard deviation of the SiB3 runs with the sunlit/shaded canopy simulation (and in the final run) that is 30% larger than observed. Intuitively this seems large. However, a detailed investigation of observed carbon flux closure is beyond the scope of this paper; we will accept the increase in correlation coefficient and larger-than-observed variability as positive results.

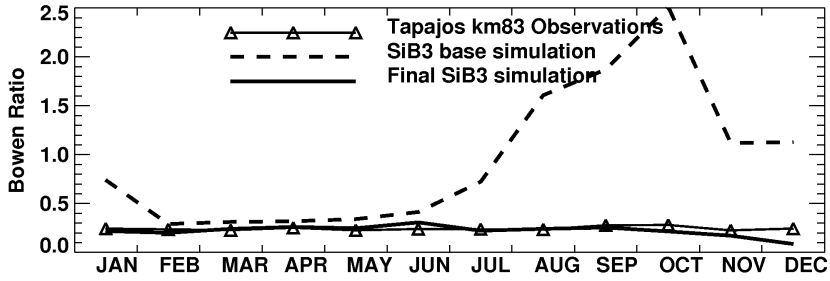

Figure 2.5: Monthly mean Bowen Ratio at Tapajos National Forest km 83 site, years 2001-2003. Observations are shown as solid line with triangular symbols. Control simulation is dashed, final simulation is solid line.

Finally, although the emphasis here has been on CO_2 flux, the large fraction of total water flux occurring as transpiration (80-85% in SiB3 simulations) tightly couples fluxes of latent and sensible heat to vegetation behavior. Modeled and observed values of Bowen Ratio are shown in Figure 2.5. In the unmodified case, Bowen Ratio becomes large during the dry season as transpiration wanes due to soil water stress and attendant stomatal closure. The Bowen Ratio in the final run is almost constant throughout the year, as is the observed. The magnitude of the individual fluxes (latent and sensible heat; not shown) is similar to observed in the final run as well.

2.5 Conclusions

We modified the model physics in the Simple Biosphere model (SiB3) to include mechanisms that allow broadleaf evergreen forests in tropical Amazonia to maintain biophysical function through seasonal drought. This changed model response from an inverted annual NEE cycle to one that has the same general behavior as observed eddy covariance fluxes. The mechanisms we included are deeper soils and a modification of the soil moisture respiration optimum value, modified root water uptake function, hydraulic redistribution, and light response. We found that each process, individually incorporated into SiB3, was not sufficient to change the sign of the annual NEE cycle to match observations.

Increasing soil depth to 10 meters and allowing roots to access this entire reservoir had the

effect of removing stress from vegetation during the dry season, although a similar response was obtained with hydraulic redistribution incorporated into SiB3. In each case, the respiration response was critical to the annual NEE. By changing the soil moisture value most favorable to respiration from 60% to 75% of saturation, we were able to induce a reduction in near-surface root respiration in the SiB3-DS case like that observed in the field [*Goulden et al.*, 2004], resulting in net carbon uptake during the drier months. In the SiB3-HR case, hydraulic redistribution kept near-surface soil layers moist, and there was no respiration response to drying soil. In fact, in the SiB3-HR case respiration actually increased in the dry season due to slightly warmer temperatures.

When canopy response was modeled explicitly for sunlit and shaded fractions (SiB3-SS), the response in the monthly mean was minimal. The largest change was in the magnitude and shape of the diurnal cycle.

The above points underscore the concept of equifinality, or multiple paths to a single solution in a model. For example, observed NEE reveals vegetation uptake of carbon in the dry season, and efflux when rain is plentiful. In the model, we can reproduce this result two ways: 1) photosynthesis is constant annually, and respiration decreases in the dry season as surface litter and soil desiccate, and 2) annual respiration is constant, and photosynthesis increases in the dry season in response to higher light levels. Observed NEE does not partition the individual contribution of photosynthesis and respiratory components, but it is intuitive to believe that the actual canopy response is a combination of 1) and 2). It is desirable to quantify the relative response of each, but that is likely to be variable in space and time.

As pointed out by *Franks et al.* [1997], eddy covariance fluxes by themselves are insufficient to provide a robust calibration of process-based biophysical models. Therefore, model simulations must be confronted with observational data from multiple sources to prevent modelers from getting 'the right answer for the wrong reason'. Open lines of communication between the observational and modeling communities are critical to this effort.

This research represents initial success in simulating the correct sign in the annual NEE cycle at an single location in the Amazon Basin. We've done so by identifying several mechanisms

identified in the literature as having a bearing on the observed behavior in the region, specifically 1) the ability of roots to access moisture in deep soil layers, 2) the ability of hydraulic redistribution of soil moisture by roots to both make water available to roots and to more efficiently use the pore space in the soil to store water, and 3) the ability of the vegetation to utilize increased light during the dry season, when more incoming radiation is available. By incorporating these mechanisms into SiB3 we are able to obtain an annual cycle of NEE that matches the observed, specifically uptake of carbon during the dry season and efflux during the wet months. We've shown the average results for three years of simulations (2001-2003), as the initial goal is to be able to reproduce the general response of the vegetation in the region. As our understanding of the biophysical processes increases, we will be in a position to investigate variability about the mean. We've shown that we can obtain the right sign for a single station. The next step is to reproduce the analysis across moisture and vegetation gradients across the Amazon Basin.

Chapter 3

MULTIPLE SITES: ECOPHYSIOLOGICAL BEHAVIOR ACROSS VEGETATION AND MOISTURE GRADIENTS IN TROPICAL AMAZONIA

3.1 Introduction

The Amazon Basin occupies a central role in our ability to understand and predict interactions between earth and atmosphere across multiple spatial and temporal scales. The dense forest and large spatial extent means this region stores a significant fraction of global biomass [*Houghton et al.*, 2001], up to 10%. It has been predicted that climate change will result in the conversion of Amazonian forest to savanna or grassland, releasing much of the carbon stored at the surface and further altering the radiation characteristics of the atmosphere [*Cox et al.*, 2000; *Huntingford et al.*, 2004; *Huntingford et al.*, 2008]. Predictions such as these place a premium on our ability to understand the surface ecophysiology of tropical systems. If we are to predict global climate under changing radiative conditions, we must be able to translate our understanding of the physical system into numerical models, and tropical Amazonia will play a significant role.

Surface ecophysiology in Amazonia is tightly coupled to the atmosphere. Seasonal temperature range is small, and annual variability is primarily defined by the intensity and duration of wet and dry seasons. Bidirectional coupling between surface and atmosphere plays a critical role in timing, duration, and magnitude of seasonal rains, and the large areal extent of the basin provides Amazonia with influence on regional to global-scale circulation patterns. The region is important to global carbon flux, due to the large carbon stores and fluxes.

The behavior of the land surface is tightly coupled to the cycles of wet and dry seasons that define seasonality in the region. In the tropical Americas, there is an annual cycle, whereby convec-

tive precipitation associated with the Intertropical Convergence Zone (ITCZ) is centered over the Amazon Basin during Austral summer (December, January, and February). In Austral fall (March, April, May) this feature moves northward and westward to a position over Central America [*Horel et al.* 1989] where it remains during Boreal summer (June, July, August). The northward position of the precipitation maximum coincides with the wet season north of the equator; south of the equator, the wet season is approximately coincident with Austral summer.

Prior to the onset of the wet season in Amazonia, the atmosphere is 'preconditioned' by an increase in latent heat flux (LE) from the surface [*Fu et al.*, 1999; *Li and Fu*, 2004]. This increase in latent heat flux increases the available potential energy in the lower atmosphere while reducing the convective inhibition energy due to cooling at the boundary layer top. In response, convective precipitation is initiated, which in turn influences the development of mid- to upper-tropospheric features that define the circulation and moisture convergence of the mature wet season [*Li and Fu*, 2004; *Fu and Li*, 2004; *Lenters et al.*, 1997]. The intrusion of cold air from southern high latitude can also trigger widespread precipitation and wet season onset [*Li et al.*, 2006]. At the latitudinal extremities of this precipitation oscillation (Central America and southern Brazil, approximately), annual precipitation variability is dominated by the annual cycle [*Adler et al.*, 2003; *Horel et al.*, 1989]. Between these spatial endpoints annual precipitation is larger, the dry season shorter or almost nonexistent, and interannual variability dominates the precipitation variance [*Horel et al.*, 1989]. Superimposed on this mean pattern is variability in circulation and vegetation behavior, which can be influenced by topography [*Lu et al.*, 2005] or other factors such as soil depth or type [*von Randow et al.*, 2004]. Ecosystem response displays this variability; *Phillips et al.* [2009] and *Saleska et al.* [2007] both show heterogeneity and variability in the ecophysiological response to the 2005 Amazonian drought as measured by allometric and satellite observations, respectively.

Interannual variability in precipitation is imposed by the dominant climate mode in the region, the El Niño-Southern Oscillation (ENSO). There are well-established connections between ENSO and South American precipitation [*Rasmusson and Carpenter*, 1982; *Ropelewski and Halpert*, 1987; *Ronchail et al.*, 2002; *Yoon and Zeng*, 2010]. *de Souza and Ambrizzi* [2002] demonstrate that

the warm eastern Pacific sea surface temperatures associated with El Niño influence the Hadley and Walker circulations, imposing anomalous subsidence over large regions of South America. The strongest response is in northeastern Brazil; furthermore, while overall continental-scale precipitation correlates well with ENSO, the spatial patterns from even to event are heterogenous [*de Souza and Ambrizzi*, 2002; *Coelho et al.*, 2002; *Ronchail et al.*, 2002]. In this study, the longest continuous record at any station is four years. This is insufficient to evaluate variability at climatic timescales. Therefore, emphasis here will be on the annual cycle.

Recent work has debated which mechanism(s) are most responsible for determining variability in ecosystem function, and, due to the tight coupling between the vegetated surface and surface-atmosphere exchange, variability in exchange of energy, moisture and carbon between the atmosphere and terrestrial biosphere in the Amazon Basin. It has been proposed that Amazonian forests are light-limited, and respond to relative drought with an increase in ecophysiological function [*Huete et al.*, 2006; *Saleska et al.*, 2007]. However, this finding has been challenged [*Samanta et al.*, 2010], citing problems with cloud and aerosol masking of remotely-sensed vegetation characteristics (i.e. *Sellers et al.*, [1996a], *Los et al.*, [2000]). As of this writing, we don't feel that the issue is closed.

Recycling, or the precipitation of water at a site or region that was locally evapotranspired rather than advected into the region, is an important component of the Amazonian hydrologic cycle. Early studies estimated that as much as half of the precipitation in the Amazon Basin was recycled [*Salati et al.*, 1979], but that number has been subsequently adjusted, to a value of 35-45% [*Eltahir and Bras*, 1994; *Trenberth*, 1999; *Costa and Foley*, 1999]. It has been suggested that the ecotone between forest and savanna, the 'transition forest', or cerradão *Eiten*, 1972; *Ackerly et al.*, 1989], plays a critical role in precipitation recycling in Amazonia [*Vourlitis et al.*, 2002]. The cerradão forms a buffer between the savanna (cerrado) to the southeast of the main tropical forest, and moistens dry air advecting over during the dry season [*Vourlitis et al.*, 2002; *Vourlitis et al.*, 2001]. This moistening reduces humidity stress on vegetation and facilitates transpiration in the forest interior.

Seasonal cycles of observed water and heat flux across vegetation and moisture gradients

from forest to savanna were investigated by *darocha et al.* [2009], and the region was partitioned into two functional types. In regions where annual precipitation was large and dry season short, evaporation increased during seasonal drought; otherwise latent heat flux was in phase with precipitation and evaporation decreased during the dry season. The authors postulated that wetter forests were light-limited, while evaporation in drier regions was controlled by soil moisture.

In this manuscript, we simulate surface ecophysiology at a subset of the stations investigated by *Darocha et al.* [2009]. We evaluate the model's ability to reproduce annual mean behavior across vegetation and moisture gradients. Additionally, we integrate carbon flux into the analysis to investigate full ecosystem behavior. The goals of this study are to 1) demonstrate an ability to capture mean annual cycles of biophysical behavior across vegetation and moisture gradients, and 2) use the model's ability to partition processes into component behavior as a means to formulating more detailed conceptual descriptions of the mechanisms involved.

We find that in the wettest interior regions of Amazonia, seasonal variability is minimal. Bowen ratio is always low, and gross fluxes of carbon uptake and efflux are consistently large. Variability is forced by high-frequency changes in meteorological forcing, on weekly to monthly scales. The small amplitude of seasonal cycles suggests that ecosystem function remains relatively constant throughout the year. Seasonal cycles begin to emerge as annual precipitation decreases and the dry season is more well-defined. At these intermediate sites we find that the seasonality is limited to carbon flux; seasonal cycles of energy and water flux have low amplitude, and Bowen ratio is small throughout the year as well.The annual carbon flux shows a seasonal cycle, as photosynthetic and respiratory fluxes lose phase cohesion due to differences in response of determinant mechanisms to climatic forcing. As annual precipitation decreases further, and length of dry season increases, a higher degree of seasonality emerges in all aspects of ecophysiological behavior. At the driest sites, the sign of the carbon flux is in phase with precipitation; that is, there is carbon uptake during the wet season, and efflux during seasonal drought. This is contradictory to the seasonal cycles of carbon flux in wetter regions. At the driest sites there is seasonality in energy and moisture fluxes, and in some locations the sensible heat (H) exceeds latent during the dry season (Bowen ratio greater than

1).

3.2 Methods

Historically, landsurface models have had difficulty reproducing annual cycles of energy, moisture, and carbon flux in tropical ecosystems. *Saleska et al.* [2003] showed that several models inverted the annual carbon flux cycle when compared to observed data. *Baker et al.* [2008] demonstrated an ability to capture the mean annual cycle of energy, moisture and carbon fluxes, at a single point in the Tapajos River National Forest (Brazil), by incorporating observed mechanisms into the Simple Biosphere Model (SiB). With that as a starting point, in this paper we again confront model results with observed quantities, this time at multiple sites and across vegetation and moisture gradients. We will focus on annual cycles of energy, moisture and carbon flux, but will evaluate diurnal and synoptic-scale behavior to support conclusions where appropriate.

3.2.1 Model

The Simple Biosphere Model (SiB) was developed as a lower boundary for atmospheric models [*Sellers et al.*, 1986], and has been coupled to GCMs [*Sato et al.*, 1989; *Randall et al.*, 1996] as well as mesoscale models [*Denning et al.*, 2003; *Nicholls et al.*, 2004; *Wang et al.*, 2007; *Corbin et al.*, 2008]. The addition of ecosystem metabolism to the code [*Sellers et al.*, 1996a; *Denning et al.*, 1996] give the model a high degree of ecophysiological realism that is valuable to ecologists as well. SiB model output has been compared to eddy covariance observations at sites in midlatitude forest [*Baker et al.*, 2003; *Schaefer et al.*, 2008], grassland [*Colello et al.*, 1998; *Hanan et al.*, 2005], and tropical forest [*Baker et al.*, 2008; *Schaefer et al.*, 2008]. The model has a proven track record for evaluating exchange between the atmosphere and terrestrial biosphere.

As a 'third generation' land surface scheme [*Sellers et al.*, 1997], SiB incorporates ecophysiological function as an additional constraint on fluxes of latent and sensible heat. Photosynthetic carbon assimilition is based on enzyme kinetics developed by *Farquhar et al.* [1980], and stomatal conductance couples vegetation behavior to the overall surface energy budget [*Collatz et al.*, 1991;

Collatz et al., 1992; *Sellers et al.*, 1996a; *Randall et al.*, 1996]. Soil heat and moisture flux has been modified to follow the Community Land Model (CLM) [*Dai et al.*, 2003]. Root distribution follows *Jackson et al.* [1996], and a fully prognostic canopy air space (CAS) for temperature and moisture follows *Vidale and Stöckli* [2005] and *Baker et al.* [2003].

Remotely-sensed information, such as Normalized Difference Vegetation Index (NDVI) was introduced into SiB [*Sellers et al.*, 1996a; *Sellers et al.*, 1996b; *Randall et al.*, 1996] to describe spatiotemporally variable vegetation phenology. However, satellite data can be obscured by masking due to cloud and/or aerosols, especially in regions with a well-defined seasonal precipitation cycle [*Los et al.*, 2001]. While variability in remotely-sensed LAI has been noted in tropical Amazonia [*Myneni et al.*, 2007], the magnitude of the seasonal phenology observed at site-level plots can be much smaller [*Malhado et al.*, 2009]. Furthermore, while seasonality in observed LAI is generally tied to wet/dry seasonal cycles [*Brando et al.*, 2010; *Miller et al.*, 2004], variability in satellite products often occur with unrealistic frequency, in obvious response to cloudy and clear periods during the wet season [*Los et al.*, 2000; *Sellers et al.*, 1996b; *Stöckli et al.*, 2008]. For this reason we have, for sites identified to be broadleaf evergreen forest, maintained a constant LAI and fPAR in SiB simulations. We concede that model simulations may not reflect actual seasonal changes in vegetation, but we argue that this limitation is more than compensated for by the fact that our forest simulations do not experience unrealistic high-frequency variability imposed by cloud or aerosol masking of spectral vegetative indices. Furthermore, observed LAI is usually above 4 [*Myneni et al.*, 2007; *Malhado et al.*, 2009; *Miller et al.*, 2004], which approaches where fPAR is saturated in SiB [*Sellers et al.*, 1996a]. Even if we had accurate LAI/fPAR phenology at all forest sites, SiB may not see a response as all points in the seasonal cycle are above the saturation level of the model.

Modifications to the code since SiB2 was introduced in 1996[*Sellers et al.*, 1996a; *Sellers et al.*, 1996b] have been described elsewhere [*Baker et al.*, 2003; *Hanan et al.*, 2005; *Vidale and Stöckli*, 2005]. *Baker et al.* [2008] identified several mechanisms that were required for the model to capture the annual cycles of energy, moisture, and carbon flux at the K83 site in the Tapajos River National Forest. They are:

- A soil reservoir large enough to store sufficient moisture to sustain ecophysiological function through periodic drought. Most landsurface models have a soil depth of 3-4 meters, which was found to be inadequate. A 10-meter deep soil was found to be sufficient at the Tapajos River K83 site, and has been incorporated into SiB as the standard.

- Adequate soil moisture is a necessary, but not sufficient mechanism to allow vegetation function to survive seasonal drought. Removal of water by roots, usually tied directly to relative root mass with depth in models, must be relaxed to allow water extraction by roots in excess of the amount suggested by relative root fraction. This phenomenon has been observed in multiple species [*Oliveira et al.,* 2005], and allows retrieval of water stored deep in the soil. In SiB, we have developed a 'relative root fraction' system, wherein soil is extracted based on root density when water is plentiful. When surface soil (where the majority of root mass resides) dries, deeper roots are allowed to extract water at a rate exceeding their absolute root density.

Global maps of soil depth are nonexistent or unreliable, so SiB employs rooting depth as a mechanism to impose heterogeneity on a global 10-meter deep soil. Maximum rooting depth of different vegetation is described in *Canadell et al.* [1996], while *Jackson et al.,* [1996] give a global map of rooting depth and distribution associated with discrete biome classes.

It has been postulated that hydraulic redistribution, or the movement of water across moisture gradients via roots, plays an important role in Amazonian forests' ability to survive seasonal drought [*Lee et al.* [2005]. In this case hydraulic redistribution facilitates the movement of water downward during wet periods, increasing soil storage, and moves water upwards, against gravity, rewetting surface soils during seasonal drought. We do not consider hydraulic redistribution in our simulations for two reasons: 1) previous simulations [*Baker et al.,* 2008] show that hydraulic redistribution alone is not sufficient to reproduce observed seasonality in SiB, and 2) simulating hydraulic redistribution requires soil-to-root exchange coefficients that are unknown without detailed soil/root surveys. We call the current version of the model SiB3

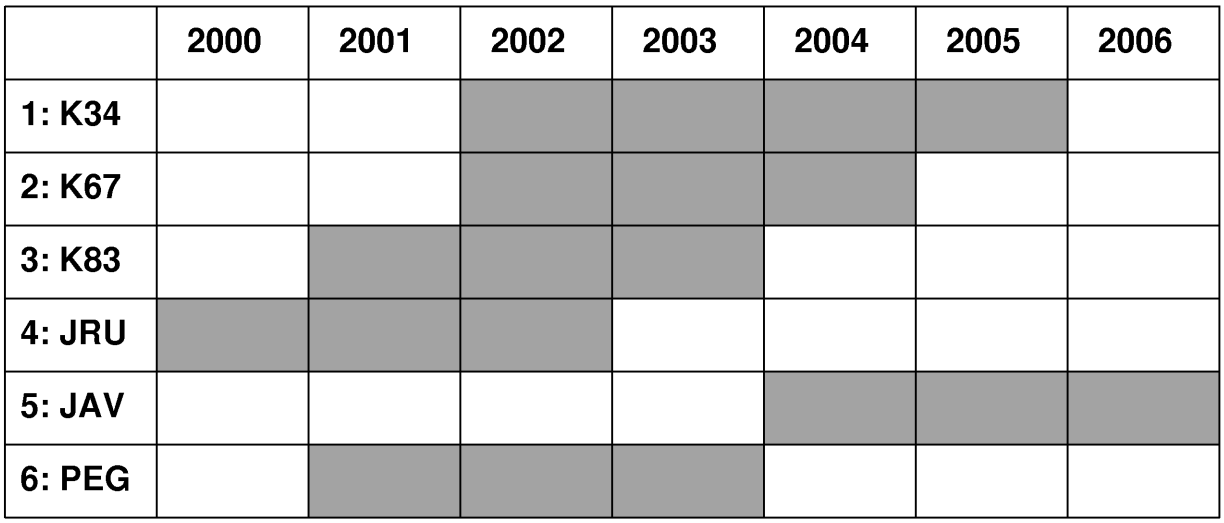

Figure 3.1: Data availability for the sites used in this study.

3.2.2 Observation Sites

The behavior of observed energy and moisture fluxes across vegetation and precipitation gradients in Amazonia was described in *da Rocha et al.*, 2009], using data from 7 stations in Brazil. We simulated ecophysiological behavior at 6 of these 7 sites, listed in order of decreasing mean annual precipitation: Manaus (K34), Jaru (JRU), Tapajos River National Forest (K67 and K83), Javaes (JAV), and Pé de Gigante (PEG) (Figure 3.1). All sites except PEG are classified as evergreen forest, and therefore do not experience annual/interannual variability in vegetation behavior in the SiB3 simulations. All sites were simulated for either 3 or 4 years over the period 2000-2006. Data availability for each site is shown in Figure 3.1.

These sites were chosen to extend across vegetation and moisture gradients, along a line running approximately Southeast to Northwest, from PEG to K34. PEG is the driest site, with an annual precipitation of approximately 1500 mm [*da Rocha et al.*, 2009], while K34 and JRU have annual precipitation well over 2000 mm. All stations but PEG are at latitude less than 10°, so seasonality in radiation and temperature are small. Seasonality is most strongly defined by annual precipitation (and associated variability in cloudiness and temperature), and the length/severity of

the dry season, defined as the number of months with monthly precipitation less than 100 mm [*Keller et al.*, 2004].

Detailed descriptions of the sites are available elsewhere: *Araujo et al.*, [2002] describe the K34 site, and JRU is covered in *von Randow et al.*, [2004]. Behavior at the Tapajos River National Forest sites (K67, K83) are recounted by *Saleska et al.*, [2003], *da Rocha et al.* [2004], *Miller et al.* [2004], *Goulden et al.* [2004], and *Hutyra et al.*, [2007] while the JAV site is described by *Borma et al.* [2009] and the PEG site by *da Rocha et al.* [2002].

Data Availability

Model simulations require data-filled meteorology (pressure, temperature, dewpoint, wind-speed, longwave and shortwave radiation, and precipitation) as model inputs. Missing data were interpolated from neighboring values where gaps were short, and from climatology when gaps were long. Longwave radiation has a significant impact on surface character, and is infrequently measured at the sites used. Techniques used to estimate longwave radiation at midlatitude sites are ineffective in the tropics; a new technique has been developed for creating incoming longwave [*restrepo et al.*, 2010a], and we use it here.

Model simulations were evaluated against measured flux of energy (sensible heat), moisture (latent heat), and carbon taken at the tower sites. However, not all observations are available at each site for all times; instrument failure, heavy rain, and low wind speed can all impair the ability of an eddy covariance instrument to accurately record data. Furthermore, the lack of CO_2 storage observations make calculation of observed Net Ecosystem Exchange (NEE) of carbon difficult. Fortunately, SiB3, with a prognostic canopy air space [*Baker et al.*, 2003; *Vidale and Stöckli* 2005], can simulate the flux of CO_2 past the sensor. Canopy storage is accounted for in the model, so model flux of carbon is analogous to what the sensor sees.

NEE is generally thought of as a robust metric of carbon source or sink over daily to multiyear timescales, and we do not have a reliable observation of this quantity. Furthermore, modeled NEE is constrained to a value of zero on an annual basis [*Denning et al.*, 1996]. What we are going to

focus on is the ability of eddy covariance instruments to detect change and/or ecosystem response to variability on multiple timescales. How does carbon flux (and for that matter, latent and sensible heat) change over an annual cycle? What general shape does the monthly-mean diurnal composite take? How does the ecosystem respond to synoptic- to monthly-scale cycles of wetting and drying?

Evaluation of model simulations against eddy covariance flux observations can be problematic. Models are generally held to energy, moisture and trace gas conservation through the formulation of their governing equations. However, determination of energy balance closure in eddy covariance data has been an ongoing issue [*Wilson et al.*, 2002; *Hollinger et al.*, 2005; *Foken et al.*, 2006]. Furthermore, the lack of closure in the eddy covariance energy budget can imply lack of closure in observed carbon budget as well [*Aranibar et al.*, 2006]. The goal of this paper is not detailed analysis of observational techniques and data. Instead, we wish to exploit the acknowledged strength of eddy covariance observations to capture ecosystem response to *variability* in forcing over multiple timescales (diurnal, synoptic, monthly) for comparison to simulations.

Monthly-mean observed carbon flux shows a net negative value (terrestrial uptake) for almost all months at almost all stations. However, it is well-known that drainage [*Araujo et al.*, 2002], energy/carbon budget closure [*von Randow et al.*, 2008], or the lack of storage observations[*Restrepo-Coupe et al.*, 2010] all contribute uncertainty to observed carbon flux. Therefore, we calculate the monthly *anomaly* for comparing observed annual cycles of carbon flux to simulations. This metric neglects determination of observed source/sink on timescales longer than diurnal, which is consistent with the annual balance property of SiB3 [*Denning et al.*, 1996]. Deviation from the monthly average carbon flux value is also used in plots of daily average. Mean values of carbon flux are *not* used in the calculation of monthly-mean diurnal composites, or in graphics showing hourly behavior, and no adjustments are ever made to observed latent and sensible heat flux.

The lack of observed storage, while problematic to calculation of observed NEE, is not an impediment to confronting SiB3 simulations with observed data. The prognostic CAS in SiB3 allows us to calculate a top-of-canopy flux into and out of the CAS, which is directly analogous to what an instrument would observe.

3.3 Analysis

If we are to use a model to parse out elements of ecophysiological behavior, we must first evaluate the model against available observations, on multiple temporal scales. In this section we will demonstrate that SiB3 demonstrates competence when confronted with observational data across all 6 sites, from hourly data and monthly-mean diurnal composites to daily- and monthly-averaged periods. Once established against observations, model representation of component mechanisms and interpretation of ecophysiological function will have more credence.

The mean seasonality (precipitation, radiation, temperature) at these sites is described in *da Rocha et al.* [2009], but will be briefly summarized here (Figure 3.2), as a review of the climatological regime gives context to the discussion of biophysical behavior. Sites K34, K67 and K83 are all very near the equator, while JRU and JAV are located at approximately 10°, south latitude. Site PEG is the farthest south, at approximately 20°. The wettest locations are in the north and west (K34, JRU), with a general decrease in annual mean precipitation towards the east and south. The driest site is PEG, in the southeast corner of the domain. The dry season is somewhat correlated with annual precipitation; K34 has a dry season, but its length is short (4 months, maximum) and monthly precipitation is frequently near or above the climatological definition of 100 mm month^{-1} for a 'dry month' [*Keller et al.* [2004] even during the dry season. There is a well-defined dry season at JRU of 5 months, even though annual precipitation is large, and 3 of these months (June, July and August) are extremely dry. Mean precipitation during May and September at JRU is close to 100 mm. The Santarem sites (K83, K67) are similar to each other with regard to annual mean precipitation and length of dry season (5-6 months). Precipitation at these sites is not infrequent during dry months, and can exceed 100 mm during an individual month. At JAV and PEG the dry season is longer, and precipitation is rare or nonexistent during most dry months.

The equatorial sites (K34, K67, K83) have very small temperature seasonality (Figure 3.2), with only one or two degrees separating the mean monthly temperature of the warmest months, during the dry season, from the cooler, rainy months. At JRU and JAV the temperature seasonality is similar or slightly larger in magnitude, but the seasonality shows a bimodal signal with relative

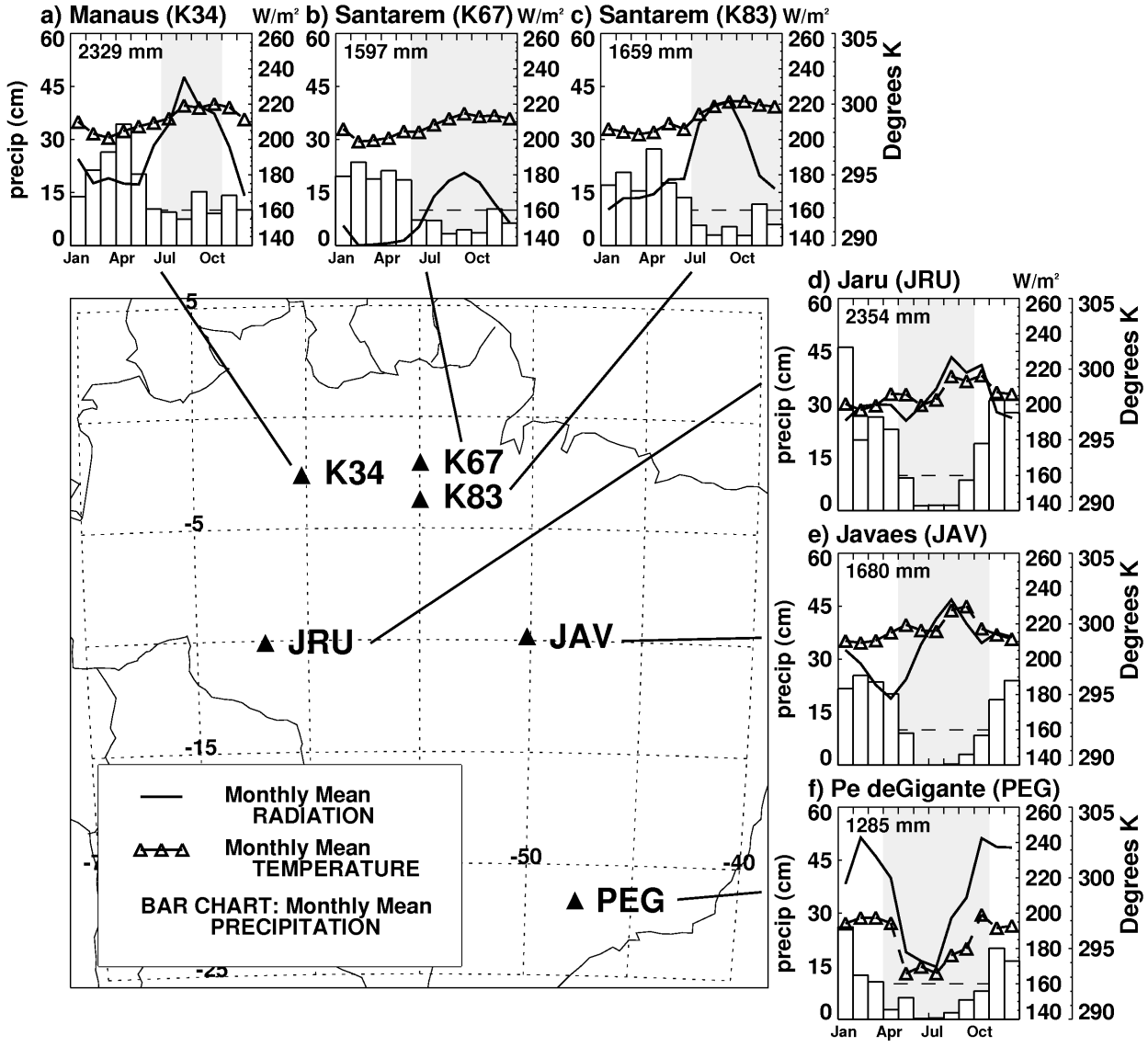

Figure 3.2: Site location and mean monthly incoming shortwave radiation, temperature and precipitation, following Figure 1 of *da Rocha et al.* [2009]. Dry season, defined as number of months with less than 100 mm of precipitation, is shaded. Annual mean precipitation for the years used in this study is listed at the top of each panel.

temperature peaks at the beginning and near the end of the dry season. At PEG, annual mean temperature is less and amplitude of the annual cycle is larger. At this location, seasonality plays a greater role. At all other sites, maximum monthly temperature occurs during the dry season, when cloudiness is less; at PEG, the dry season is coincident with Austral winter, so temperature is lower during the dry season. Radiation is consistent with temperature: at all sites but PEG insolation rises considerably as cloudiness decreases during dry season and insolation (and temperature) rise. At PEG the main radiation variability is due to latitude and therefore solar angle/day length; January is characterized by both higher midday insolation, as well as longer photoperiod, when compared to June.

Figures 3.3 and 3.4 compare model results at all 6 sites against observations. Figure 3.3 shows net radiation (R_{net}), latent and sensible heat flux superimposed over the mean annual precipitation cycle. Figure 3.4 shows modeled and observed carbon flux, with simulated GPP and total respiration included for reference. In both Figures, the dry season is shaded.

Monthly-averaged incoming radiation at K67 is significantly lower than at K83 (Figure 3.2). These sites are located near each other ($<$20 km apart), yet this difference does not appear to be due to instrument bias or degradation. A persistent low-level convergence (LLC) area on the east bank of the Tapajos River has been described [*Dias et al.*, 2004; *Lu et al.*, 2005], where a cloud frequently forms. The LLC is frequently located over K67, yet rarely over K83. This can be seen in the hourly radiation observations taken at the two sites (not shown), which commonly show a reduction in midday maximum insolation over the K67 site when compared to K83. We postulate that clouds resulting from the influence of the LLC at K67 are not as prevalent at K83, resulting in a systematic reduction in incoming solar at K67.

The mean annual cycle of net radiation, latent and sensible heat flux, comparing model values to observations, is shown in Figure 3.3. Seasonal cycles of R_{net} are captured by the model, although modeled net radiation is larger than observed at 4 of the 6 sites. Exceptions are K83, where observed net radiation exceeds modeled, and K67 where observed and modeled net radiation are similar. Modeled net radiation is a function of vegetation type, Leaf Area Index (LAI), frac-

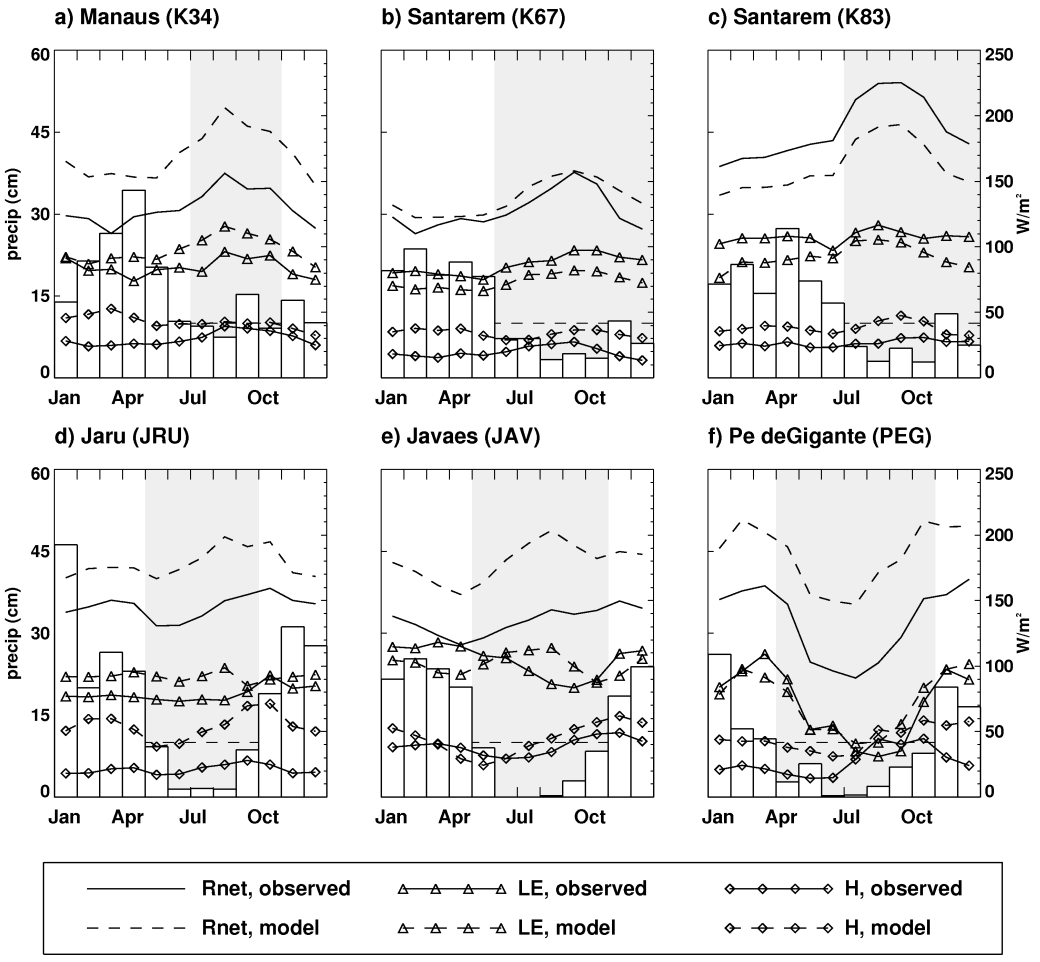

Figure 3.3: Mean annual cycles of modeled and observed net radiation (Rnet), latent heat (LE), and sensible heat (H) for the 6 stations superimposed on a histogram of monthly-mean precipitation. Locations are shown in Figure 1, dry season is shaded as before.

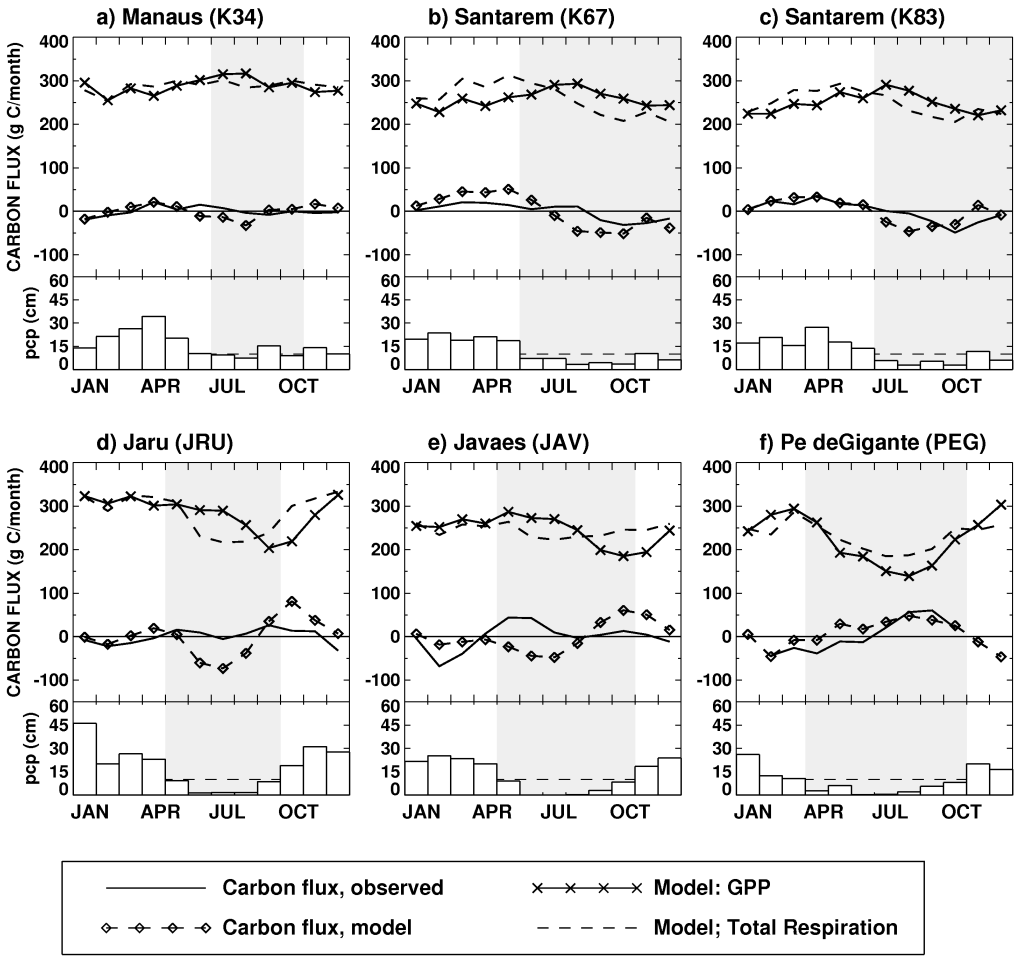

Figure 3.4: Mean annual cycles of modeled and observed carbon flux for the 6 stations, superimposed on a histogram of monthly-mean precipitation. Locations of towers are shown in Figure 1. Modeled Gross Primary Productivity (GPP) and total respiration are shown at the top of the plot; dry season is shaded.

tion of Photosynthetically Active Radiation absorbed (fPAR), and the fraction of radiation in beam and diffuse components. There are real variations in leaf absorption/reflectance characteristics, leaf angle distributions, and canopy gap fraction between sites. Much of this variability will not be captured fully by the model, as in the model all sites except PEG are classified as 'evergreen broadleaf forest' and will have identical parameter values for leaf angle distribution, vegetation cover fraction, and leaf character [*Sellers et al.*, 1996b]. Model heterogeneity in vegetation between sites is determined by maximum Global Inventory Monitoring and Modeling Study (GIMMSg) NDVI [*Brown et al.*, 2004; *Tucker et al.*, 2005; *Pinzon et al.*, 2006] value over the observation record, as calculated by the methods outlined in *Sellers et al.* [1996b]. High NDVI maximum values at K34, K67, and JRU set LAI, fPAR and green fraction values are close to the maximum (saturation), or 7.0, 0.95 and 0.99, respectively. Maximum NDVI at JAV and K83 are slightly lower, and result in slight reduction in LAI; fPAR and green fraction are still high. Furthermore, SiB3 parameterizes the partition of a single incoming shortwave radiation value into visible/near-infrared and beam/diffuse components [*Sellers et al.*, 1986]. These differences can explain differences between modeled and observed net radiation, and suggest an avenue for future model development.

3.3.1 forest sites: K34, K67, K83, JRU

The forest sites in these simulations are the equatorial sites (K34, K67, K83) along with JRU (Figure 3.2). JAV, while considered forest in the model, is a unique transitional forest site and will be described later. The forest sites are characterized by large annual precipitation ($>$1500 mm), low temperature variability (Figure 3.2), and maximum radiation during the dry season. The forest sites are characterized by extremely small annual cycle of observed carbon flux at the two wettest sites (K34, JRU); an annual cycle is observed at K67 and K83, although the amplitude is small, on the order of 50-60 g C m^{-2} $month^{-1}$ (Figure 3.4).

The forest site at JRU is distinct from the others. *von Randow et al.* [2004] report a relatively thin soil at JRU, with depth less than 4 meters overlying a solid bedrock layer. For this reason we did not incorporate the deep soil modifications at this site, as reported in *Baker et al.* [2008]. This

local information was incorporated into the model simulations; we retained the root mechanisms for water extraction as discussed in *Baker et al.* [2008], but limited soil depth to approximately 3.5 meters.

At the forest sites, latent heat is large and relatively constant throughout the year (Figure 3.3). In both model and observations, LE increases during the dry season. Using the Ohm's Law analog, we can express latent heat flux as

$$\lambda E_m = \frac{\rho c_p}{\gamma r_a} (e_m - e_a) \tag{3.1}$$

where

λE_m = latent heat flux (W m^{-2})

ρ = air density (kg m^{-3})

c_p = specific heat of air at constant pressure (J kg^{-1} K^{-1})

γ = psychrometric constant (hPa K^{-1})

r_a = aerodynamic resistance between canopy and boundary layer air (sec m^{-1})

e_m = water vapor pressure of boundary layer (hPa)

e_a = water vapor pressure of canopy air (hPa)

In this context, increased LE during the dry season can arise from increased e_a (due to increased transpiration as light levels increase), or from a decrease in e_m as the boundary layer dries in response to large-scale moisture divergence. Additionally, higher temperatures during the dry season may contribute to greater buoyancy in the canopy, and an increase in turbulent exchange between the CAS and atmosphere, expressed as a smaller value of r_a. Overall magnitude of LE generally follows net radiation at the forest sites. Where model R_{net} exceeds observed, model LE exceeds observed and vice versa, but the general shape of the observed annual LE cycle is captured at all sites by SiB3. We can consider sensible heat and carbon flux in the same manner; the magnitude and direction of the flux is a combination of the magnitude/direction of the gradient between the value in the CAS and atmosphere combined with the conductance or ease of the turbulent coupling

between the two.

Annual mean H at the forest sites is much smaller than LE, and shows less amplitude during the year. Maximum H occurs during the dry season (Figure 3.5). Modeled monthly H is larger than observed for all forest sites, both for monthly average and maximum midday values. Monthly-mean diurnal composites of LE for wet and dry seasons at the 4 forest sites are shown in Figure 3.6. In general, SiB3 can reproduce the diurnal cycle, although modeled H is frequently higher than observed. An exception is at JRU, where model H and LE precede observed by one or two hours. In the model, these fluxes follow net radiation, and positive values of H/LE are seen shortly after sunrise. The observations at most sites display this coincidence between R_{net} and energy/moisture as well. At JRU, there is a lag of between one and two hours between sunrise and heat flux response for both LE and H (see Figure 9 in *von Randow et al.* [2004]). We postulate that this lag must be due to the unique configuration of vegetation and topography at the JRU site, as this tendency is not seen at the other sites. It is not possible to reproduce this behavior in a model without detailed local information.

Monthly-mean diurnal composites of carbon flux for wet and dry seasons at the forest sites are shown in Figure 3.7, as was done for latent and sensible heat in Figures 3.5 and 3.6. In this case we do not calculate the deviation from a mean value, but calculate the observed diurnal average as the actual movement of CO_2 past the sensor. We are less concerned with the integrated value than we are with the general shape of the carbon flux signal throughout the day.

Carbon flux at the wettest sites (K34, JRU, Figure 3.4) show little evidence of an annual cycle in the observations. Monthly uptake/efflux deviation amounts are small, and show slight coherence to wet and dry seasons in the form of a slight positive (efflux) anomaly at the end of the wet season. However, the thin soil at JRU imposes significant constraint on ecophysiology, so this site will be considered separate from K34. At K67 and K83 a regular cycle of wet season efflux and dry season uptake is observed [*Saleska et al.*, 2003; *Baker et al.*, 2008]. The processes at K67 and K83 are relatively similar, and will be discussed jointly.

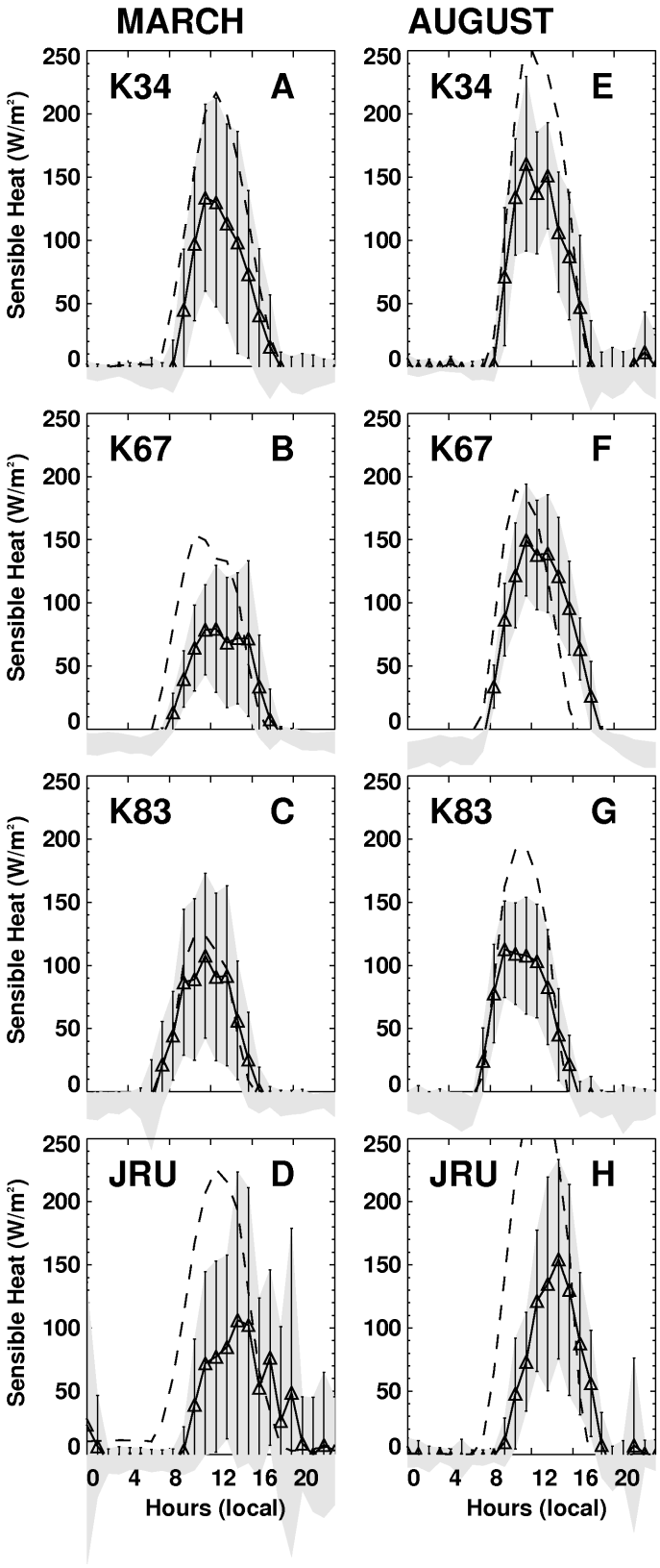

Figure 3.5: Monthly-mean diurnal composites of Sensible Heat flux, wet season (March) and dry season (September) months, at the forest sites (K34, K67, K83, JRU). Standard error (+/- 1 standard deviation) of the observed data is shaded.

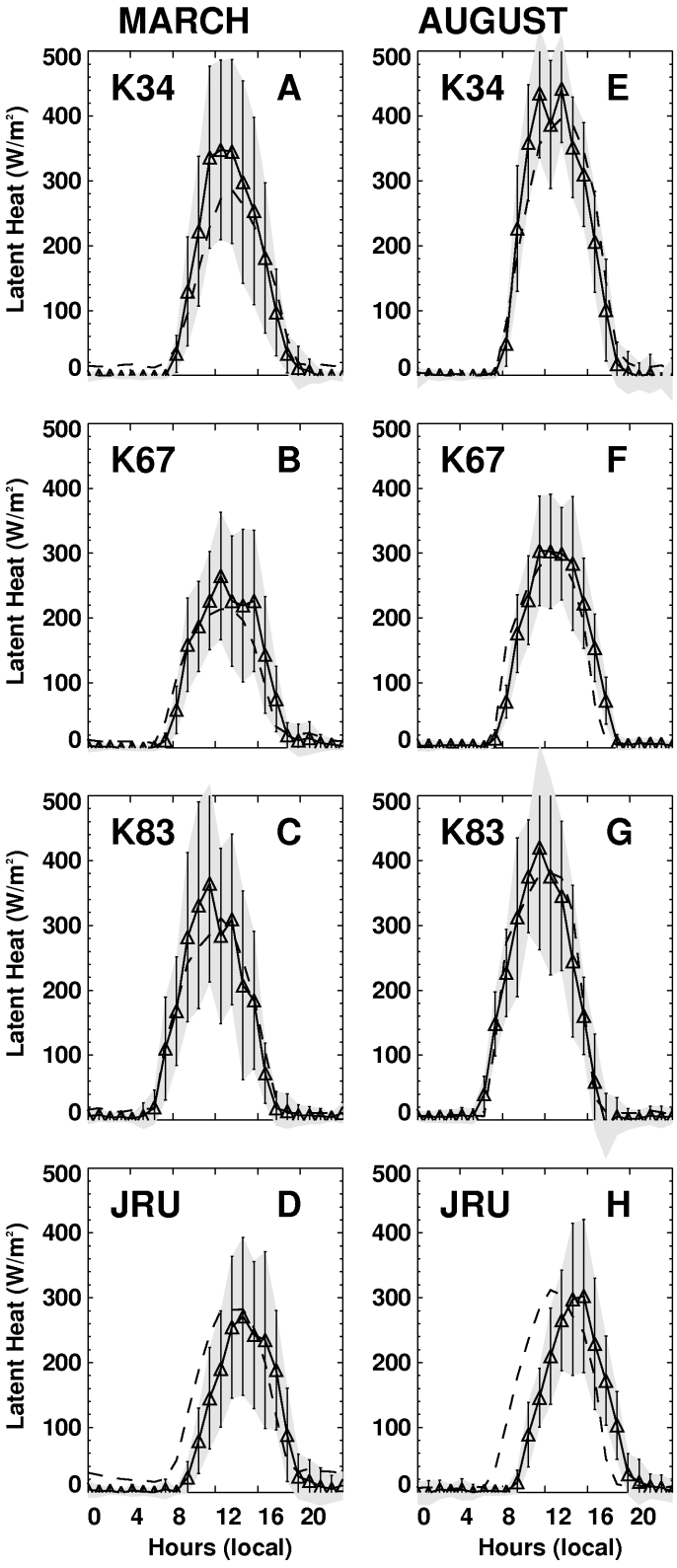

Figure 3.6: Monthly-mean diurnal composites of Latent Heat flux, wet season (March) and dry season (September) months, at the forest sites (K34, K67, K83, JRU). Standard error (+/- 1 standard deviation) of the observed data is shaded.

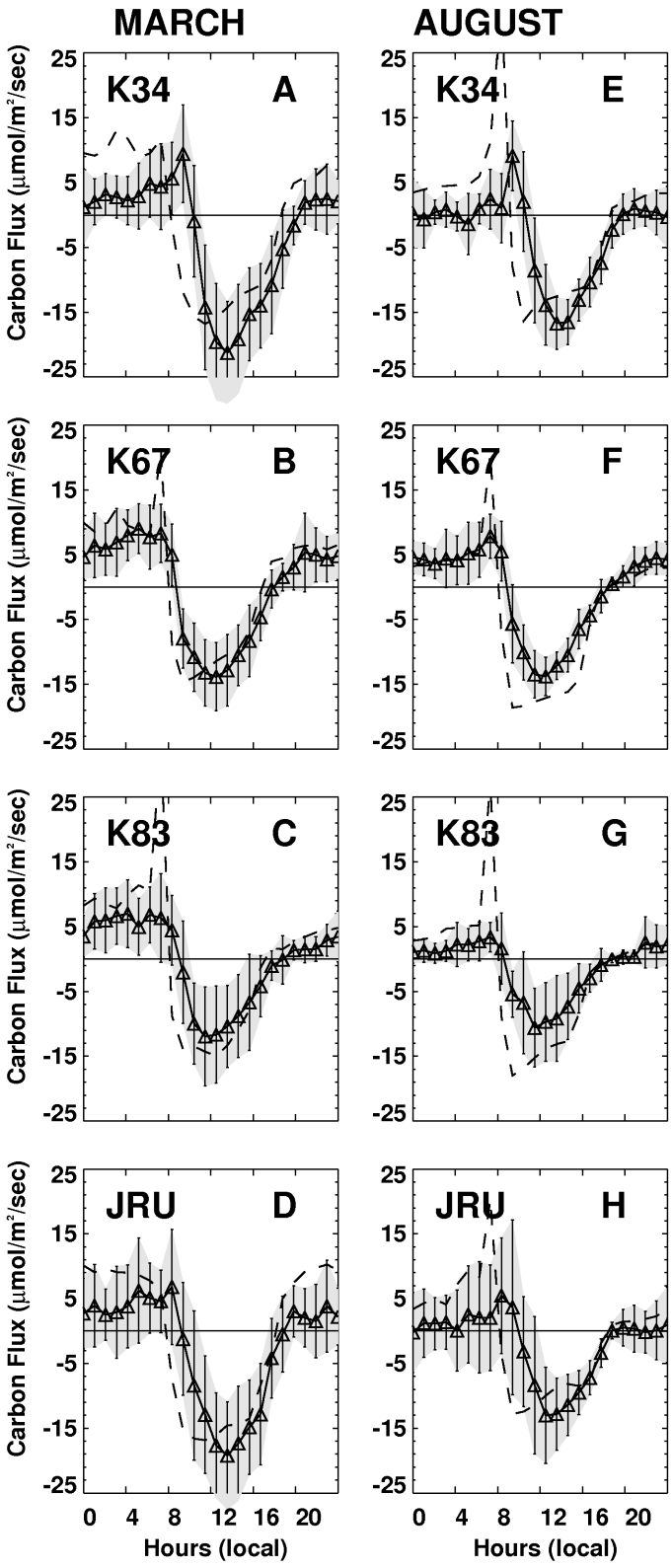

Figure 3.7: Monthly-mean diurnal composites of carbon flux, wet season (March) and dry season (September) months, at the forest sites (K34, K67, K83, JRU). Standard error (+/- 1 standard deviation) of the observed data is shaded.

Manaus: K34

Annual precipitation at K34 averages 2329 mm for the 4 years studied. Annual temperature variability is small, and both incoming and net radiation is highest during the dry season (Figures 3.2 and 3.3, panel a). Observed LE and H is nearly constant on an annual basis (Figure 3.3, panel a), as is annual carbon flux (Figure 3.4, panel a). However, some cycle is evident: Observed LE, H and R_{net} all show maximum values during the dry season (Figure 3.3 panel a). Observed carbon flux shows very little annual cycle, with maximum relative efflux late in the wet season, with slight relative uptake from late dry season through early wet season (Figure 3.4 panel a).

Comparing model to observations at K34, we see that simulated R_{net} follows the seasonal cycle observed, with a consistent positive bias. This is likely due to specific canopy characteristics at K34, as this bias is not uniform at all forest sites. The overall energy budget of the model will reflect this bias, so we can expect simulated LE, H, and/or ground heat flux (G) to exceed observed. The annual cycle of model LE (Figure 3.3,panel a) matches observed on a monthly basis. Simulated values are slightly higher, but maximum values occur during the wet season. Model H exceeds observed during the wet season (Figure 3.3, panel a), and maximum model H takes place during the wet season, as opposed to the dry season in the observations. However, simulated H is less than LE, and amplitude of the annual cycle is small.

Simulated carbon flux closely matches the mean annual cycle observed (Figure 3.4, panel a). Amplitude is small, with relative uptake in January and in July-August. Simulated GPP and total respiration (Figure3.4, panel a) are large and do not show obvious seasonality. There is a suggestion of increased GPP during the dry season, but total respiration follows a similar path. Carbon flux lacks an obvious annual cycle in both model and observations, suggesting that relative direction of carbon flux (uptake or efflux) at K34 is a function of high-frequency variability in meteorological forcing (radiation, precipitation), on synoptic- to monthly timescales. This is supported by Figure 3.8, which shows K34 daily-average values of LE, H, carbon flux, GPP/total respiration, and precipitation for February 2002. Maximum LE, in both model and observations, show maximum values in the relatively dry periods between days 8-15 and 26-28. Modeled H follows observed generally,

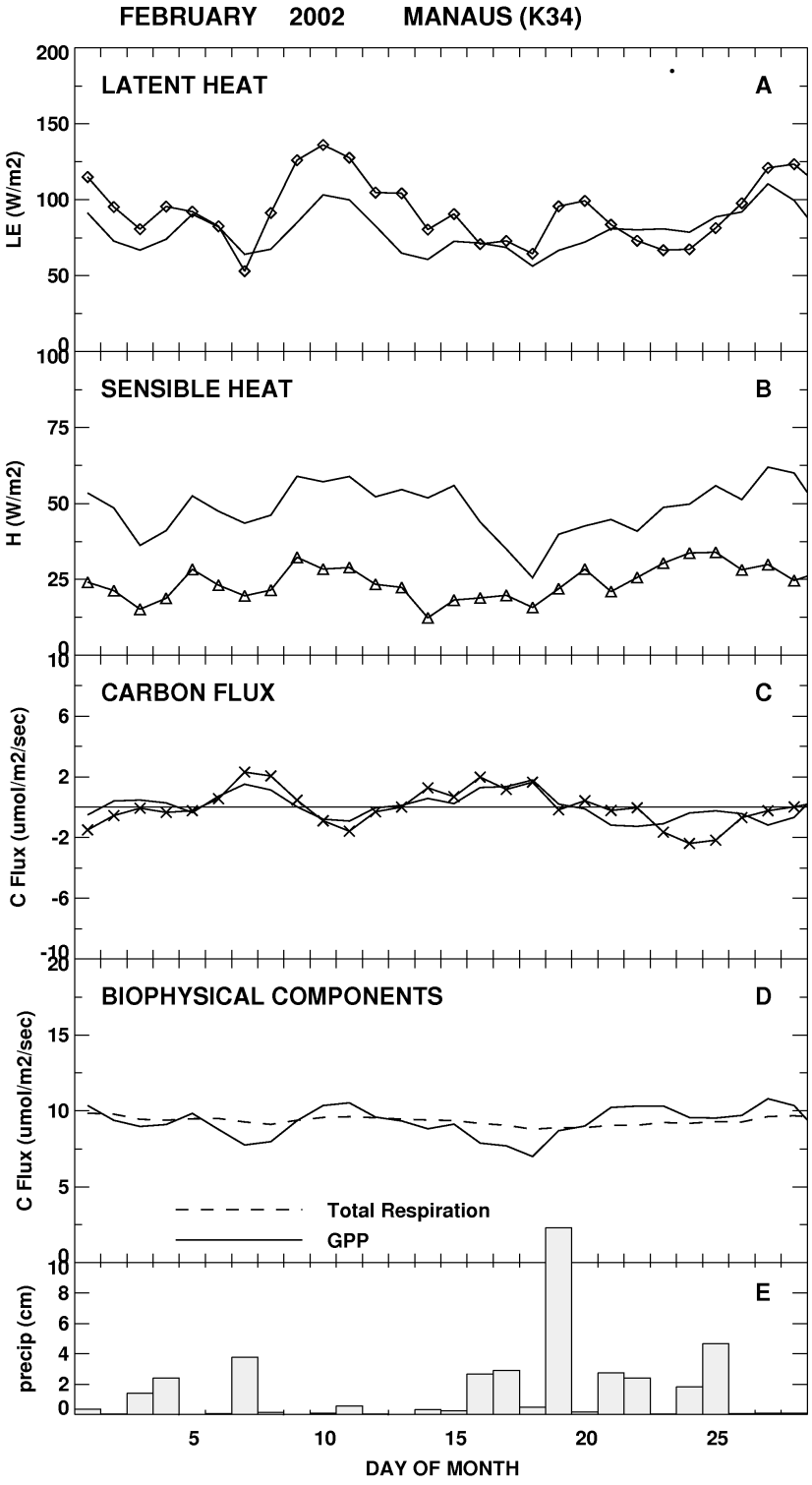

Figure 3.8: Daily mean (modeled and observed) Latent, Sensible and Carbon flux for the month of February 2002 at K34 (Panels A-C) Observations are shown as lines with symbols, simulated value as solid lines. Modeled partition of Carbon flux is shown in Panel D, daily precipitation in Panel E.

with a positive bias of between 10 and 25 W m^2 on a daily basis. This sensible heat bias is seen in the monthly average, shown in Figure 3.3, (panel a). Modeled carbon flux matches observed quite well on a daily basis, keeping in mind we are showing observed anomaly to emphasize response to changes in forcing rather than the absolute value of uptake or efflux. In the simulations, daily respiration is almost invariant during the month; relative uptake/efflux is determined by high-frequency variability in GPP, as vegetation responds to rapid changes in insolation. Since February is a very damp month, we expect soils to be near saturation; the large, almost invariant respiration supports this. GPP responds to high-frequency variability in forcing. Therefore, we might expect that the increased GPP during days 8-12 and following day 20 is responding to higher levels of light. Day 8 has very little precipitation, yet light levels are still low (only 3-4 hours with insolation greater than 300 W m^{-2}; not shown), resulting in low GPP.

Monthly-mean diurnal composites of latent and sensible heat are shown in Figures 3.5 and 3.6: K34 is shown in panels A (wet season month) and E (dry season month) in each Figure. Observed LE (Figure 3.6)is has larger midday maximum during the dry season, and modeled values concur. As for sensible heat, observed maximum midday values are similar for both wet and dry season months. However, H maintains higher values slightly longer in the dry season, resulting in the larger monthly-averaged observed sensible heat seen in Figure 3.3, panel a). In the simulations, midday maximum H is larger during the dry season. However, positive H values are present for a slightly longer period of time in during the wet season, with the result that modeled monthly-average H is larger during the wet season (refer again to Figure 3.3, panel a).

Monthly-mean diurnal composites (observation and model) of carbon flux are shown in Figure 3.7 (K34 shown in panels A-wet month/E-dry month). Both observations and model show an efflux spike shortly after sunrise: This reflects the release of accumulated carbon from the canopy air space as the nocturnal stable layer is broken by buoyancy. It is interesting to note a unique feature of SiB3-the prognostic canopy air space-is crucial to simulation of this feature. However, it is also worthwhile to note that the timing of the simulated efflux spike does not match the timing of the observation. This may be due to nocturnal drainage of CO_2 through the complex terrain at the

K34 sites [*Araujo et al.*, 2002].

Reserva Jaru: JRU

Mean annual precipitation at JRU is large (2354 mm yr^{-1} for the years used in this study), but latitude (JRU is at 10° South), thin soil and pronounced dry season lead to differences in ecophysiological function when compared to K34. At JRU, wet season insolation is greater than K34 (Figure 3.2, panel d) due to slightly longer day length. Dry season day length at JRU is slightly shorter than at K34, and midday insolation less as well. The seasonal cycle of net radiation displays a bimodal nature (Figure 3.3, panel d), with maxima at the end of the wet and dry seasons. Modeled R_{net} captures the annual cycle, with a regular bias of 20-50 W m^{-2} on a monthly basis.

Mean annual cycles of observed LE and H (Figure 3.3, panel d) reveal limited seasonality. LE is almost constant annualy, with a slight increase in magnitude in September and October, the end of the dry/beginning of wet season. Amplitude of the annual H cycle is small, with small increases corresponding to the relative maxima in R_{net} at the end of the dry and wet seasons. Simulated LE is relatively constant and slightly larger than observed. However, the modeled LE decreases slightly at the end of the dry season, where observed LE increases. Simulated H shows seasonal maxima consistent with observed, but amplitude of the annual cycle is overestimated in addition to a positive bias.

The observed annual cycle of carbon flux anomaly is similar to K34, showing little variability throughout the year (Figure 3.4, panel d). There are relative tendencies towards efflux at the end of the dry and wet seasons, with relative minima (uptake) at the midpoint. Simulated carbon flux reproduces this general pattern, but overestimates the amplitude. Model GPP has a significant annual amplitude, reflecting the inability of the shallow soil to store sufficient moisture to maintain ecophysiological function completely through annual drought. Interestingly, simulated LE does not respond as strongly as photosynthesis. As at other forest sites, model LE initially increases during the dry season (Figure 3.3, panel d), responding to increased moisture gradient across the canopy top as well as increased transpiration due to greater light (refer to Equation 3.1). At JRU, at the

very end of the dry season a slight decrease in LE is seen in the simulations. The large amplitude in simulated carbon flux (Figure 3.4, panel d) is due to phase incoherence between photosynthetic and respiratory response. Following the method outlined in *Baker et al.* [2008], respiration is tightly linked to moisture levels in near-surface soil; litter respiration is responsive to surface soil moisture levels, and relative root mass is greater near the surface as well. As surface moisture is depleted, total respiration decreases. There is no concurrent decrease in GPP, as roots are able to access water at deeper levels in the soil. It is only after several dry months, when total column soil moisture has been depleted, that GPP decreases.

Monthly-mean diurnal composites of modeled LE (Figure 3.6, panels D and H) show similar magnitude to observed, with the temporal offset mentioned earlier. Midday maximum LE is slightly larger in August (when compared to March) for both model and observations. Modeled H (Figure 3.5, panels D and H) is significantly larger in magnitude, when compared to observations, during both dry and wet months. This is likely attributable to the bias in R_{net} discussed previously.

Diurnal cycles of carbon flux, simulated and observed, are shown in Figure 3.7, panels D and H. Magnitude of carbon uptake is lesser during the dry season month (August) for both simulations and observation. However, there is an early-afternoon decrease in simulated carbon flux that is not seen in the observations. This may be partially due to temperature stress imposed on model vegetation by excessive sensible heat flux.

The hysteresis between morning and afternoon ecophysiological function, as reflected by diurnal cycles of latent heat and carbon flux, has been attributed to a circadian response in vegetation [*Keller et al.*, 2004]. The model does not parameterize a purely circadian response, but imposes stress on potential photosynthesis by temperature, humidity, and soil moisture factors as described in *Sellers et al.* [1992]. Simulated soil moisture stress operates on timescales of moistening and drying around precipitation events, but temperature and humidity stress operate in regular diurnal cycles. We can explore the diurnal nature of the vegetation response (and compare simulated to natural processes) by plotting monthly-mean diurnal cycles of carbon flux against monthly-mean diurnal cycles of latent heat (Figure 3.9). Hours 9, 10 and 12 are plotted as an 'x' on the observed

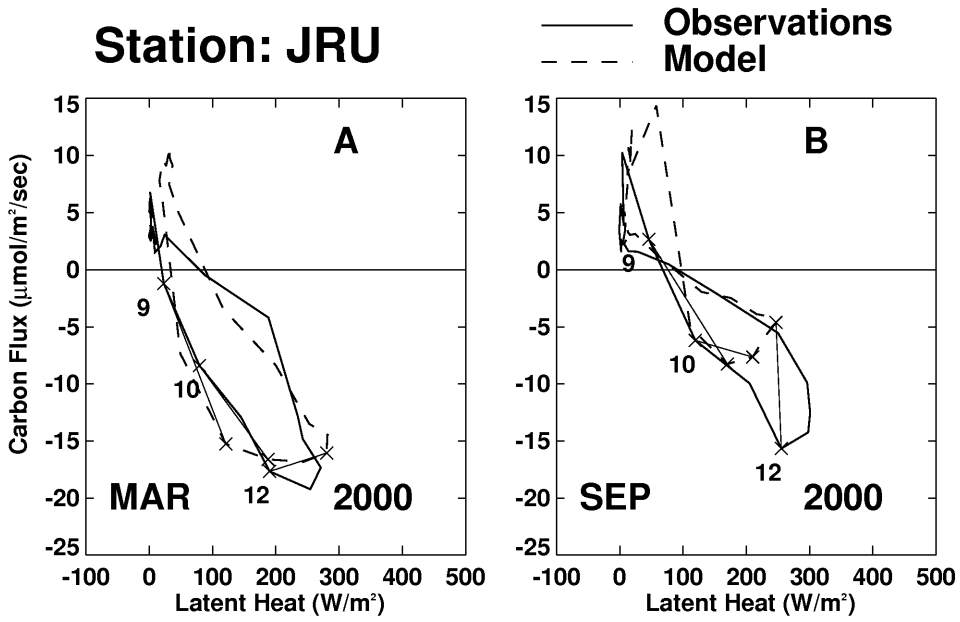

Figure 3.9: Monthly-mean diurnal composite of Latent Heat (X-axis) plotted against Carbon flux (Y-axis) for JRU, March and September 2000. Symbols (x) and thin lines connect equivalent times for model and observations.

cycle, so we can see that the observed LE/Carbon flux cycle in the wet season (panel a) moves in a 'counterclockwise' direction; LE increases following sunrise concurrently with carbon uptake. The same hours are signified with an 'x' on the simulated cycle, and thin lines connecting indicate temporal agreement between model and observations. In the afternoon, the process is reversed (concurrent decrease in LE and carbon uptake), but shifted slightly towards larger latent heat. This is due to a buildup in water vapor pressure in the CAS during the day. Increased water vapor pressure, along with higher temperatures can act to increase the gradient term or decrease the resistance term in Equation 3.1, resulting in larger afternoon LE. There is not a concurrent increase in the carbon uptake: Increased daytime respiration and mixing of high-CO_2 air into the CAS from the atmosphere combine, with the result that CAS CO_2 levels reach a minimum value shortly after daybreak and remain at that value during the day. During the dry season (Figure 3.9), both observed and simulated carbon flux/LE patterns resemble a 'figure-8'. in the morning, carbon uptake is strong while latent flux increase is minimal, due to much lower water vapor pressure (in both the CAS and atmosphere) when compared to the wet season. In the afternoon, latent heat flux decreases more rapidly than carbon uptake, resulting in a 'figure-8' diel pattern. The exact timing is not the same between simulation and observation, and modeled maximum carbon uptake in September is underestimated, but the basic pattern is reproduced.

Tapajos River National Forest: K67, K83

The ecophysiological response at the Santarem sites (K67, K83) are consistent with each. At these sites, an annual cycle has been observed[*Saleska et al.* [2003], wherein there is regular carbon efflux during the wet season and uptake during seasonal drought. Our simulations, corroborated by observed carbon flux (Figure 3.4, panels b) and c), shows annual amplitude of 80-100 g C m^{-2} in both the GPP and respiration cycles, but with a shift in phase that determines the annual carbon flux signal. Maximum respiratory flux at the Tapajos River sites occurs late in the wet season or soon after rains have diminished; soils are at maximum moisture levels, and increased temperature warms the soil slightly. Without replenishing rains, surface litter and near-surface soil

dries out, and respiration decreases. Annual minimum respiration occurs just prior to the onset of the rainy season. Photosynthetic processes show a similar annual cycle in amplitude, but phase-lagged to respiration by 2-3 months. Respiration is quickly responsive to cessation of rainfall, while evolved mechanisms allow forest ecophysiological function to be maintained for longer periods. This difference in response time, coupled with the annual rainfall amount, soil depth, and length of dry season determine the annual cycle in carbon flux. Monthly-mean diurnal composites of carbon flux are shown in Figure 3.7, panels D and F/C and G. The magnitude of uptake is similar in both wet (March) and dry (August) season months, although observed nocturnal efflux is larger during the wet season. Simulated carbon uptake is slightly exaggerated during the dry season. The simulated post-dawn release of stored CO_2 exceeds the observed. This may be due to the fact that there is no mechanism for air drainage in the model, so CO_2 respired during the night is accumulated in the CAS.

Latent heat flux, both observed and simulated (Figure 3.3, panels b and c), increases at the outset of the dry season and decreases slightly as seasonal drought progresses. Monthly-mean diurnal composites of LE (Figure 3.6, panels B and F/C and G) show an increase in midday maximum in both observations and simulations during the dry season. Observed sensible heat diurnal cycles show a marked increase from wet season to dry at K67 (Figure 3.5, panels B and F), but not at K83 (Figure 3.5, panels C and G). Interestingly, simulated H exceeds observed at K67 significantly in the wet season, and only slightly in the dry season, although simulated R_{net} is similar to observed. At K83, simulated wet season H is close to observed, and overestimated during the dry season, but observed R_{net} exceeds observed.

Forest: Summary

At all forest sites, our simulation results are generally consistent with those of *Saleska et al.* [2003] from the Tapajos River National Forest (see also, *Baker et al.*, [2008]); we show a general pattern of carbon efflux during wet periods, uptake during dry. This cycle is dependent upon intensity and duration of the dry season. At the Tapajos River sites (K67, K83) there is a

consistent phase shift between photosynthetic and respiratory processes. Surface soil dries during the dry season, and there is an attendant drop in respiration. GPP shows an initial increase with increased radiation as rains decrease, and decreases only when soil moisture is depleted later in the dry season. The net result is the offset between GPP and respiration, resulting in dry season uptake of carbon. At K34 the dry season is short with frequent rains; at this site, gross fluxes are always large, and net flux is dependent upon high-frequency variability. JRU is unique, due to the short yet intense dry season and the thin soil. Observed carbon flux anomaly at JRU does not have the magnitude of the regular annual signature seen at K67 or K83, but more closely resembles K34. Model simulations capture the general tendencies of this cycle, but with an exaggerated amplitude.

Latent heat is large at all forest sites. At K34, K67 and K83 there is an increase in LE during the dry season, while at JRU LE is maintained during seasonal drought, and shows a slight increase with resumption of seasonal rains. Monthly-mean sensible heat has magnitude generally on the order of one-half of LE at all forest sites. Simulated H exceeds observed at all tower sites, with the largest overestimation at JRU.

3.3.2 Ecotone: Javaes River, JAV

The southern and eastern edge of the tropical Amazonian forest is defined by an ecotonal region known as the 'transition forest', or cerradão. The cerradão occupies the transition from forest to savanna (cerrado), and can consist of closed canopy forest, savanna, open arboreal woodland, or even distinct vegetation types exhibiting intermediate characteristics [*Eiten*, 1972; *Ackerly*, 1989; *Vourlitis et al.*, 2001; *Borma et al.*, 2009]. Therefore, it is difficult to characterize a typical cerradão, and we can expect a high degree of heterogeneity in regions classified as such. Observations taken in a semi-deciduous forest near Sinop, in Mato Grosso state, Brazil [*Vourlitis et al.*, 2001; *Vourlitis et al.*, 2002; *Vourlitis et al.*, 2004; *Vourlitis et al.*, 2005; *Vourlitis et al.*, 2008] indicate a ecosystem where evapotranspiration is tightly coupled to precipitation with carbon neutrality during the dry season, uptake during seasonal rains, and efflux during transition seasons between rain and drought.*Borma et al.* [2009] describe a seasonally flooded transition forest along the Javaes River

(JAV, simulated here) near Cantão State Park in Tocantins state, Brazil, that also shows a tight coupling between rainfall and evapotranspiration. At JAV, we can see an annual carbon flux cycle somewhat similar to that described by *Vourlitis et al.* [2001] (Figure 3.4, panel e). The greatest relative carbon uptake is during the wet season, with relative efflux at the end of the wet season/beginning of dry, as well as at the end of the dry season. There is a brief period of 'neutrality' during the dry season as well. The seasonal flooding plays a large role in the overall ET, as does the rapid drainage of sandy soil following inundation [*Borma et al.*, 2009]. It is to be expected that these features will influence carbon dynamics as well.

At JAV, the dry season is longer than at the forest sites, with precipitation events during annual drought more infrequent. Seasonality in radiation is defined by cloudiness (JAV is at latitude 10° S), with maximum insolation in dry season (Jul-Sep) and minimum at the end of the wet season in April (Figure 3.2, panel e). Overall latent heat flux shows an annual cycle, with maximum at or near the end of the dry season and minimum just prior to the start of seasonal rains in September (Figure 3.3, panel e). Sensible heat flux is less than latent in all months, and the amplitude of the annual cycle is less pronounced; annual maximum/minimum in sensible heat are negatively correlated with maximum/minimum in latent heat.

Simulating the transition forest in a computer model presents unique problems. Heterogeneous assemblages of varied landcover types challenges traditional classification methods, and uncommon characteristics such as seasonal flooding and change of soil character with depth require model tuning if close adherence to local conditions is to be obtained. Ultimately, we decided against tuning the model at this site; detailed site-level observations are not available globally, and ultimately we hope to expand knowledge gained during local simulations to regional- or global scale simulations. We can evaluate differences between model simulations and local observations, and comment on these differences and potential reasons for them. This is distinct from JRU, where a simple modification, using know values (soil depth) could be easily incorporated into SiB3 simulations.

Mean annual cycles of precipitation and simulated/observed latent and sensible heat are

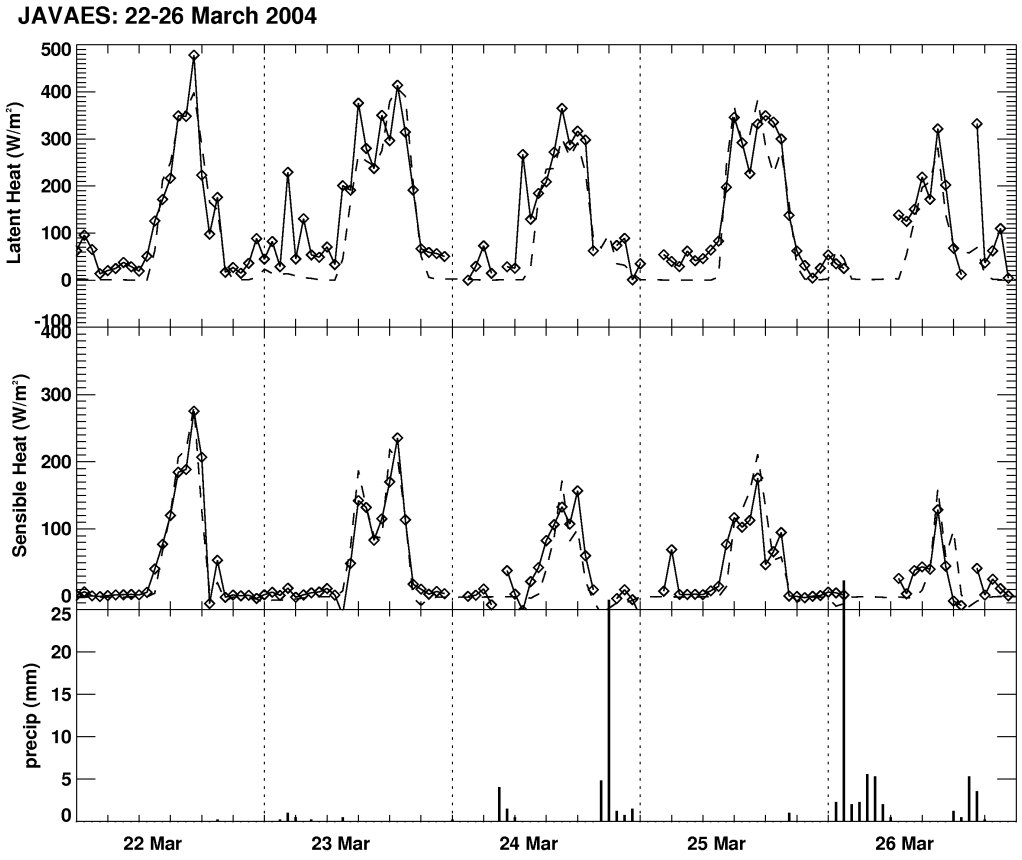

Figure 3.10: Hourly latent and sensible heat, and precipitation at site JAV for 22-26 March 2004. Observed data plotted as solid lines with symbols, model results dashed lines.

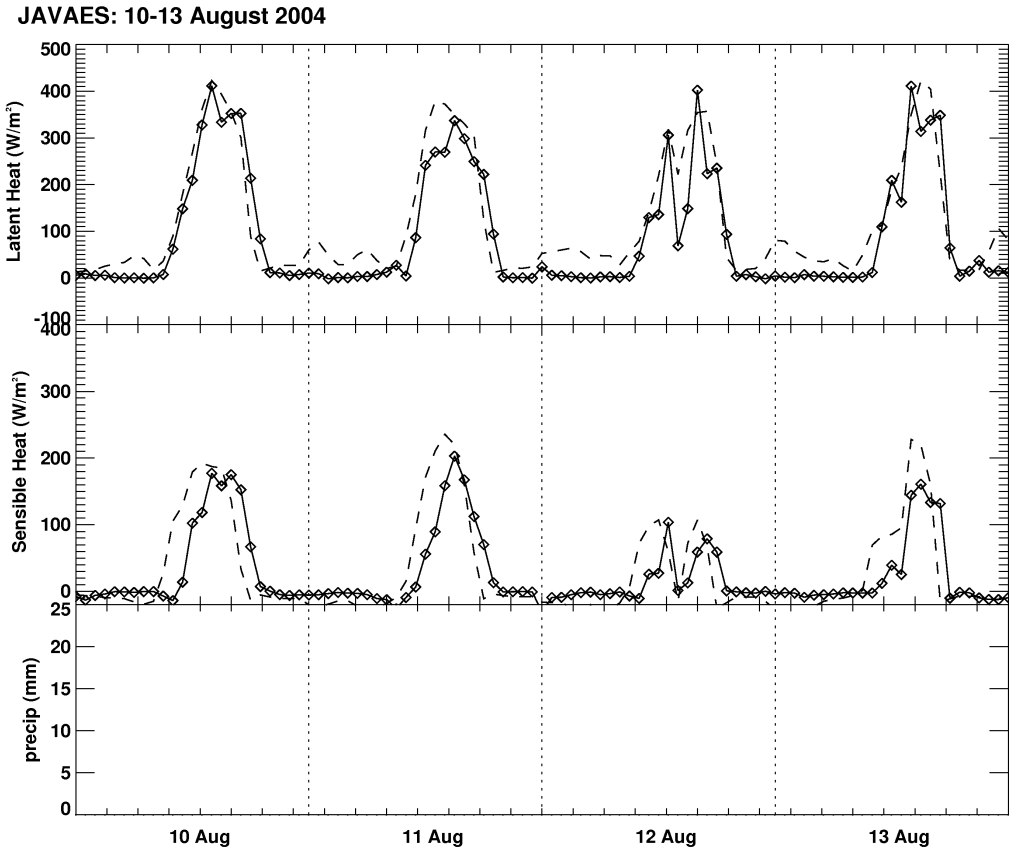

Figure 3.11: Hourly latent and sensible heat, and precipitation at site JAV for 10-13 August 2004. Observed data plotted as solid lines with symbols, model results dashed lines.

shown in Figure 3.3 (JAV; panel e). In general, the annual cycle of simulated sensible heat matches the observed, and both follow the annual cycle of net radiation. Simulated latent heat flux is lower than observed during the wet season/inundation maximum, and greater than observed during the middle of the dry season. We can attribute the wet season LE underestimation to the lack of inundation in the model; *Borma et al.* [2009] attribute a significant fraction of overall ET during flooding to evaporation from water surface. We can see this behavior in Figure 3.10, which shows hourly observed and simulated latent and sensible heat fluxes and precipitation for 5 days in March 2004, a period of inundation. Latent heat flux during daylight hours is remarkably similar between model and observations, but there is a consistent nighttime evaporative flux in the observations, consistent with evaporation from a plane water surface (not represented in the model). Sensible heat fluxes are very similar between model and observations during this entire period. Following dry season onset, observed ET reaches its minimum value in 5 months, while modeled minimum is reached in 6 months (Figure 3.3, panel e). During the dry season (Figure 3.11) simulated midday LE peaks are again consistent observed, with a value near 400 W m^{-2}, but at night there is a simulated flux of 10-50 W m^{-2} that is not present in the observations. *Borma et al.* [2009] describe a soil at JAV that dries out quickly following inundation. In the simulations, the mean CAS water vapor pressure is higher during March 2004 (wet season) than in August (dry season), but nighttime LE is higher in August due to a larger ventilation mass flux associated with greater nocturnal wind speeds and a slightly larger gradient in water vapor pressure between the CAS and atmosphere.

The annual cycle of simulated H is close to the observed, but there are differences between simulated and observed LE and carbon flux (Figures 3.3 and 3.4, panel e) at JAV. For additional insight into stomatal constraint on evaporative flux, we can plot LE vs. carbon flux at JAV, as was done at JRU (Figure 3.12), in this case for June and October 2006. In this case, the observed diurnal cycle moves in a counterclockwise direction for both months, as opposed to the clockwise cycle seen in the observations at JRU. maximum carbon efflux occurs at either 7-8 local time, and in both wet (June) and dry (October) months there are several hours in the morning where LE increases while carbon flux is either steady or increasing in efflux rate. The slope of the observed

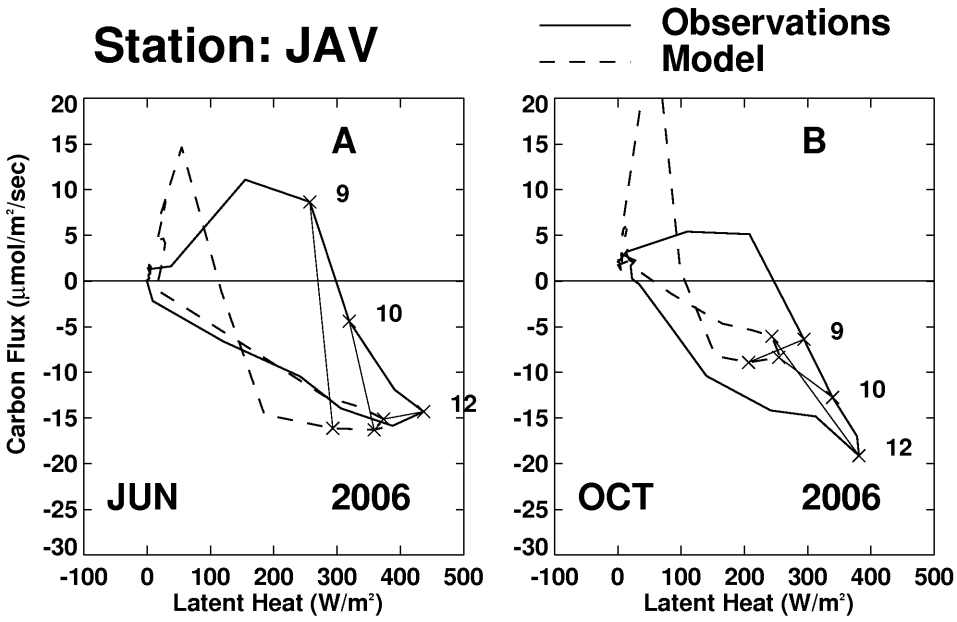

Figure 3.12: Monthly-mean diurnal composite of Latent Heat (X-axis) plotted against Carbon flux (Y-axis) for JAV, June and October 2006. Symbols (x) and thin lines connect equivalent times for model and observations.

LE/carbon flux line (both months) is steeper in the morning hours; this implies a steady increase in LE, but that once carbon flux switches sign from efflux to uptake, carbon is rapidly assimilated by the canopy. During the afternoon hours, assimilation and evaporation decrease at similar rates. Simulated behavior resembles observed during the afternoon hours, but diverges in the morning. There is a consistent overestimation of the magnitude of the initial flush of CO_2 from the canopy following sunrise, and the simulated flush precedes observed by 1-2 hours. Following CO_2 flush, carbon uptake flux increases rapidly with little or no attendant increase in LE. By the mid- to late-morning hours, carbon uptake flux plateaus, while LE increases; during the afternoon the decrease in carbon uptake and LE has similar magnitude, producing the 'figure-8' shape. The observed behavior in June is intuitive: In June the site is either flooded, or flooding has recently abated, in all years simulated. The observed morning increase in LE without carbon uptake is consistent with evaporation of water surfaces. In October, the observed LE increase prior to carbon uptake is less. This is to be expected if flooding is not present. Simulations of both months, however, show excessive carbon uptake during the morning hours. This may be due to circadian processes in natural vegetation [*Keller et al.*, 2004]. It may also be coupled to simulated radiative transfer and heating of the CAS in the model. This second hypothesis is supported by the fact that the simulated flush of CO_2 out of the canopy occurs several hours earlier than observed, with greater magnitude. This behavior is consistent with premature heating, perhaps associated with errors in modeled radiative transfer at low sun angles.

Simulated canopy ecophysiology at JAV (Figure 3.4, panel e) behaves in a manner remarkably similar to that described at another cerrradão site, near Sinop in Mato Grosso state, Brazil [*Vourlitis et al.*, 2001]. Our simulations show relative carbon uptake during the wet season and early dry season, with nearly neutral conditions later in the dry season (Aug-Sep). The largest efflux values were noted during the transition from dry to wet (Oct-Nov). *Vourlitis et al.* [2001] ascribe this to a combination of large surface litter and decreased Leaf Area Index (LAI) following maximum litterfall rates in the late dry season, along with a increase in surface moisture (and attendant heterotrophic respiration) as rains resume. In the model, we do not explicitly resolve carbon

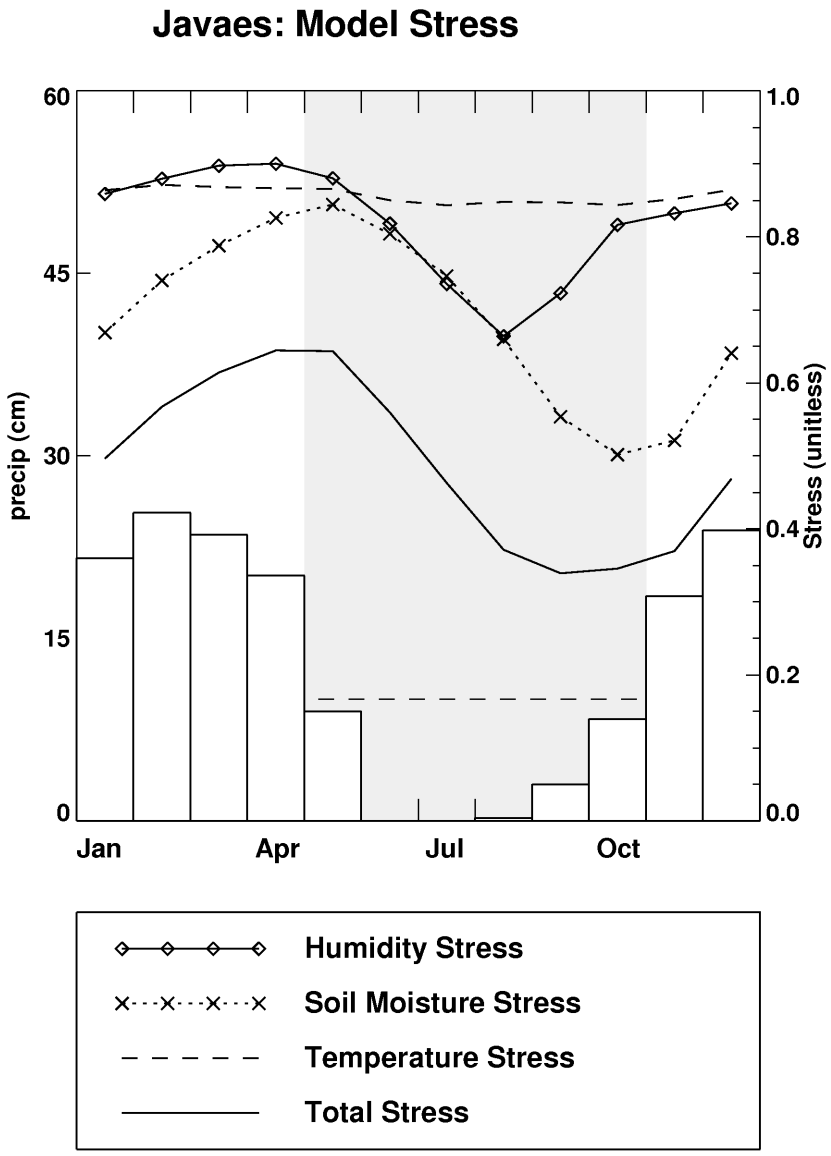

Figure 3.13: Monthly averaged stress values at the Javaes (JAV) site. Annual precipitation cycle is shown for reference.

pools; simulated respiration response at the transition from dry to wet season is directly controlled by soil temperature and moisture conditions, as described in *Denning et al.* [1996]. As rains replenish soil moisture, the relative carbon efflux diminishes, eventually changing sign (to uptake) as photosynthetic processes achieve greater magnitude than respiration.

Figure 3.13 shows simulated annual mean stress on GPP. Model stress factors act as multi-

pliers on photosynthetic processes, with a value of 1 implying no stress and a value of 0 associated with stomatal closure. The 3 stress factors are multiplied together to obtain a total stress value in the model. With the cessation of annual rains, dry air is advected into the forest from the cerrado, and humidity stress imposes a constraint on photosynthesis, although soil moisture is still sufficient to maintain GPP. By September, it has begun to rain again, and humidity stress on GPP is eased. However, transpiration load exceeds the rainfall recharge to the soil, and soil water stress is imposed upon photosynthesis. It can be seen that the exact relationship that controls GPP at cerradão sites (humidity stress, soil moisture stress, and precipitation dynamics) are highly heterogeneous. The exact annual cycles of GPP and surface energy/hydrologic budget will be dependent on local vegetation and precipitation. However, we believe the presence of forest indicates a combination of annual precipitation/dry season length and storage capability that serves to decouple GPP from precipitation to some extent. In all but the driest transition forests we would expect to see forest function maintained in the dry season once surface soil has drained, imposing a constraint on respiration. In these cases, the phase shift would be created, and dry season uptake of carbon would result. The amount and duration of this uptake will be highly variable.

3.3.3 Cerrado: Pé de Gigante, PEG

Carbon, energy, and moisture flux over a woodland savanna (cerrado Sensu stricto) site has been described by *da Rocha et al.* [2002], and *da Rocha et al.* [2009]. The site is located in southeast Brazil, in São Paulo state, and has the largest temperature and radiation seasonality of any sites in this study (Figure 3.2, panel f). Fluxes were recorded in Vassununga state park, in a region that contains closed canopy forest, and open shrubland in addition to woodland savanna.

Heterogeneity is a defining characteristic of savanna, and as such poses challenges for simulations. In SiB3, the use of satellite data to specify phenology requires a single-layer canopy [*Sellers et al.* 1996a, 1996b], so explicit representation of heterogeneous assemblages of grasses, shrubs and trees is not possible. The site is simulated as C4 grassland in SiB3. However, the spectral characteristics of NDVI captures the inclusion of green trees during periods when grasses are dormant.

The Pé de Gigante site is water-limited [*da Rocha et al.*, 2002; *da Rocha et al.* 2009], meaning that ecophysiological function is tightly coupled to precipitation. In contrast to all the other sites, where incoming radiation is regulated by cloud amount, seasonality at PEG is defined by latitude. The dry season occurs during Austral winter, so that radiation levels are actually higher during the rainy season, and temperatures are warmer. Latent heat is larger than sensible during the seasonal rains, but the Bowen ratio drops below one for a short period at the end of the dry season in both simulations and observations (Figure 3.2, panel f).

Simulations and observations [*da Rocha et al.*, 2002] suggest that PEG is a carbon sink until early in the dry season, at which time respiration exceeds GPP. Simulations show that GPP drops rapidly following cessation of seasonal rains, while Respiration subsides at a lower rate. This is in contrast to the ecophysiological mechanisms postulated for forest sites, where GPP is maintained during the dry season while respiration decreases. The reasons for this are several, including 1) reduced annual precipitation and longer, more severe (meaning very few precipitation events) dry season result in smaller water storage in the soil, 2) shrubs and grasses have shallower rooting systems than tall trees, and therefore lack the ability to access water stored deep in the soil. For these reasons, GPP and respiration at PEG are in phase, and coupled tightly to water availability in the near-surface soil.

3.4 Discussion

Climatological control of ecophysiology is spatially heterogeneous in Brazil. *da Rocha et al.* [2009] showed that evapotranspiration in the wettest areas (central Amazon) is tightly linked to radiation levels (light-limited), while water availability regulates ET in the drier regions to the south and east. Our simulations reproduce this behavior. Forest sites K34, JRU, K67 and K83 maintain a consistently small Bowen ratio (sensible smaller than latent heat); maximum annual values for both H and LE occur during the dry season, when net radiation is greatest, and annual amplitude of LE/H cycles is relatively small. The dry season increase in both LE and H suggests an ecosystem response to increased radiation levels, without ecosystem stress, since evaporation is maintained.

At JAV, annual precipitation is less, and the dry season is more clearly defined. Here, seasonality is more pronounced, and LE actually decreases midway through the dry season in conjunction with increasing sensible heat. This implies that stress is being imposed upon the vegetation, as the Bowen ratio is increasing. Our simulations at JAV are consistent with reported behavior at another cerradão site near Sinop in Mato Grosso state, but inconsistent with some elements of the observed carbon flux; we believe that inundation at JAV, combined with rapid drainage of the soil following cessation of flooding are the reasons. At the savanna site (PEG), evaporation is tightly coupled to precipitation. Latent heat flux decreases immediately with cessation of seasonal rains, and Bowen ratio exceeds one during the dry season. Simulated annual cycle of latent and sensible heat at PEG is very similar to observed.

Vegetation couples carbon dynamics to the Bowen ratio by stomatal regulation of transpiration. Overall carbon flux is defined by the interaction of photosynthetic and respiratory processes. We've demonstrated that SiB3 can simulate observed annual cycles of carbon flux, and we use model diagnostics to partition GPP and respiration as a means to construct a conceptual model of photosynthesis and respiration across vegetation and moisture gradients. We do not address overall source/sink of CO_2 on an annual or interannual basis for these individual sites. Local to regional-scale Net Ecosystem Exchange of CO_2 over long timescales is dependent upon storage pools, which are themselves the residual from large gross photosynthetic and respiratory fluxes. These pools cannot be determined from model simulations performed on 3 or 4 years of observational data.

At K34, gross uptake is large during all months, and there is little sign of an annual GPP cycle, with the exception of a slight increase in the dry season. Respiration is consistently large at K34, as even the 'dry season' there has appreciable precipitation. At K34, variability in carbon flux is high-frequency, as GPP and respiration will respond to variations in precipitation and cloudiness on scales from the synoptic to monthly. At the other wettest site, JRU, annual precipitation is large, but the dry season is well-defined; June, July and August are very dry. Observed annual carbon flux anomalies are similar to K34; simulated annual carbon flux shows similar shape but exaggerated amplitude when compared to observations. During seasonal drought simulated surface

soil desiccates, with an attendant drop in respiration. GPP is maintained, and carbon flux shows uptake by the terrestrial biosphere.

At the Tapajos sites (K67, K83), GPP increases in response to higher light levels at dry season outset. GPP decreases slightly by the end of the dry season, but respiration decreases rapidly due to drying of litter and surface soils. The combination of increased GPP and reduced respiration combine to produce relative carbon uptake during the dry season in both simulations and observations.

At JAV, observed carbon flux is tightly coupled to periodic inundation and rapid drainage following flooding. Simulated carbon flux produces uptake during the wet season and early dry season, with largest carbon efflux at the end of the dry season, 3-4 months following observed efflux maximum. the cerrado site, PEG, is water- rather than light-limited. Observed and simulated carbon flux is positively correlated to precipitation, with relative uptake during seasonal rains and efflux during drought. GPP and respiration both have large amplitude in the annual cycle, and both are correlated with rainfall.

A conceptual model of ecophysiological behavior emerges: In the wettest regions of the forest, ecosystems are light- rather than water-imited. Gross carbon fluxes are continuously large, and small magnitude uptake or efflux is determined by high-frequency variability in forcing. A dry week, for example, may result in increased GPP due to higher light levels, while slight drying of near-surface soils may result in a small decrease in respiration. Moving downgradient in precipitation, annual total is less, and dry season obtains definition. At these locations seasonality in carbon flux may be imposed by the mechanistic concepts outlined in *Baker et al.* [2008]: A combination of GPP elevation in response to enhanced light levels and respiration decrease as surface soil desiccates results in carbon uptake during the dry season. At these sites, seasonality in carbon flux is distinct while seasonality in energy and moisture flux are minimal. Photosynthetic function is not compromised during the seasonal drought, and transpiration maintains the Bowen Ratio at small values. At drier sites, vegetation has stress imposed upon it by the combination of even less annual precipitation and a longer dry season. The imposition of water limitation in the drier regions has

the effect of forcing the precipitation and carbon cycles into phase with each other. Water limitation also has the effect of imposing larger annual cycles on the latent and sensible heat flux cycles. As vegetation experiences water stress, evapotranspiration rates cannot be maintained, and the Bowen ratio increases.

3.5 Conclusions

Tropical forests have an evolved resistance to annual drought (dry season), as well as to variability in the precipitation seasonality, and carbon flux is inextricably coupled to weather and climate. Evapotranspiration is critical to precipitation recycling not only locally, but across regional and continental scales [*van der Ent et al.*, 2010]. It has been shown that simulations of atmospheric processes are responsive to improved physical realism at the land-atmosphere interface [*Harper et al.*, 2010]. The results of climate simulations that predict large-scale conversion of Amazonian forest to grassland or savanna [*Cox et al.*, 2000; *Betts et al.*, 2004; *Cowling et al.*, 2004; *Cox et al.*, 2004; *Huntingford et al.*, 2004; *Huntingford et al.*, 2008] will be more robust if they can show consistency with ecophysiological behavior under current conditions. Errorbars on predictions of future climate will be greatly reduced if biological response under present climate is resolved.

Our simulations have demonstrated an ability to rectify unrealistic ecophysiological stress in forest ecosystems [*Saleska et al.*, 2003; *Baker et al.*, 2008] while maintaining response across vegetation and moisture gradients. But removing unrealistic stress on vegetation is only half of the battle; forests have evolved mechanisms to protect against annual drought and, it is expected, interannual drought as well. But if sustained drought in Amazonia occurs during the 21st century due to perpetual El Ñino conditions [*Cattanio et al.*, 2002; *Li et al.*, 2006] or a combination of climatological and sociological pressure on the ecosystem [*Nepstad et al.*, 2008], it is realistic to expect that forest collapse, or a 'tipping point' may be reached. Previously, models were unable to withstand even seasonal drought, in the form of a dry season. Now that we've adjusted our model physics to achieve greater resiliency to seasonal drought, we need to ensure that we have not created models that are impervious to drought.

Recent experiments in the Tapajos River National Forest have evaluated forest response to artificially reduced rainfall, as a measure of forest resiliency to extended drought. A significant fraction of wet season rainfall was captured and not allowed to infiltrate the soil, and forest response was monitored over several years [*Markewitz et al.*, 2010; *Nepstad et al.*, 2007; *Nepstad et al.*, 2002]. Their results indicate that forest function was maintained for 2 years when up to 40% of wet season rainfall was removed, followed by partial stress stratified by vegetation height/diameter. These results provide insight into forest drought tolerance levels, and a logical next step will be to reproduce the exclusion experiments in SiB3.

Chapter 4

REGIONAL BEHAVIOR: MEAN VALUES, ANNUAL CYCLES, AND RESPONSE TO INTERANNUAL VARIABILITY

4.1 Introduction

Human activity, in the form of fossil fuel burning, cement production, and land cover/land-use change, has increased the concentration of CO_2 in the atmosphere [*Keeling*, 1995, *IPCC* 2007]. The radiational changes imposed by the increase in this and other greenhouse gases are predicted to change the earths climate [*IPCC* 2007; *Solomon et al.*, 2009], although the exact nature of global response is uncertain[*IPCC* 2007; *Friedlingstein et al.*, 2006], and future conditions depend upon sociopolitical as well as environmental factors.

The rate of CO_2 increase in the atmosphere has been mediated by an increase in marine and terrestrial consumption, the so-called missing sink, whereby only about half of the anthropogenic CO_2 remains in the atmosphere in a given year [*Oeschger* 1975; *Keeling*, 1995; *IPCC* 2007]. Maritime CO_2 flux is relatively constant temporally [*Friedlingstein et al.*, 2006] but terrestrial CO_2 flux is highly variable in space and time. Furthermore, it is not known how either the maritime or terrestrial sink mechanisms will respond under changing climate, although it is expected that the sink mechanisms will diminish [*Friedlingstein et al.*, 2006]. The uncertainty in the land behavior under future climate is such that it is not currently resolved whether the the land will be a net source or sink of carbon by the year 2100; it is generally accepted that the oceans will continue to provide a net sink of CO_2 [*Friedlingstein et al.*, 2006].

Tropical forests are critical to terrestrial response to rising CO_2. Inversion studies have shown that tropical forests are generally a carbon source [*Gurney et al.*, 2002, *Stephens et al.*, 2007],

although uncertainty around the flux is large enough that the absolute magnitude, or even the sign of the flux, is not fully known. Furthermore, tropical forests exhibit temporal variability in flux magnitude as well as sign; these regions are a primary driver in the variability of the growth rate of global atmospheric CO_2 concentration [*Rayner and Law*, 1999; *Bosquet et al.*, 2000; *Rödenbeck et al.*, 2003; *Baker et al.*, 2006].

The Amazon basin and surrounding regions comprise the largest tropical forest on the planet. It has been estimated that up to 10% of terrestrial biomass resides in this forest [*Houghton et al.*, 2001], making tropical South America a major constituent in global determination of and response to climate change. It has been put forth that current climate is marginal for sustainability of Amazonian forests [*Cowling et al.*, 2004], and that small changes there in temperature and moisture regimes (increasing temperature, decreasing precipitation) will result in conversion of forest to grassland over large scales [*Cox et al.*, 2000; *Huntingford et al.*, 2004; *Cowling et al.*, 2004; *Huntingford et al.*, 2008]. This conversion will result in massive release of CO_2 currently stored in vegetation, providing a positive feedback for further radiational forcing. However, this response is not unanimous among climate predictions; of the 11 models that participated in the Intergovernmental Panel on Climate Change (IPCC) 4th Assessment Report (AR4), using the Special Report on Emission Scenarios (SRES) A1B scenario, five reported an increase in Amazon Basin precipitation, three reported a decrease, and three reported little or no change [*Li et al.*, 2006].

Additionally, uncertainty around predictions of future ecophysiological behavior resides in an historic inability to capture annual cycles of CO_2 flux [*Saleska et al.*, 2003] as well as latent and sensible heat [*Baker et al.*, 2008] in tropical forests. Adding another level of complexity to the issue is the question of what the mechanisms that determine ecophysiological function in the Amazon are. Some authors [*Saleska et al.*, 2007, *Huete et al.*, 2006] describe the region as light-limited, and claim that the forests green-up during anomalous drought, in opposition to the traditional concept of the region as experiencing biological stress during drought. This finding has been challenged [*Samanta et al.*, 2009; *Phillips et al.*, 2009], although the latter work shows a heterogeneous response of vegetation to the 2005 drought. At present, we dont consider the issue closed, a conclusion supported

by *Brando et al.* [2010].

It is known that there is a decoupling of biophysical function from rainfall, as the forests have evolved to survive a dry season that can last several months or more. What is not known is the exact spatiotemporal nature or the resiliency/durability of this decoupling. It seems intuitive also that the forests have evolved to withstand drought (beyond the seasonal cycle) over the timescales most frequently imposed upon them. These would be timescales of ENSO, or 2-7 years. Studies where precipitation is allowed to be intercepted by the canopy, but excluded from reaching the ground support this, as forests at Tapajos River National Forest showed little to no ill effects of partial exclusion of rainfall for several years [*Nepstead et al.*, 2008]. Exclusion studies further east, at Caixuana, showed more rapid stress and mortality, but total-season rainfall was excluded there, not just part of the wet season rainfall. In neither case was stress and mortality immediate, suggesting an additional tolerance, or buffer against stress, of from 1-3 years.

Overall source/sink of carbon is determined by the unique spatiotemporal variation in multiple component terms. Carbon uptake (GPP) is a function of vegetation type and ecophysiological status, while respiration depends on multiple carbon pools (labile, recalcitrant and armored) as well as temperature and moisture conditions in the soil. Fire is an important component as well [*Randerson et al.*, 2005; *van Der Werf et al.*, 2003], and can occur naturally or due to human activity. Quantification of long-term carbon status at any point on the globe requires reasonable understanding of the component terms, as well as an ability to simulate them across wide-ranging changes in ecophysiological parameter space.

The current study does not address all elements of carbon status in Amazonia/South America. We concentrate on ecophysiological function across large spatial and temporal gradients as a means to quantify both annual cycles of energy, moisture, and carbon exchange as well as large-scale responses to the dominant modes of climate variability. We do not address the absolute magnitude of net carbon flux on the continent, nor do we evaluate whether tropical South America is a long-term source of sink. Reduced uncertainty in ecophysiological behavior will translate to more realistic simulations of overall carbon flux, whether in long-term climate simulations, or as *a priori* fluxes

for inversions. Furthermore, realistic vegetation behavior in models used as a lower boundary for meteorological simulation is critical to an accurate simulation of Bowen ratio, which will impact circulation and by extension, weather and climate.

This paper represents the culmination of a series, aimed at providing a picture of regional ecophysiological behavior in Amazonia that is anchored to available observational data. The large-scale Biosphere-Atmosphere Experiment in Amazonia (LBA, *Keller et al.*, 2004) provided a wealth of observational data, across vegetation and moisture gradients in Brazil. These data shed light on unexpected ecophysiological behavior [i.e. *Saleska et al.*, 2003] and provide an opportunity for us to challenge our understanding of ecophysiological behavior as represented by numerical models. In the first paper of the series[*Baker et al.*, 2008] we demonstrated an ability to capture the seasonal cycle at a single site in the Tapajos River National Forest; in the second [*Baker et al.*, 2011] we extended the analysis, again limited to observation tower sites, across vegetation and moisture gradients. At this time, we believe the model has shown sufficient skill, when confronted directly with observational data, to merit a regional simulation. Section 2 summarizes the precipitation regime, as well as results from inversion and process-based model studies. In section 3 we will describe the model and summarize past results. Section 4 will describe regional patterns and behavior, the mechanisms that control spatiotemporal variability, and regional response to major modes of climate variability. In section 5 we will integrate the information from the previous sections into a coherent picture of regional behavior.

4.2 Background

4.2.1 Precipitation

Annual precipitation and seasonal variability in tropical South America is determined by the movement of the Intertropical Convergence Zone (ITCZ), towards the north during Boreal summer and southward in Austral summer. *Horel et al.* [1989] looked at variability in outgoing longwave radiation (OLR) and show that in central america and the Amazon basin south of the equator, precipitation variability is dominated by the seasonal cycle. From the equator to 5 north, variance

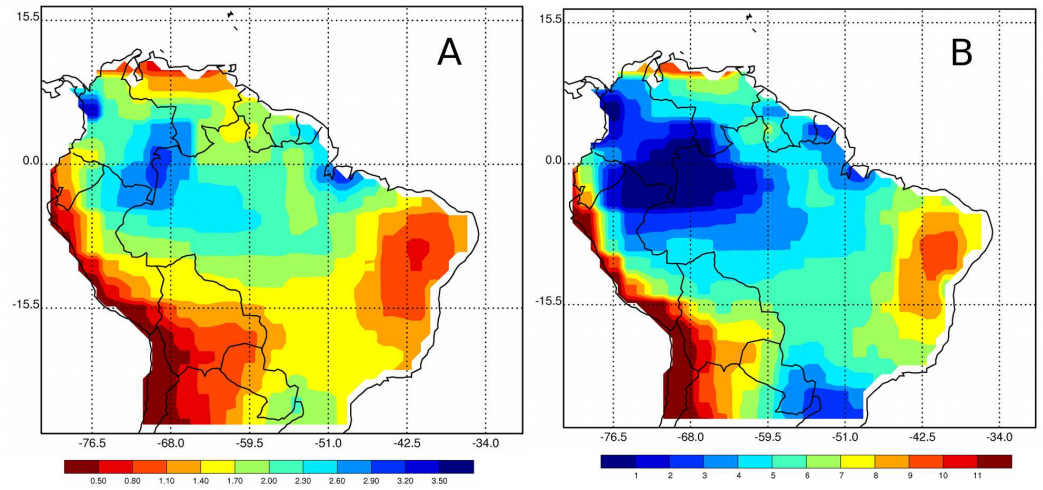

Figure 4.1: Panel A: Annual mean precipitaion, meters, for South America. Panel B: Annual mean length of dry season, months.

attributable to interannual variability (IAV) dominates. We can picture convective precipitation oscillating along a northwest-southeast line, with maximum seasonality at the terminal points along the line. In the center, annual precipitation is larger, and seasonality less. In the majority of the region, the wet season occurs during Austral summer, centered when the ITCZ reaches its southern terminus; in parts of Colombia, Venezuela, Northern Brazil, Guyana, Suriname and French Guyana the wet season is offset 6 months, and is centered on Boreal summer. Figure 4.1 shows annual precipitation and length of dry season (defined as number of months with precipitation less than 100mm) for years 1983-2006 from the Global Precipitation Climatology Project (GPCP; *Adler et al.*, 2003). Maximum precipitation is located in the northwestern sector of the Amazon basin, which we may envision as being almost continually located under the ITCZ as it oscillates annually along the northwest-southeast line. Precipitation decreases to the south and east; the forest-savanna boundary lies approximately along the line of 1.5 meters annual precipitation. Dry season length is inversely related to annual precipitation amount. In general, we can assume that at wetter sites the dry season is shorter and precipition during dry months greater than at dry sites, although precipitation during dry months is somewhat variable across the region.

Further variability is imposed on precipitation, on inter-annual to intraseasonal scales by modes of climate variability such as El Nino-Southern Oscillation (ENSO) as well as sea surface temperature (SST) variability in the tropical Atlantic Ocean north of the equator (TNA) and south of the equator (TSA). Rainfall during Austral summer (wet season, south of the equator) is also associated with the South American Convergence Zone (SACZ), which exhibits variability as well [*Carvalho et al.*, 2004]. Positive-phase ENSO (El Niño) is associated with decreased precipitation over South America. *Souza and Ambrizzi* [2002] describe a situation where anomalously warm SST over the eastern Pacific Ocean influence the Hadley and Walker cells, inducing anomalous descent (and precipitation inhibition) over northeast Brazil (and Guyana, Surinam, and French Guyana) as well as anomalous ascent (and precipitation increase) over south-southeast Brazil. This pattern, and the associated precipitation anomalies have been known for years [*Rasmusson and Carpenter*, 1982; *Ropelewski and Halpert*, 1987; *de Souza and Ambrizzi*, 2002; *Ronchail et al.*, 2002; *Yoon and Zeng*, 2010]. However, regional behavior is not homogeneous; response can vary from event to event in spatial distribution and magnitude of precipitation anomaly, although El Niño events are frequently phase-locked to Austral summer [*Rasmussen and Carpenter*, 1982] resulting in a strengthened pattern during this time [*Ropelewski and Halpert*, 1987; *Yoon and Zeng*, 2010]. The correlation patterns found during El Niño are generally reversed during periods when east Pacific SST is anomalously cool (La Niña).

There has also been a correlation established between TNA and TSA and South American precipitation. There is an inverse relationship between positive TNA SST anomaly and precipitation [*Moron et al.*, 1995, *Ronchail et al.*, 2002, *Yoon and Zeng*, 2010]. This pattern is similar to that related to El Niño, although it is possible that positive TNA SST may be influenced by El Niño, complicating the relationship [*Yoon and Zeng*, 2010]. TSA positive SST anomalies are associated with a negative precipitation bias in southeastern Brazil, and a positive precipitation anomaly in the region of northeast Brazil most strongly impacted by ENSO. In the case of both TNA and TSA, the precipitation influence is reversed by opposed SST anomalies. *Cox et al.* [2007] predict an increase in positive-phase TNA in the future due to reduced aerosol emissions over North America. This

change in TNA will shift the ITCZ northward, resulting in decreased Amazonian precipitation due to mechanisms similar to those described by *de Souza and Ambrizzi*, [2002].

While statistically significant relationships have been established, their spatial and temporal behavior is variable. *de Souza and Ambrizzi* [2002] show that while the 1982-1983 El Nino was stronger than the 1986-1987 event, precipitation anomaly during December, January and February was of a higher magnitude in the 1986-1987 event, and spatial patterns were different as well. Spatial heterogeneity in ENSO response is also seen by *Coelho et al.* [2002] and *Ronchail et al.*, [2002]. An additional source of variability is the behavior of the South American Convergence Zone (SACZ), a persistent feature of Austral summer (wet season). ENSO has been shown to exert influence on the SACZ, while the Madden-Julian Oscillation (MJO) has shown correlation with extreme precipitation events [*Carvalho et al.*, 2004].

A detailed analysis of South American precipitation mechanisms and their intraseasonal to interannual variability is beyond the scope of this paper. We wish to give a brief outline of the general relationships that have been observed, with the understanding that there is spatiotemporal variability around these influences. It has been postulated that warm TNA SST was chiefly responsible for the 2005 drought in the southwest Amazon Basin [*Zeng et al.*, 2008]. However, interactions between the principle modes of climate variability that influence South American precipitation (ENSO, TNA, TSA) make exact prediction of precipitation, given a certain SST configuration, difficult. Additionally, it has been suggested that ecophysiological behavior acts to moisten and destabilize the atmosphere prior to wet season onset [*Li and Fu* 2004, *Fu and Li*, 2004]. This behavior may add another layer of complexity to an already knotty problem.

4.2.2 Inversions

Inversion studies use Bayesian synthesis techniques to combine CO_2 concentration measurements with atmospheric circulation data to provide an estimate of global CO_2 flux. These are considered 'top-down' techniques, as they infer carbon source/sink from observed concentration data and simulated atmospheric transport. While uncertainty is inherent, due to spatiotemporal variability

in observation networks and imperfect transport, these techniques provide insight into both spatial patterns and IAV of CO_2 exchange between the atmosphere and surface (ocean and land). The globe is generally broken into 11 land and 11 ocean regions, following the TransCom3 experiment [*Gurney et al.*, 2002]. Carbon flux with an anthropogenic source is considered better-constrained than natural flux, and is generally removed from the inversion prior to calculation, with the exception of fires started by humans. It is important to remember that inversion studies, while based upon observational data, retrieve only total flux; attribution of component fluxes (photosythesis, respiration, fire) is impossible, as is spatial resolution beyond the large regions used in the inversions.

Tropical South America was found to be a small source of CO_2 by both *Gurney et al.* [2002] and *Stephens et al.* [2007], although uncertainty was large. The lack of observational data in tropical America, as well as the large vertical transport inherent with deep convection, make constraint of net flux difficult. *Stephens et al.* [2007] went so far as to suggest that tropical land may be a strong sink of CO_2 if land-use emissions are removed.

The calculation of IAV using synthesis inversions is more robust than the calculation of net flux [*Rayner and Law*, 1999; *Bosquet et al.*, 2000; *Peylin et al.*, 2005]. It has been found that land is a larger contributor to variability in global CO_2 flux than ocean [*Bosquet et al.*, 2000; *Rödenbeck et al.*, 2003; *Peylin et al.*, 2005; *Baker et al.*, 2006; *Gurney et al.*, 2008]. Of the land fluxes, tropical land-especially in South America, has been found to contribute a large fraction of the variability in overall land flux [*Bosquet et al.*, 2000; *Rödenbeck et al.*, 2003; *Peylin et al.*, 2005; *Baker et al.*, 2006; *Gurney et al.*, 2008]. While inversion studies suffer from under-constraint in tropical areas, it is not unreasonable to expect that a forest such as the Amazon, with large spatial extent and significant carbon stores, would play a significant role in overall land influence on atmospheric CO_2 growth rates.

Bacastow [1976] noticed a correlation between observed atmospheric CO_2 growth rate (measured at Mauna Loa, Hawaii and the South Pole) and the Southern Oscillation Index (SOI, similar to ENSO). Initially, the relationship was attributed to oceanic flux, but it has since been determined that anomalous westerly flow in the eastern Pacific during El Niño events suppresses upwelling and

attendant release of CO_2 from nurient-rich waters. Ultimately, it has been determined that terrestrial flux dominates IAV in the atmospheric CO_2 growth rate, and that tropical regions are of prime import. In general, positive-phase ENSO (El Niño) events have been correlated with efflux of carbon to the atmosphere from tropical South America [*Rayner and Law*, 1999; *Bosquet et al.*, 2000; *Rödenbeck et al.*, 2003; *Peylin et al.*, 2005; *Baker et al.*, 2006; *Gurney et al.*, 2008].

However, this observation is not universal. Full CO_2 observation flask networks have only been available since the early 1980's, providing slightly less than 30 years of available data. Furthermore, volcanic events (El Chichon in 1983, Pinatubo in 1991) may complicate the picture; global CO_2 growth rates were found to be negative in the early 1990's, a result of either (a reduced respiration due to lower temperatures or b) increased penetration of diffuse light into vegetation canopies, increasing GPP [*Gu et al.*, 2002; *Niyogi et al.*, 2004]. But even in years not considered contaminated by volcanic activity, a universal response of tropical South American carbon flux to ENSO was not found; *Bousquet et al.* [2000] observed both anomalous source and sink during El Niño years. This finding is supported by a study performed using eddy covariance flux tower data [*Schwalm et al.*, 2011] which also determined that ENSO status is insufficient to determine sign on the global CO2 growth rate.

It also must be kept in mind that top-down studies are unable to partition overall carbon flux into detailed spatiotemporal maps, nor are they able to partition flux into component processes. Fire, both naturally-occurring and human-caused, are an important element of carbon flux both globally [*van der Werf et al.*, 2003] and in South America [*Aragaõ et al.*, 2007]. In this study we are considering the response of unmanaged ecosystems to annual cycles and interannual variability imposed by the dominant mode of climate forcing, namely, ENSO. Fire will not be considered.

4.2.3 Canonical Viewpoint

By the late 1990's, inversion studies were drawing attention to the tropics in general, and Amazonia in particular, as playing an important role in global carbon flux and variability in the annual growth rate of atmospheric CO_2. Furthermore, a correlation between ENSO status and growth

rate was emerging, although ambiguity remains around the particulars. Simultaneously, 'bottom-up', carbon fluxes, or fluxes produced by process-based ecophysiological models, were arriving at similar conclusions. These process-based models encompass a wide variety of form, from models that emphasize vegetation and nutrient cycles, to ecophysiological models using satellite phenology products such as Normalized Difference Vegetation Index (NDVI) or Enhanced Vegetation Index (EVI), to fully prognostic ecosystem models developed for use as the lower boundary for AGCMs, to Dynamic Global Vegetation Models (DGVMs) used to predict ecosystem response to changing climate. Verification has been problematic; prior to the Large-Scale Biosphere-Atmosphere project in Amazonia (LBA), surface observations, especially eddy covariance flux towers that measure surface-atmosphere exchange explicitly, were sparse. Stations were few, and available data was generally either of short duration or temporally spotty. The LBA dataset has been invaluable for informing our understanding of ecophysiological processes in Amazonia, as well as the incorporation of this knowledge into ecophysiological models.

The spatial pattern of Net Primary Productivity (NPP, defined as Gross Primary Productivity (GPP) less autotrophic respiration) is shown by *Raich et al.* [1991] to be strongly correlated with annual precipitation amount. A strong gradient in dry season NPP from the wettest part of the basin towards the the savanna (cerrado) in the drier southeast is shown by *Foley et al.* [2002]. This pattern is generally supported, and *Potter et al.* [2001] note the requirement of sufficient moisture *and* adequate insolation for the development of a carbon sink in the Carnegie-Ames-Stanford-Approach (CASA) model.

We can consider the Net Ecosystem Exchange (NEE, or overall carbon flux) as the sum of three components: 1) GPP, the initial uptake of carbon by photosynthesizing plants, 2) R_{auto}, autotrophic respiration, or the respiration produced by plant metabolic processes, and 3) R_{hetero}, heterotrophic respiration, or respiration from 'pools' of carbon such as leaf litter/coarse woody debris or dead roots. Total respiration is the sum of R_{auto} and R_{hetero}. The interaction of these three processes is influenced by variability in precipitation and temperature, and interact to determine anomalous behavior in NEE. The known relationships between ENSO, TNA and TSA and precipi-

tation come into play when determining these interactions.

Anomalously high temperature during dry El Niño events suggests an increase in R_{auto}, thereby decreasing NPP, by *Kindermann et al.* [1996]; *Potter et al.*, [1999, 2001, 2003, 2004, 2005] find a strong reliance of NEE on GPP reduction due to decreased rainfall during El Niño events. This precipitation reliance is supported by *Tian et al.* [1998]. *Zeng et al.* [2005] note a 'conspiracy' of processes, in that the reduction of precipitation during El Niño events not only suppresses GPP, but elevates respiratory efflux via an increase in temperature due to an increase in the Bowen ratio. *Zeng et al.* [2005] note a partitioning of GPP/respiration influence of approximately 2/3 and 1/3 respectively, supported by *Qian et al.* [2008] in a study using the same model. A GPP decrease/Respiration increase is also seen by *Jones et al.* [2001] in the Amazon, in a study using a fully coupled global model.

These interactions become more complex due to time lags. Precipitation follows ENSO signal by a season (4 months) or so [*Potter et al.*, 1999; *Zeng*, 1999; *Foley et al.*, 2002). There is a further lag between precipitation variability and runoff [*Zeng*, 1999; *Nijssen et al.*, 2001] which can be considered a proxy for soil moisture anomaly. Soil moisture is tightly coupled to GPP [*Zeng et al.*, 2005, *Baker et al.*, 2010], so GPP response can lag ENSO status by 6 months to one year or more.

From these studies, a canonical explanation of the process sequence has emerged;

- El Niño events are associated with reduced rainfall in tropical South America.
- Reduced rainfall imposes stress on vegetation, resulting in reduced carbon uptake by biospheric processes.
- Additionally, reduced cloudiness and/or evapotranspiration (ET) result in warmer temperatures and subsequent increase in respiration.
- Also, drier conditions are more favorable for fire, either natural or of anthropogenic origin.

Extensive research has been performed, from both the top-down and bottom-up perspective,

into the ecophysiology and variability of the Amazon region. However, we believe that uncertainty remains in multiple aspects of the analysis. First, models have had difficulty capturing observed annual cycles of land-atmosphere exchange. In many cases, bottom-up regional simulations have been performed without evaluating model performance against observations. In these studies defense, a network of observational data has only recently become available. In the case of top-down (Inversion) studies, uncertainty inherent to the analysis makes retrieval of an annual cycle of carbon flux in tropical land regions difficult. Secondly, mechanistic attribution has been inconsistent. This speaks to the controversy over light- versus water-limitation on photosynthesis in the region, and the disagreement over ecosystem response to variability in forcing. Finally, while bottom-up models have established a canonical response to ENSO forcing, inversion results have been less robust. This implies a complexity in actual ecophysiology that is not capture by process-based models.

4.3 SiB3 Model Simulations

We use the Simple Biosphere Model (SiB3) as a means to represent our understanding of the physics of surface-atmosphere exchange of momentum, mass, energy and trace gases. SiB was developed as the lower boundary for Atmospheric General Circulation Models (AGCMs; *Sellers et al.*, 1986, *Sellers et al.*, 1996a), but contains sufficient ecophysiological detail to be useful to ecologists. SiB is a third generation model, and simulates stomatal behavior as a means to constrain Bowen ratio. SiB determines stomatal conductance through the use of enzyme kinetics following *Farquhar et al.* [1980] with additional photosynthesis and transpiration mechanics following *Collatz et al.* [1991, 1992].

The analysis here is subsampled from a global simulation, covering years 1983-2006, utilizing a 1x1 degree cartesian grid. Vegetation is taken from maps provided by *DeFries and Townshend*, [1994], and does not reflect deforestation or other land cover change during the simulation. We use a 10-minute timestep, and meteorological forcing is provided by National Centers for Environmental Prediction (NCEP2) [*Kalnay et al.*, 1996; *Kanamitsu et al.*, 2002]. Reanalyses have known biases in precipitation [*Costa and Foley*, 1999] , temperature and humidity [*Zhao et al.*, 2006; *Zhang*

et al., 2007], as well as radiation [*Ricciuto et al.*, 2011]. We have scaled precipitation to values provided by the Global Precipitation Climatology Product [GPCP; *Adler et al.*, 2003], but other biases are not addressed [*Baker et al., 2010*]. Vegetation phenology is obtained from the GIMMSg NDVI product [*Brown et al.*, 2004; *Tucker et al.*, 2005; *Pinzon et al.*, 2006], and used to obtain time-varying phenological parameters following *Sellers et al.* [1996b]. There are known biases in NDVI in the tropics [*Los et al.*, 2000; *Sellers et al.*, 1996b]; vegetation properties can be masked by clouds during the wet season, and by smoke and/or aerosols during seasonal drought. We have, therefore, removed variability in NDVI for grid cells identified as evergreen broadleaf forest (EBF; tropical forest). This technique removes anomalous variability in canopy characteristics as retrieved by spectral methods, but neglects real changes in the canopy as well. EBF has leaves at all times, and observed seasonality is generally below the response threshold in SiB3. See *Baker et al.* [2011] for more detail.

It is important to reconcile descriptions of domain. The legal Amazon, which consists of all or part of nine Brazilian states (Acre, Amapá, Amazonas, Pará, Rôndonia, Roraima, Tocantins, Mato Grosso, Maranhão) is not identical to the area defined as the Amazon Basin, which is a purely hydrologic boundary. The term 'Amazonia' often refers to the forest that covers most of the Amazon Basin. The domain in our simulations is all of South America, as far as 30° south. This encompasses all of tropical South America, as well as the cerrado region to the southeast.

Prior to a domain-wide simulation, we established model performance against local observations taken at eddy covariance tower sites [*Baker et al.*, 2011]. We find that in the forest center, gross fluxes of carbon are large, and net flux has little or no seasonality and is determined by high-frequency changes in forcing. Bowen ratio is always small, and shows little variability in the annual as well. Moving away from the forest center, towards the south and east, annual precipitation decreases and dry season length increases. Here, a seasonal cycle emerges, due to differential response between GPP and respiration to seasonal drought. We find that GPP is maintained, or increases, during the dry season, while respiration is suppressed due to drying at the ground surface. This mechanistic relationship produces overall carbon flux similar to observed [—textitSaleska et

al., 2003; *Baker et al.*, 2008]. This phase shifting induces carbon uptake during the dry season, and efflux during seasonal rains. Moving further downgradient in moisture, into the cerrado, we find that moisture availability and carbon flux are in phase. There is carbon uptake during season rains, and photosynthesis is suppressed enough during the dry season to induce the land surface to be a source of carbon. A more detailed description of SiB3 comparison to observations is given in *Baker et al.* [2011].

We can evaluate reanalyzed drivers by comparing model simulations driven by tower-based meteorology against those forced by reanalysis products. In this case we emphasize mean annual cycles, as opposed to actual years, due to the inability of reanalysis products to exactly capture observed interannual variability. A map showing model domain, evaluation sites and vegetation type is shown in Figure 4.2. We evaluate NCEP against observational data at four forest sites (Manaus, K34; Tapajos River National Forest/Santarem, K67, K83; Reserva Jaru, JRU), one savanna site (Pé de Gigante, PEG) and one site located in the transition forest, or cerradão (Bananal Island, Javaes River, JAV) in Figure 4.2. Figure 4.3 shows the relationship between NCEP2 precipitation (scaled to GPCP) and observed precipitation at each site. The annual mean value is enclosed by a box, and individual years are indicated with a number trailing the station name. For all but JAV, the annual mean of the reanalysis and observed precipitation are very close; even at JAV, reanalysis precipitation exceeds observed by only slightly more than 10%. However, significant differences between observed and reanalysed precipitation is seen during individual years, especially at the wetter sites (K34, JRU). Also, these comparisons look at annual precipitation only; no consideration is given to the seasonality, or distribution of precipitation through the year.

Annual mean flux of latent and sensible heat, carbon flux, and precipitation are shown in Figure 4.4. Observed values are shown in black (with symbols), while tower-driven model results [*Baker et al.*, 2011] are shown in red. Model results, acquired by selecting the 1x1 degree grid cell where the tower resides, are shown in blue. The low-amplitude seasonality at the K34 forest site is well captured by the model forced by reanalysis (SiB-R) when compared to the model forced by tower meteorology (SiB-T). As shown in Figure 4.3, reanalysed precipitation is slightly less than

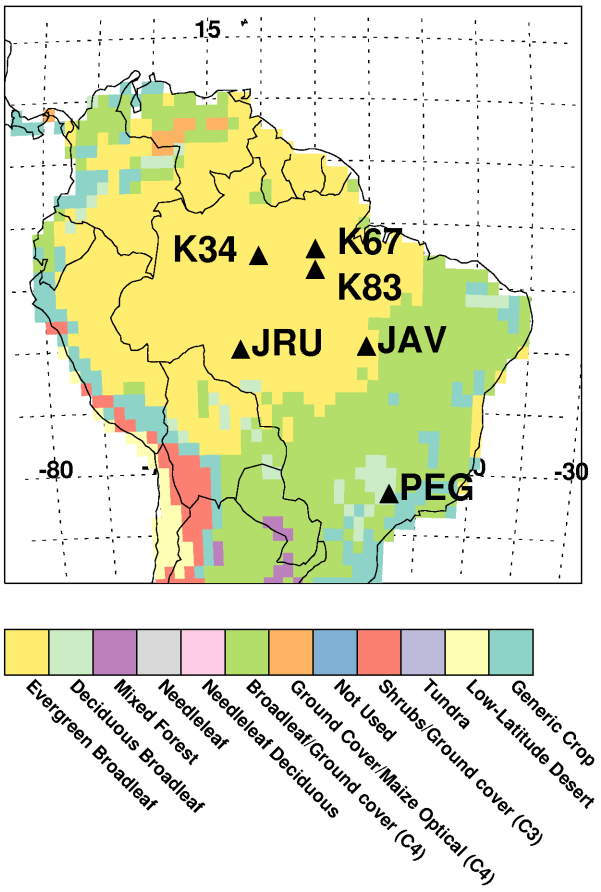

Figure 4.2: Vegetation classification for South America. Tower Sites are superimposed.

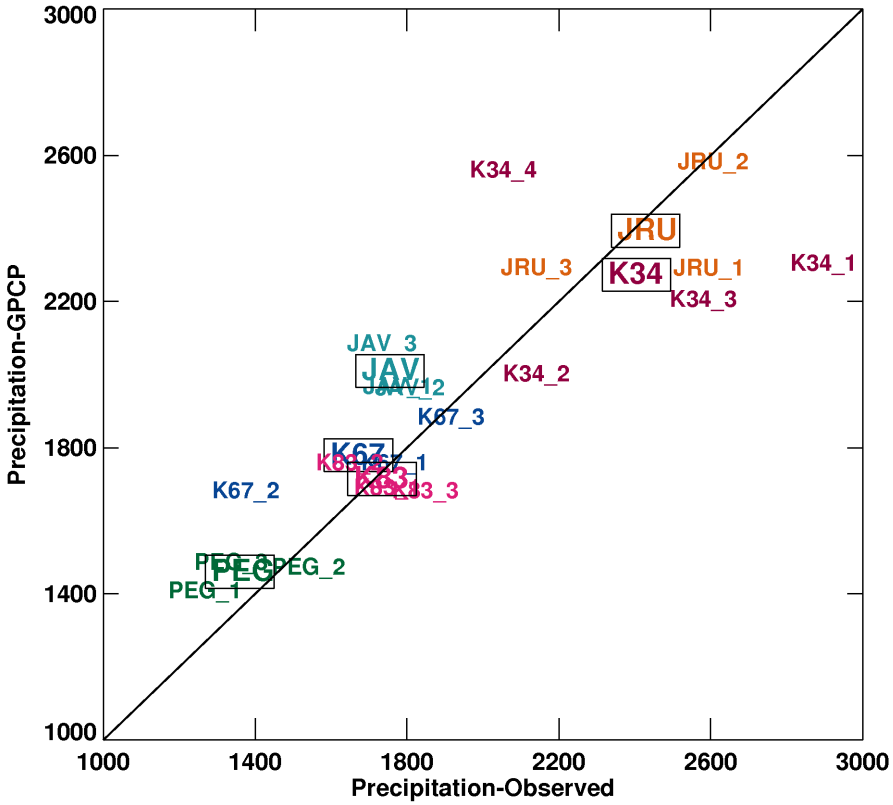

Figure 4.3: Comparison of observed vs. reanalysis precipitation (in mm), for 6 sites shown in Figure 4.2. Annual mean values are enclosed by boxes, individual years are indicated by a subscript that indicates the year in the tower record.

observed; seasonally, this difference falls mainly during the wet season.. At the Santarem/Tapajos River National Forest sites (K67, K83) there is more precipitation during the wet season in the reanalysis. There is little difference between SiB-R and SiB-T latent and sensible heat fluxes. However, the amplitude of the SiB-R carbon flux (both GPP and respiration) are enhanced compared to SiB-T; this results in an increased amplitude of the annual cycle of NEE. At the JRU forest site, annual precipitation is similar (Figure 4.4), but reanalysed precipitation is slightly less than observed in November-January, and higher in March-June. Latent and sensible heat fluxes are similar between the two runs, while the magnitude of the carbon flux (GPP, respiration) is slightly larger as at K67 and K83. However, at JRU, the SiB-T respiration shows more suppression during the dry season. This may be due to local effects at the site, such as the thin (3 meters depth) soil [*von Randow et al.*, 2004; *Baker et al.*, 2008 *Baker et al.*, 2011]. It is not possible to implement local information as a tuning agent into global- or regional-scale simulations; the model is restricted to available large-scale datasets. At the transition forest site (JAV), annual precipitation in the reanalysis is larger than observed (Figure 4.4E), due to larger wet season monthly amounts. Latent and sensible flux is similar between SiB-R and SiB-T, while the carbon flux shows increased amplitude common to the forest sites. There is enhanced suppression of dry season respiration in SiB-R, resulting in anomalous uptake of CO_2 when compared to observations. This is another site with unique properties such as seasonal inundation [*Borma et al.*, 2009], which cannot be easily captured in a model simulation with 1-degree resolution. At PEG, SiB-R precipitation is slightly larger than SiB-T. However, annual cycles of latent, sensible, and carbon flux are very similar between the two treatments. The upshot here is that we do not see a divergence between SiB3 simulations driven by tower meteorology or those driven by the reanalysis; weve established model competence in the former group of model runs [*Baker et al.*, 2008, *Baker et al.*, 2011], and that competence is maintained when the domain is extended from point- to regional-scale. We contend that this establishes a basis for trust in relationships obtained during the regional-scale simulations. We‘ve established the model at the point scale prior to simulating wall-to-wall.

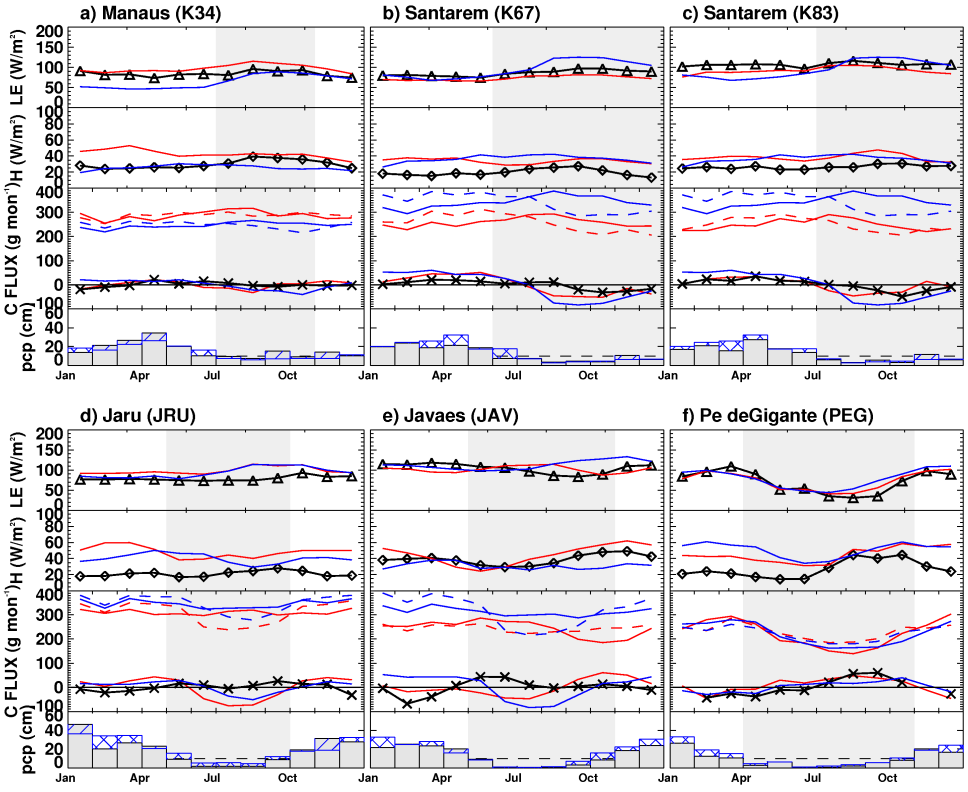

Figure 4.4: Annual mean cycles of latent heat, sensible heat, carbon flux, and precipitation for the 6 tower sites shown in Figure 4.2. Observed data is shown as solid black line with symbols; SiB3 simulations driven by meteorological data recorded at tower sites (SiB-T) is shown as red lines; SiB3 simulations driven by reanalysis data (SiB-R) is shown as blue lines. Carbon flux is broken in GPP (solid) and respiratory (dashed) components.

4.4 Results

Prior to evaluating regional- to continental-scale results, we are careful to verify that the model provides a reasonable approximation of ecophysiological behavior when confronted with observational data from multiple sites across vegetation and moisture gradients [*Baker et al.*, 2008; *Baker et al.*, 2011). Further, we have verified that model simulations forced by reanalysed meteorological datasets is not materially different from simulations driven by observations (Figure 4.4). At this point, we feel confident in our ability to simulate both annual cycles and interannual variability in the undisturbed land surface of South America. Unquestionably, some elements of behavior will not be captured (i.e. seasonal inundation, as at Bananal Island/Javaes River), but the general result is robust. We will compare our results with inversions, but only qualitatively. SiB does not contain fire, and annual flux of carbon is constrained to a zero annual flux by methods outlined in *Denning et al.* [1996]. We have relaxed the carbon balance restriction by lagging respiratory response by one year, so that assimilated material is respired in the following year; this has the result of allowing imbalance during a given 12-month period, but the long-term balance between photosynthesis and respiration is very close to unity. We are unable to capture the absolute year-to-year magnitude in variability, but we believe that our representation of variability in surface processes is realistic.

4.4.1 Regional Behavior

Annual mean GPP, and the standard deviation of variability about that mean, is shown in Figure 4.5. If annual mean GPP is compared with annual mean precipitation (Figure 4.1, panel A), it is easily seen that maximum productivity is not co-located with maximum precipitation (as in *Raich et al.* [1991]), but actually forms almost a U-shaped 'ring' around the region of maximum rainfall. *Potter et al.* [2001] describe a situation where ample precipitation in addition to adequate insolation is required to produce a carbon sink; if we extend this idea to the annual cycle, it can easily be thought of that the wettest regions will actually be too dark to assimilate as much carbon as regions that have significant precipitation, but higher light levels for the canopy to absorb. Tropical forest (EBF; Figure 4.2) is very productive, assimiliating 3 to 4 kg of carbon per square meter annually.

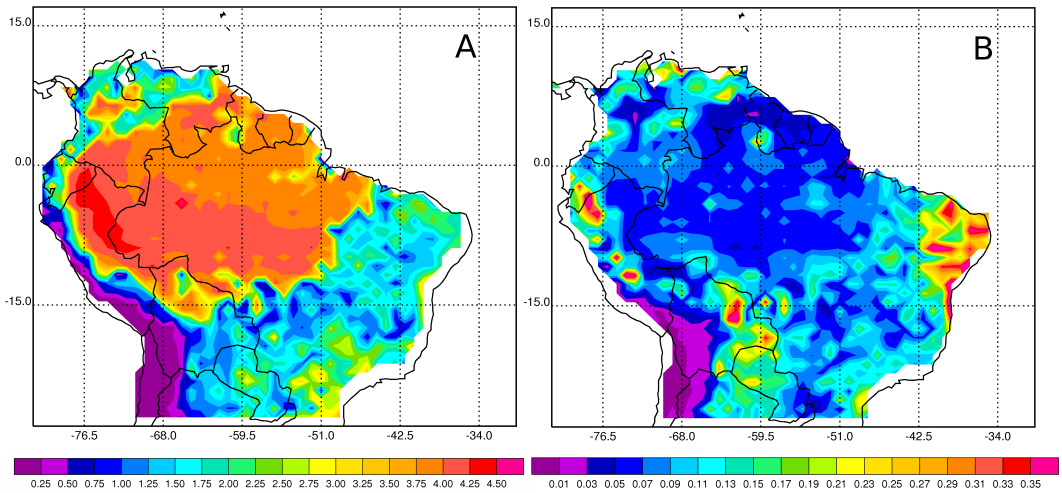

Figure 4.5: Panel A: Annual mean GPP, kg. Panel B: standard deviation in annual GPP, kg.

Seasonality within the forest is also small, as GPP in the month of maximum photosynthetic activity is usually less than 10% of the annual total (not shown; compare with 8.3% if all months have identical fraction). Variability in the forest is small as well, usually less than 1 kg on an annual basis. Since respiration is constrained to match GPP, the only difference between the two is small variations in standard deviation.

The savanna/cerrado is much less productive, with a GPP that is half or less than that of the tropical forest. Variability is similar, meaning that the coefficient of variation (standard deviation divided by the mean) is much larger in the cerrado. Maximum productivity occurs during the wet season (Austral summer), and seasonality is greater; some in the southern part of the domain (not shown) assimilate as much as 15% of the annual amount during the month of maximum photosynthesis.

Seasonality in the region is essentially symmetric across the equator; the wet season is during each hemisphere's summer. We can integrate over the domain to obtain seasonal cycles for the region as a whole, shown in Figure 4.6. Keep in mind that in northern and southern regions (about the equator) seasonality will be reversed, but the fraction of area in the south is much larger. Also, seasonality in the cerrado is more tightly linked to precipitation than in the forest, and maximum productivity is during seasonal rains. In the forest, it appears that highest productivity is during drier

months, when moisture is available yet light levels are high [*Saleska et al.*, 2003,2007, *Baker et al.*, 2008).

We integrate over all points and years to obtain annual cycles, shown in Figure 4.6. Taken as a whole, maximum precipitation (Figure 4.6, panel A) occurs during Austral summer, consistent with the large fraction of the domain south of the equator. Radiation incident at the surface shows a generally inverse pattern to precipitation, reflecting the impact of clouds, and implicating that zenith angle and day length are not the only factors. Annual cycles of GPP and total respiration are shown in Figure 4.6, panel B. Gross fluxes are large, and seasonal amplitude is a small fraction of the mean. Maximum assimilation occurs at the beginning and end of the southern wet season. At the end of the wet season, this is intuitive; soils will be very wet, and as rains recede greater insolation will reach the canopy. At the end of the wet season the mechanisms are more complex. Our simulations show that along the southern boundary of the forest, interspersed with the regions where maximum GPP occurs in March, are areas where maximum GPP takes place in November (not shown). We speculate that these may be regions that respond to higher light levels during the approach of Austral summer, prior to the onset of seasonal rains. This explanation is consistent that the findings of *Fu and Li* [2004] and *Li and Fu* [2004] who describe an increase in surface evapotranspiration (ET) in advance of the wet season. This increased moisture flux serves to moisten and destabilize the atmosphere, and helps 'precondition' the atmosphere for the large-scale convergent features that define the wet season. Large fractional canopy cover in the forest implies a large component of transpiration in overall ET; it makes sense that if transpiration increases, then the vegetation must not be experiencing stress, and carbon flux can be expected to increase as well. This annual cycle contradicts that put forth by *Potter et al.* [2001], who predicted an annual minima in GPP coincident with or slightly lagging precipitation minimum. Our simulations predict a partial decoupling of ecophysiological function from annual precipitation cylcles.

Respiratory flux is maximized during Austral summer, or the southern wet season (Figure 4.6, panel B). Temperatures are warm year-round, and ample moisture at the surface of the soil maximizes respiration potential. As seasonal rains move north and surface (litter and surface soil)

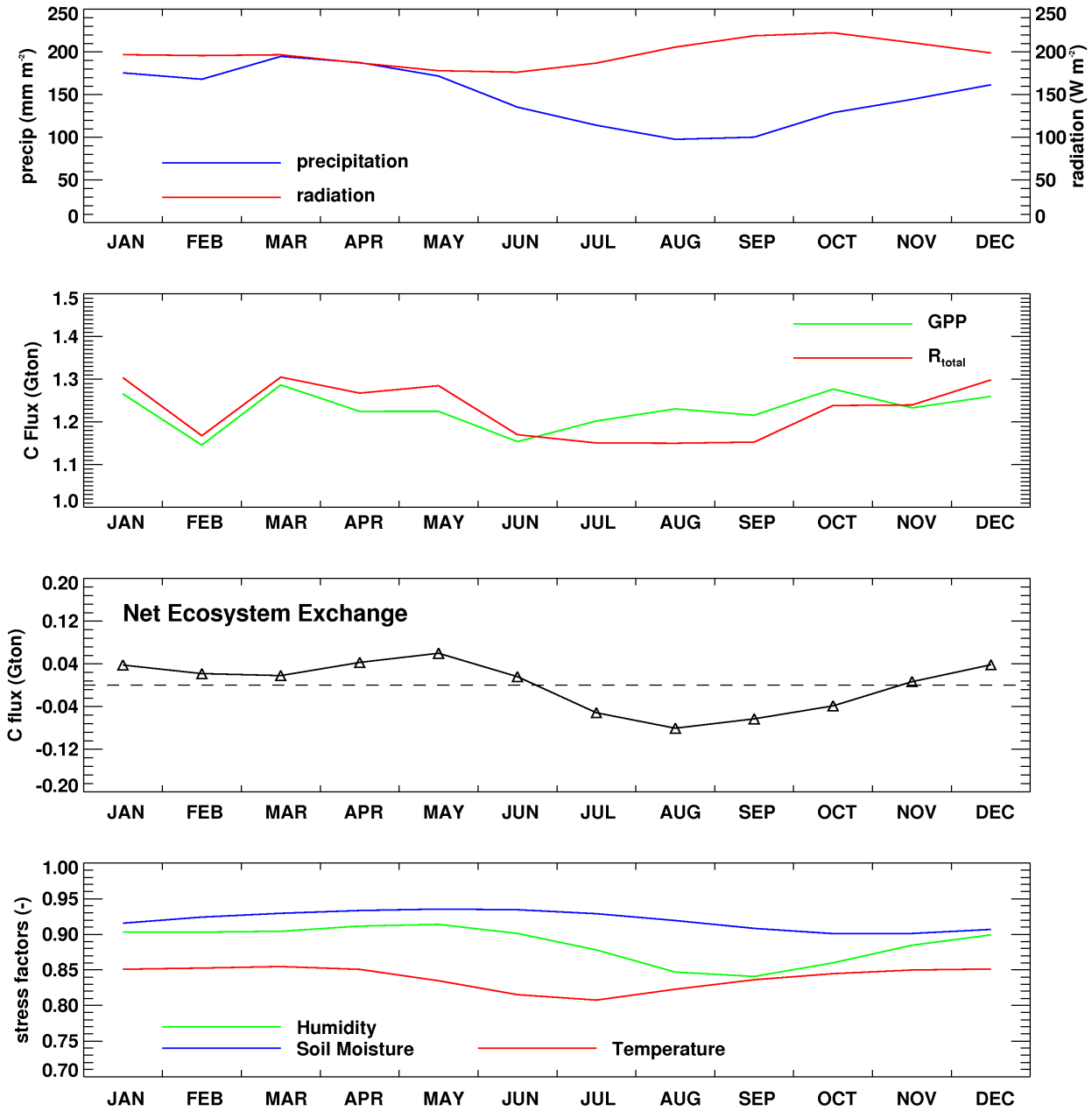

Figure 4.6: Simulations of domain-wide annual cycles of precipitation, radiation and carbon flux from SiB3 simulations. Mean values of precipitation and radiation are found by area-weighting individual gridcells prior to calculating the mean. Carbon flux is accumulated over the entire domain. Panel A: domain-averaged precipitation (blue) and radiation (red). Panel B: mean GPP (green) and total respiration (red). Panel C: domain-wide Net Ecosystem Exchange (NEE) of carbon.

desiccates, respiratory flux decreases.

The annual cycle of NEE is shown in Figure 4.6, panel C. The photosynthetic and respiratory fluxes combine to produce a net efflux of carbon during the southern wet season, and uptake during seasonal drought. This cycle closely resemble seasonal cycles observed at tower locations in the Tapajos River National Forest [*Saleska et al.*, 2003] and simulated using SiB in *Baker et al.* [2008]. In *Baker et al.* [2011] it was found that the wettest forests had little or no annual cycle in carbon flux; in the cerrado, carbon flux was tightly linked to precipitation. In many forest sites, however, a phase-shifted pattern was found. Carbon uptake increased (or was at least maintained) during seasonal drought, while respiratory flux decreased as surface soils dried out. The current simulations suggest that this behavior is common over a large enough fraction of the total region to be the defining mechanism for regional carbon flux as a whole.

4.4.2 Process Variability

For insight into the mechanisms that influence variability, we regress variability in GPP against variability in forcing mechanisms: precipitation, light, temperature, and soil moisture. To determine independence of observations, we calculated the degrees of freedom (dof) following *Bretherton et al.*, [1998] on both annual and monthly data. We find a low level of autocorrelation (not shown) for all of the domain, with the exception of the thin strip of desert on the western South American coast. This justifies the use of monthly data for the regression. We utilize simple statistics, calculating a linear regression and use a two-ended Student's T-test to determine significance at the 95% level (Figure 4.7). Variability in radiation determines the greatest fraction of variability in GPP for a large fraction of the tropical forest, and explains a significant fraction of the variability-up to 70% in regions. Along the southern and eastern forest boundary, soil moisture explains a the most variability, albeit at a smaller fraction than in the forest interior. In the cerrado, there are locations where each of the mechanisms explains the most variability, but the fraction explained is always small, generally less than 25-30%. We note that where radiation explains the most variability in the cerrado, the relationship is negative; higher insolation is correlated with lower GPP.

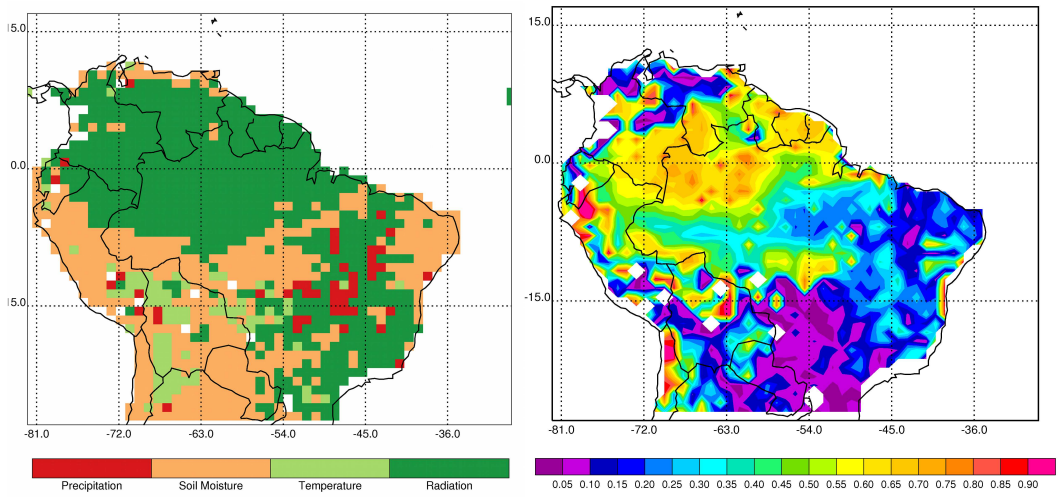

Figure 4.7: Panel A: Mechanism that explains the largest amount of variability in monthly GPP anomaly. Panel B: fraction of total variability explained by the dominant mechanism.

If we perform the calculation on an annual basis (not shown), the results are similar, but not identical. On an annual basis, radiation is the dominant mechanism in forested regions, explaining a high fraction of the variability, but the total area where radiation is dominant is smaller than that found with the monthly calculation. Soil moisture is the dominant mechanism for much of the forest south of the equator, explaining a significant (up to 90%) fraction of the GPP variability. At the boundary between the soil moisture and radiation regions, the variability explained by the dominant mechanism is less, suggesting an interplay between soil and radiation properties in determining interannual variability in GPP.

Respiration variability and reliance on a single mechanism does not show the patterns seen in GPP. Total variance explained is small throughout the domain, and the mechanism pattern is heterogeneous. Since respiration is a function of temperature, moisture, and carbon pool size (approximated in SiB by previous year's assimilation, following *Denning et al.*, [1996]), it is not unexpected that these multiple interactions will result in a complex picture of respiration variability.

Synthesizing these results, we can formulate a picture of basin-scale ecophysiological behavior, and predict large-scale response to meteorological variability over larger temporal scales. In the forest interior, precipitation is large, even in drought years. GPP in this interior region responds

to higher insolation, and exhibits limitation properties similar to those described by *Saleska et al.* [2007] and *Huete et al.* [2006]. To the south and east, where annual precipitation is less, forest productivity is more dependent upon soil moisture. We might anticipate that in this region plant response will depend on magnitude, duration, and timing (wet season/dry season) of a drought event. It is interesting to note that in this region, forest that shows dependence upon soil moisture, contains the portion of the southwest Amazon most directly affected by the 2005 drought. In that case, a drier-than-normal dry season followed several years of suppressed annual precipitation [*Zeng et al.*, 2008], resulting in significant stress on vegetation. Our findings are consistent with that evaluation.

Respiration patterns are much more heterogeneous. Therefore, when considering continental-scale NEE we can envision a situation where complex respiration response couples with slightly more predictable, but still somewhat variable, GPP patterns to determine large-scale response. We predict that overall carbon flux will exhibit complex patterns in response to climatic variability. This will be investigated in the next section.

4.4.3 Climate Variability

There are clearly established relationships between ENSO and South American precipitation, and a relationship between water status and carbon flux has been proposed from both bottom-up and top-down investigations. Under this paradigm, regional precipitation decreases during (or following a lag) an El Niño. This precipitation decrease results in a suppression of photosynthesis, an increase in respiration, or both, resulting in increased carbon flux to the atmosphere. However, there are some indications that this paradigm may not hold universally. First, there is an historic inability of landsurface models to accurately capture seasonality in Amazonia [*Saleska et al.*, 2003; *Baker et al.*, 2008]. Secondly, there is an unresolved debate over whether Amazonian forests are light-limited [*Saleska et al.*, 2007; *Huete et al.*, 2006] or not [*Samanta et al.*, 2010]. Finally, our regression of GPP anomalies against indicate that there are regions in the tropical South American forest where water status defines carbon assimilation, and regions where the forest is light-limited, even on an interannual basis. This implies a more complex picture, one that defies simplistic explanation. This

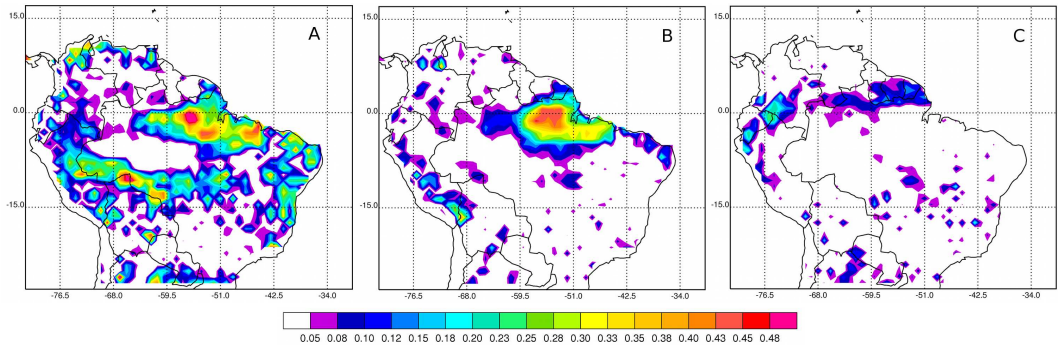

Figure 4.8: Annual NEE anomaly regressed against modes of climate variability. Panel A: NEE vs. MEI. Panel B: NEE vs. TNA. Panel C: NEE vs. TSA. Scale shows amount of variability in NEE explained by the individual climate index. Only areas that are significant at the 90% level are shown.

complexity is mentioned in both top-down [*Bousquet et al.*, 2000] and bottom-up *Schwalm et al.*, [2011] studies.

The Multivariate ENSO Index (MEI; *Wolter and Timlin*, 1993, 1998) is an expression of the strength of the ENSO signal based on the first principle component of 6 variables over the Pacific Ocean; pressure, zonal and meridional wind components, SST, air temperature, and cloudiness. The North Atlantic SST (TNA) and South Atlantic SST (TSA) indices are described in *Yoon and Zeng* [2010]; we obtained TNA/TSA indices from NOAA [*Enfield et al.*, 1999]. We regressed annual anomalies of precipitation against MEI, TNA, and TSA and obtained results (not shown) similar to multiple previous studies linking ENSO and precipitation status. Following *Yoon and Zeng* [2010], we applied a running mean to monthly data prior to calculation, and determined annual anomalies over the period September-August. We then applied the same regression tool to GPP, total respiration, and NEE. NEE correlation to MEI, TNA and TSA is shown in Figure 4.8. It should be noted that we do not consider the strong El Niño event of 1982-1983, as only the latter half of the event is available for analysis. Additionally, we do not emphasize evaluation of ENSO events during 1992-1995, as it has been postulated that global aerosol from the Pinatubo eruption were the driving force in global CO_2 growth rate during this period.

MEI is positively correlated with NEE near the mouth of the Amazon River, a region that also shows strong precipitation dependence. There is a secondary region along the southern border of

the forest where positive phase MEI (El Niño) is correlated with carbon flux into the atmosphere. In northeast Brazil, There is a tendency for large GPP suppression and small respiration increase during positive MEI. Extending west along the river/equator, the photosynthetic response diminished, and the respiration signal intensifies. Near the Brazil-Columbia border, there is an enhancement of the overall carbon cycle in response to positive MEI-both GPP and respiration increase, but the impact on NEE is not significant. In the southern forest, along the border of Brazil and Peru/Bolivia, there is a small decrease in GPP and small increase in respiration during positive MEI, resulting in carbon efflux.

TNA influence on NEE is limited to northeastern Brazil. Here, the response is similar to that seen for MEI; GPP is suppressed and respiration enhanced during positive-phase TNA. There is also a region near the Brazil-Peru-Bolivia border that experiences significant responses in both GPP and respiration to TNA. In this region, however, the responses cancel; GPP and respiration both decrease during positive phase TNA. This reduction in amplitude of the carbon cycle is not significant for NEE.

There is a smaller, but also positive, correlation between TSA and NEE along a line just north of the equator. In this case, there is a dipole between enhanced respiration in northeast Brazil and suppressed GPP in Colombia. As with TNA, there is a suppression of the overall carbon cycle along the southern forest boundary (both GPP and respiration decrease with positive TSA) that does not significantly impact NEE.

These individual patterns are integrated into a domain-wide summary of precipitation, carbon flux components, and NEE in Figure 4.9. In panel A, it is easily seen that precipitation anomalies are inversely correlated with MEI over the large scale. The canonical model suggests that GPP will lag precipitation anomalies by 6-12 months. Panel B shows that while this is sometimes the case (1997-2001), it does not always hold. In some cases precipitation and assimilation anomalies are concurrent (1984-1985; 1990-1992), out-of-phase (1988) or even one case where GPP anomaly precedes precipitation (1992).

Two distinct and very different situations can be seen in Figure 4.9, panel C, which shows

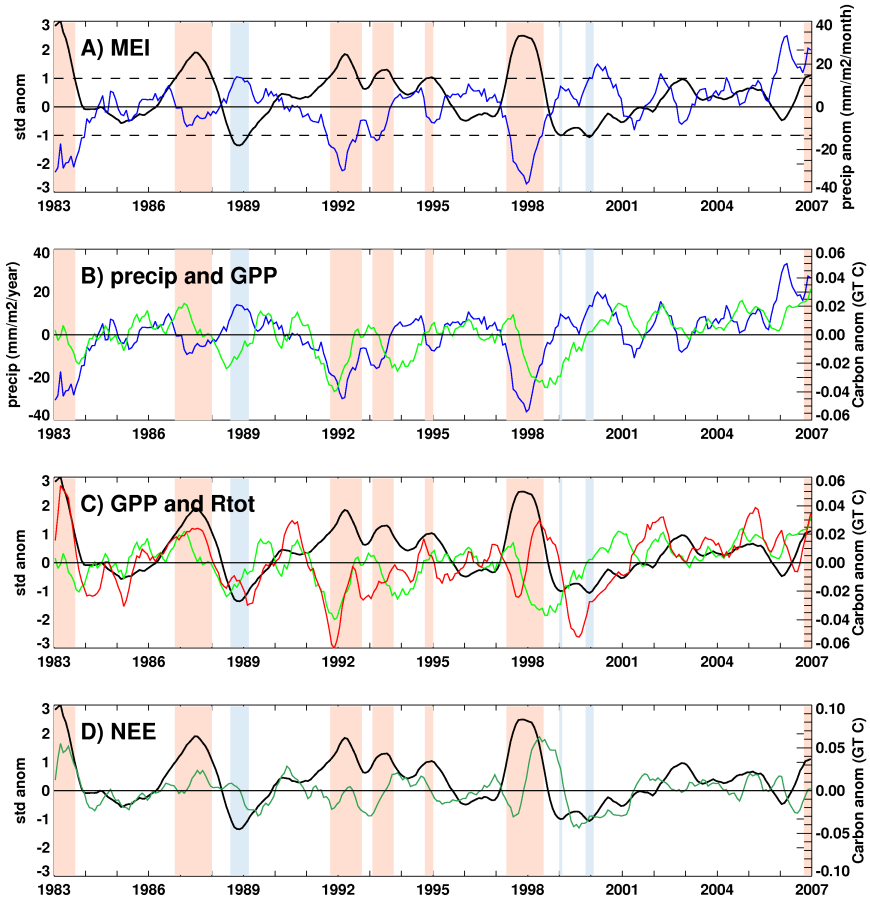

Figure 4.9: Time series of MEI vs. domain-wide anomalies in precipitation, carbon flux components (GPP and total respiration) and NEE. Panel A: MEI and precipitation. Panel B: precipitation and GPP. Panel C: MEI, GPP, total respiration. Panel D: MEI and NEE.

the interrelationship of assimilation and respiration anomalies. During the 1997-1998 El Niño, the canonical behavior is seen. There is an initial sink of carbon (Figure 4.9, panel D) at the surface, a result of a positive anomaly in GPP and negative in respiration. This may be an initial response to enhanced light levels, while moisture is still relatively prevalent, while respiration decreases as surface soils begin to desiccate. Subsequently, GPP drops sharply, at a 6-12 month lag from precipitation, and respiration increases at a lag from GPP of 1-2 months. This adheres closely to the 'conspiracy' of processes noted by *Zeng et al.* [2005]. During the El Niño of 1987, however, a distinctly different pattern emerges. In 1987, both GPP and respiration are anomalously high, or near mean values, during the duration of the event. In this case, both GPP and respiration increase initially during the event; carbon efflux is found during the latter 6 months, when GPP drops to mean values while respiration is still enhanced.

During the La Niña event of 1989, the relationship is approximately the inverse of the paradigm. Precipitation increases, followed at an approximate 6-month lag by GPP, followed another 3-4 months by respiration. This results in anomalous uptake of carbon at about a 6 month lag from MEI.

During the 1997-1998 El Niño negative precipitation anomalies followed the ITCZ and the wet season as it moved from north to south. Warm temperature anomalies accompanied the decrease in precipitation. Initially there were large positive GPP anomalies along the Amazon river, in the early wet season. Subsequently, domain-wide high temperatures, which were not dramatic (well below 1 K), were sufficient to induce a domain-wide positive respiration anomaly, driving the NEE towards larger efflux. In 1987 the El Niño was centered on the dry season in the south. In this case, spatial patterns were more disjoint, and lacked cohesion.

The 1997-1997 El Niño possessed a coherent pattern. This was due to both coherence in the precipitation anomaly and the temperature anomaly it spawned. These patterns were fundamental to behavior in 1997-1998, as it was not seen in an El Niño episode of similar magnitude, but centered on the southern domain dry season in 1987. This underscores the complex behavior in the basin, as magnitude, duration, spatial pattern and timing all influence ecosystem response to variations in

climatological forcing.

4.5 Discussion and Conclusions

The canonical causal chain of events in tropical South America starts with a decrease in precipitation, often concurrent with or lagging positive-phase ENSO. This leads to dryer soil, and imposes stress on photosynthesis, with a lag of 4-6 months. As ET decreases, temperature rises due to an increase in the Bowen ratio, also on a 4-6 month lag. Increased temperature leads to an increase in heterotrophic respiration; therefore both the stomatal and the respiratory signals positively reinforce a positive CO_2 flux from the land to the atmosphere. We do not question the validity of this sequence: However, spatiotemporal variability in the precipitation response to ENSO, the timing of precipitation anomalies around the annual cycle, and the length/magnitude of the ENSO event result in a heterogeneous response from the vegetation. Therefore, we do not believe that there is a 'typical' response of the tropical South American land surface to an El Niño/La Niña event.

Ecophysiological behavior in tropical South America has implications for global atmospheric CO_2 growth rate [*Rayner and Law*, 1999; *Bousquet et al.*, 2000; *Rödenbeck et al.*, 2003]. The large amount of carbon stored in tropical forests [Houghton] has the potential to provide a strong positive feedback to changes in radiative forcing if released, which has been postulated as a strong possibility for the near future [*Cox et al.*, 2000; *Cowling et al.*, 2004; *Huntingford et al.*, 2004; *Huntingford et al.*, 2008]. Therefore, predictions of future climate depend materially on an ability to accurately describe, and predict, the large-scale behavior of land-atmosphere interaction in South America, both on annual and interannual scales [*Friedlingstein et al.*, 2006].

We believe that previous predictions of South American biophysical behavior, while not fundamentally flawed, do not present an accurate picture of basin-wide behavior. The canonical behavior assumes an over-reliance on precipitation, signified most strongly by an inability to to capture mean annual cycles of carbon flux [*Saleska et al.*, 2003] as well as of latent and sensible heat [*Baker et al.*, 2008]. This inability suggests an underestimation of the amount of decoupling between physiological function and precipitation, and implies that tropical forests are fragile systems

that can barely survive a dry season-let alone anomalously low precipitation over multiple years that may be imposed by ENSO. This multi-year resiliency has been demonstrated by studies that exclude precipitation from the soil, and show an ability of the forest to survive several dry years before exhibiting stress and mortality [*Nepstead et al.*, 2008].

The dense canopy in tropical South American forests force a tight linkage between forest function and ET. Ecophysiology determines carbon flux, and will play a critical role in determination of Bowen ratio as well. It has been shown that surface behavior can influence the onset and cessation of seasonal rains [*Fu and Li*, 2004; *Li and Fu*, 2004]. It has also been shown that incorrect treatment of land-atmosphere exchange can influence atmospheric characteristics [*Harper et al.*, 2010]. Therefore, we can expect that uncertainty in representation of surface ecophysiology will be propagated through simulations of present and future climate.

We take a bottom-up approach, and simulate Amazonian ecophysiology on a regional scale, over multiple years. Our model has been confronted with data from multiple tower sites in Brazil. We‘ve established the model on the local scale, across vegetation and moisture gradients, prior to performing regional studies. We establish an ability to predict annual cycles of carbon, energy and moisture flux; we also verify that the reanalysis products used to drive regional studies do not substantially alter our results.

We cannot definitively resolve the light-limited/water-limited question put forth by the papers of *Huete et al.* [2006], *Saleska et al.* [2007], and *Samanta et al.* [2010]. We find that there are regions that tend towards light- or water-limitation, but these areas are not rigidly defined boundaries may move based on precipitation dynamics.

Our simulations agree qualitatively with inversion results. We show a large carbon efflux during the 1997-1998 El Niño, with heterogeneous behavior among other events. This is consistent with both inversion [*Bousquet et al.*, 2000;] and data-based bottom up [*Schwalm et al.*, 2011] result.

Future behavior of ENSO is uncertain [*IPCC*, 2007); However, Cox 2007 predicts a shift in the ITCZ position due to a modification in TNA imposed by changes in aerosol loading of the atmosphere. As understanding of large-scale climate variability increases, we need our biophysical

models to have the scientific underpinnings necessary to accurately capture ecophysiological response to this new understanding. This requires an ability to capture and reproduce behavior under present climate.

Chapter 5

APPENDIX: THE SIMPLE BIOSPHERE MODEL, VERSION 3. MODEL DESCRIPTION AND NUMERICAL SCHEME

5.1 Introduction

The Simple Biosphere Model (SiB) was introduced in 1986[*Sellers et al.*, 1986] with the intent to be used as a lower boundary condition for Atmospheric General Circulation Models (AGCMs). SiB simulates the processes that control the exchange of mass, energy, momentum and trace gases between the atmosphere and terrestrial biosphere, and was developed to provide a valuable modeling function for meteorologists and ecologists alike. The model was written with a high level of biophysical realism that give it appeal to a wide range of research applications.

A second version of the model (SiB2) was released in 1996 [*Sellers et al.*, 1996a]. Canopy representation was bolstered with improved stomatal physics [*Sellers et al.*, 1992; *Collatz et al.*, 1991; *Sellers* 1987] and inclusion of the C4 photosynthetic pathway following *Collatz et al.*, [1992]. Vegetation phenology, previously determined by lookup table, was coupled to satellite-observed phenology using Normalized Difference Vegetation Index (NDVI) information [*Sellers et al.*, 1996b].

In the intervening years, SiB has been used as a lower boundary for global [*Sato et al.*, 1989; *Randall et al.*, 1996] and mesoscale [*Denning et al.*, 2003; *Nicholls et al.*, 2004; *Wang et al.*, 2007; *Corbin et al.*, 2008] atmospheric models. Offline simulations have investigated global [*Schaefer et al.*, 2002; *Schaefer et al.*, 2004; *Schaefer et al.*, 2005] and regional [*Baker et al.*, 2010] surface flux behavior. Local ecophysiology as measured by eddy covariance flux towers have been compared to SiB in midlatitude forest [*Baker et al.*, 2003; *Schaefer et al.*,2008], grassland [*Colello et al.*, 1998; *Hanan et al.*, 2005; *Schaefer et al.*,2008], tropical forest [*Baker et al.*, 2008; *Baker et al.*, 2011] and

in savanna [*Baker et al.*, 2011]. These studies substantiate the utility of SiB in multiple applications across diverse ecosystems and spatial domains.

Since 1996, a number of model modifications have been added to the SiB code. Some of these are in direct response to model shortcomings when confronted with observations, while others are implemented when a particular biophysical mechanism is found to be either lacking or over-simplified in the code. A prognostic Canopy Air Space (CAS) formulation has been added to the equation set [*Vidale and Stóckli*, 2005; *Baker et al.*, 2003]. A prognostic CAS provides a storage or integrating volume between flux sources (vegetation, ground) and the atmosphere above the canopy. This volume has mass and therefore adds inertia to component fluxes in complex situations such as change in radiative forcing (sunup/sundown) or frontal passage. This inertia results in more realistic simulations of mass and energy exchange on diurnal scales. The capacity to store individual species is critical to the calculation of fractionation of carbon and oxygen isotopes [*Suits et al.*, 2005] as CO_2 and other trace gases can be traced explicitly through the ecophysiological processes that determine their concentration and exchange rate with the atmosphere. To our knowledge, SiB is unique among landsurface models in this regard. All other models define a diagnostic CAS, in which fluxes are summed to obtain canopy values. This latter method has the advantage of perfectly closing energy and moisture budgets, but retrieves suspect values at times when forcing changes sign, such as sunup and sundown.

Model hydrology has been improved by adopting the Community Land Model (CLM; *Dai et al.*, 2003) soil/snow submodel as well as alterations to the soil water stress on photosynthesis and ground water calculation [*Baker et al.*, 2008]. Model carbon cycle has been made more realistic by the inclusion of frost stress and autotrophic respiration terms, and more accurate phenology has resulted from a modified NDVI interpolation scheme. An internal tiling module [*Hanan et al.*, 2005] has been shown to improve simulations in mixed C3/C4 grasslands. This 'multiple physiology' framework also provides a framework, as yet unexploited, for simulating individual species or heterogeneous assemblages of woody and herbaceous cover.

5.2 SiB3 Equation Set

The SiB prognostic variables represent the state variables governing the vegetation, canopy air space, and soil. Canopy conditions are described by vegetation temperature and depth of water intercepted on leaves; canopy conductance controls rates of carbon uptake and transpirational water loss. Water vapor concentration, temperature, and CO_2 concentration are explicitly resolved in the CAS. Surface water is described by interception storage (puddles) and snow depth. Adopting the method used in the Community Land Model (CLM), snow can occupy up to 5 layers dependent on mass and depth; these snow layers have explicit treatment of liquid and ice fraction. Also following CLM, the soil provides co-located soil temperature and soil moisture layers, again with explicit treatment of liquid water and ice. Soil depth and number of layers can be user-specified as applications warrant, but a common configuration contains 10 layers, and a total soil depth of around 10 meters [*Baker et al.*, 2008].

The basic governing equations are similar to those used in previous versions of the model, with the addition of an equation for the canopy air space (CAS) temperature and moisture. These equations are

canopy

$$C_c \frac{dT_c}{dt} = R_c - H_c - \lambda E_c \tag{5.1}$$

ground

$$C_g \frac{dT_g}{dt} = R_g - H_g - \lambda E_g - G \tag{5.2}$$

CAS

$$C_a \frac{dT_a}{dt} = H_c + H_m + H_g + H_s \tag{5.3}$$

where

T_c, T_g, T_a = temperature, K

R_c,R_g = absorbed net radiation, W m^{-2}

C_c,C_g,C_a = heat capacity, J m^{-2}K^{-1}

H_c,H_g,H_m,H_s = sensible heat flux, W m^{-2}

λE_g, λE_c = latent heat flux, W m^{-2}

The subscript *c* refers to the vegetation, *g* to ground, *s* to snow, *a* to canopy air space, and *m* to reference height or lowest atmospheric level. The governing equations for canopy/ground intercepted water storage and CAS vapor pressure are

canopy

$$\frac{\partial M_c}{\partial t} = P_c - D_c - E_{wc}/\rho_w \tag{5.4}$$

ground

$$\frac{\partial M_g}{\partial t} = P_g - D_g - E_{wg}/\rho_w \tag{5.5}$$

CAS

$$\frac{\rho_a c_p \Delta z}{\gamma}\frac{\partial e_a}{\partial t} = \lambda E_c + \lambda E_g + \lambda E_s + \lambda E_m \tag{5.6}$$

where

M_c,M_g=depth of water storage, m

P_c,P_g=rate of precipitation interception, m sec^{-1}

D_c,D_g=water drainage rate, m sec^{-1}

E_{wc},E_{wg}=evaporation rate from wet fraction of canopy/ground, kg m^{-2}sec^{-1}

ρ_w=mass of water, kg m^{-3}

ρ_a=mass of air, kg m^{-3}

c_p=specific heat of dry air, J K^{-1}kg^{-1}

Δ z=depth of CAS, m

γ=psychrometric constant, Pa K^{-1}

e_a=CAS vapor pressure, Pa

Soil moisture and soil temperature are now calculated in co-located layers. This is a departure from SiB2, where soil moisture was calculated in three layers; surface, root zone, and deep recharge, respectively, to a total soil depth of 3.5 meters. The governing equation for subsurface soil temperature layers is

$$C_j \frac{\partial T_j}{\partial t} = F_{j-1} - F_j \tag{5.7}$$

where

C_j=heat capacity of soil layer j, J $K^{-1}m^{-2}$

T_j=soil temperature of layer j, K

F_j,F_{j-1}=heat flux across lower (F_j) and upper (F_{j-1}) control volume boundaries, W m^{-2}

Change in soil moisture within a given soil layer must balance mass flow across layer boundaries as well as sources or sinks. Liquid and ice-phase water are treated explicitly, so there is a phase change term that must be accounted for, and there is a sink term for liquid water for removal by roots. The soil water equations follow Darcy's law while soil hydraulic conductivity and matric potential depend on volumetric soil water content and soil texture, based on *Clapp and Hornberger*, 1978]. The soil water governing equation is

$$\frac{\partial w_j}{\partial t} = [q_{j-1} - q_j] - E_{tr} + M \tag{5.8}$$

where

w_j=water content of soil layer j, kg m^{-2}

q_{j-1},q_j=moisture flow across lower (q_j) and upper (q_{j-1}) control volume boundaries, kg m^{-2} sec^{-1}

E_{tr}=removal of water by roots for transpiration, kg $m^{-2}sec^{-1}$

M=phase change, kg $m^{-2}sec^{-1}$

Roots can act as conduits in the soil, moving water from moist to dry regions during night, or other times when stomates are closed. The process can act upwards against gravity if deep layers are more moist than the surface, or near-surface water can be transported to depth following precipitation events. This process, known as hydraulic redistribution, has been observed in many ecosystems worldwide. *Lee et al.,* 2005] incorporated hydraulic redistribution to model ecosystem behavior in the Amazon Basin, following observations [*Oliveira et al.*, 2005; *da Rocha et al.*, 2004], and *Baker et al.* [2008] incorporated hydraulic redistribution in SiB. However, site-specific coefficients are required to calculate redistribution, based on soil and root characteristics. Since global maps of these coefficients do not exist, hydraulic redistribution is not a standard feature in SiB3, but can be implemented simply if soil-root transfer coefficients are known.

By combining the thermal properties of snow with the surface soil layer, SiB2 did not provide adequate insulation, resulting in anomalous cooling of the soil in cold regions [*Baker et al.*, 2003]. The implementation of a multi-layer snow model based on the Community Land Model [*Dai et al.*, 2003] and SNTHERM [*Jordan*, 1991] provides a mechanism to insulate the soil, as well as more realistic simulation of snow accumulation and ablation. Snowpack is metamorphosed by destructive pressure, overburden, and melt, and layer numbers and depths are continually reallocated as snow accumulates or melts/compacts.

The calculation of photosynthesis as outlined in*Sllers et al.*, 1992, 1996a] has not been modified and will not recieve more attention here. However, other elements of the CO_2 budget have undergone modification, to the degree that simulation of CO_2 flux is significantly different in SiB3. Foremost, the prognostic formulation used for calculating CAS temperature and moisture has been adopted for CO_2 with the following governing equation

$$C_{CO_2}\frac{\partial CO_2}{\partial t} = R_{hetero} + R_{auto} - GPP - F_m \quad (5.9)$$

where

CO_2=CO_2 concentration in CAS, mol mol^{-1}

C_{CO_2}=CO_2 capacity in CAS, mol m^{-2}

R_{hetero}= heterotrophic respiration, mol m^{-2}sec^{-1}

R_{auto}=autotrophic respiration, mol m^{-2}sec^{-1}

GPP= gross primary productivity, mol m^{-2}sec^{-1}

F_m=CO_2 flux between CAS and reference level, mol m^{-2}sec^{-1}

By incorporating the prognostic CAS into SiB we provide a storage volume for CO_2 which gives inertia to the system when fluxes change sign rapidly, such as sunup or sundown (see *Baker et al.*, 2003). The inclusion of prognostic canopy airspace carbon strongly affects modeled net ecosystem exchange (NEE) on the diurnal scale, while two other modifications (interpolation of canopy phenology information and partitioning of respiration into autotrophic and heterotrophic compontents) are reflected in annual cycles of carbon uptake and release. The fully prognostic CAS make SiB unique among landsurface models. By explicitly resolving scalars within the canopy air SiB3 has the computational framework, or 'hooks', to incorporate detailed ecophysiological processes into the model physics. Isotopes of carbon (^{13}C/ ^{12}C)are currently incorporated into the code, and calculation of fluxes and concentration of other trace gases such as carbonyl sulfide, radon, or methane can be easily included. Futhermore, the computational framework is easily adaptable to accommodate multiple-layer canopy or detailed radiation submodels as well.

SiB has historically diagnosed respiration from canopy, roots and soil microbes to balance photosynthetic uptake [*Denning et al.*, 1996]. There is a small autotrophic canopy respiration term that is dependent upon vegetation temperature and maximum Rubisco velocity, but this approach emphasizes microbial (heterotrophic) respiration over canopy/root (autotrophic) respiration. *Hogberg et al.* [2001] show that there is a significant autotrophic component to soil respiration linked to

photosynthesis. In SiB2, all soil respiration is heterotrophic and dependent only upon soil temperature and moisture [*Denning et al.,* 1996]. Hogberg and others [*Waring et al.,* 1985; *Gifford et al.,* 2003] suggest it is not uncommon for half of soil respiration to be autotrophic, and directly linked to recently assimilated carbon.We have now partitioned respiration into heterotrophic and autotrophic components. Heterotrophic respiration follows *Denning et al.* [1996]. Canopy respiration associated with the maintenance of leaf photosynthetic enzyme infrastructure is currently included in the model formulation; instantaneous root and stem respiration is calculated as

$$R_a = R_{fa} f_{par} + R_c \tag{5.10}$$

where

R_a = root and stem autotrophic respiration

R_{fa} = autotrophic respiration factor

f_{par} = fraction of photosynthetically active radiation absorbed

R_c = autotrophic photosynthetic maintenance respiration

Annual carbon balance is maintained by the computation of the autotrophic respiration factor R_{fa}, as follows:

$$R_{fa} = \frac{f_a \sum GPP - \sum R_c}{\sum f_{par}} \tag{5.11}$$

where

f_a = fractional partition between autotrophic and heterotrophic respiration, currently 0.5

$\sum GPP$ = annual gross primary productivity

$\sum f_{par}$ = annual sum of fraction of photosynthetically active radiation absorbed

$\sum R_c$ = annual photosynthetic maintenance respiration

SiB3 can be utilized with the concurrent R_{fa} respiration, in which case annual carbon flux

will be very close to zero. In a diagnostic CAS configuration, the balance will be to machine precision. However, with a prognostic CAS carbon balance is not achieved until 2 or 3 iterations using concurrent year R_{fa} are run. It is also possible to use the value of R_{fa} calculated at the end of a given year during the subsequent year. This has the result of respiring carbon assimilated in year N during year $N + 1$, which makes intuitive sense.

The use of satellite-derived vegetation phenology in SiB and various datasets used are described in *Sellers et al.* [1996b]. The convention in SiB was to assign the termporal location of the reported NDVI to the midpoint of the compositing period. This can be problematic in regions with a large annual phenological cycle. When a monthly compositing period is used, it is not uncommon for the maximum value to occur at the end of the month in spring, when leaf-out occurs. Similarly, maximum canopy greenness can be observed at the beginning of the compositing period in the fall. By assigning these maximum values to the midpoint of the compositing period, spring bud burst/leaf-out can be 'moved forward' in time (or earlier in the year) and senescence 'moved back' (later), resulting in an increase in the length of growing season. In fact, a common characteristic of SiB2 was an early conversion from efflux to influx of CO_2 in the annual cycle modeled in boreal regions [*Baker et al.*, 2003]. By evaluating the trend of the NDVI timeseries we are able to determine whether the canopy is static, greening or browning during a particular compositing period and assign the observed value to the appropriate location (beginning, middle, end) accordingly.

Carbon assimilation, and by extension transpirational latent heat flux, is materially controlled by soil water stress. Since its inception [*Sellers et al.*, 1986] SiB has scaled photosynthesis by a soil water stress factor based on observations taken in corn [*Choudhury et al.*, 1983; *Sellers et al.*, 1989; *Collatz et al.*, 1991]. A stress factor value of one implies no stress to photosynthesis, and a stress factor value of zero is associated with total stress and closure of stomates. The soil water stress factor is based on how root zone soil water potential (calculated following*Clapp and Hornberger* [1978]) is related to a pre-defined moisture potential value identified with a stress value of 0.5 using the following relationship

$$stress_{soilmoisture} = \frac{1.0}{\{1.0 + exp\,[0.02\,(\psi_h - \psi_r)]\}} \tag{5.12}$$

where

ψ_h=1/2-stress moisture potential value

ψ_r=moisture potential of root zone

In practice, this formulation resulted in very little soil moisture stress on photosynthesis/transpiration until root zone moisture potential approaches the 1/2-stress value, at which time soil moisture stress increases exponentially. This has the effect of a stepwise function, whereby canopy function is unaffected by soil moisture stress until a critical value is reached and stomates close rapidly with incremental decrease in soil moisture thereafter. This has been shown realistic in individual plants [*Choudhury et al.*,1983], but heterogeneity on the landscape scale can be expected to encompass a range of soil moisture potential across topographical gradients. A distribution of moisture amount within a model gridcell can be envisioned [*Sellers et al.*, 2007], which would result in an integrated response to overall drying on the canopy scale.

We've modified soil moisture stress in SiB3 to give smoother behavior as the soil dries. There is more stress at higher soil moisture values (near field capacity), but the stepwise behavior at critical soil potential has been removed. As previously mentioned, the soil configuration in SiB3 has been modified; soil moisture and soil temperature layers are co-located, and roots are no longer confined to a single layer (soil moisture layer 2 as in SiB2), but are distributed exponentially through the column dependent on biome type as described in *Jackson et al.* [1996] and *Canadell et al.* [1996]. This allows consideration of the entire column when calculating soil water stress on photosynthesis. However, if water availability is a function of root density alone, model vegetation is unrealistically stressed. Several mechanisms have been observed that allow vegetation to utilize water from deep sources when surface layers (where the greatest root mass resides) desiccate, including increased conductance of deep roots [*Jipp et al.*, 1998] and hydraulic redistribution [*Dawson et al.*, 1993, 1996; *Lee et al.*, 2005]. We have not explicitly parameterized these processes, but instead have

created a 'modified bucket'-type simulation that provides reasonable results [*Baker et al.*, 2008].

We assume total stress when moisture contents drops to or below wilt point, no stress when moisture content is at or above field capacity. We use -15 J/kg for field capacity, -1500 J/kg for wilt point. The calculation is looped through the entire soil column, so the calculation of stress is made without consideration of root density as long as roots are present in a given layer. A curvature parameter is used to give a smooth transition into stress as the soil dries, in the following manner

$$stress_{soilmoisture} = \frac{\left[(1+ws)\left(\frac{\theta_{soil}-\theta_{wp}}{\theta_{fc}-\theta_{wp}}\right)\right]}{\left[ws+\left(\frac{\theta_{soil}-\theta_{wp}}{\theta_{fc}-\theta_{wp}}\right)\right]} \tag{5.13}$$

where

ws=curvature parameter (currently =0.2)

θ_{soil}=column-total volumetric soil water content (m^3water per m^3soil)

θ_{wp}=column-total volumetric soil water content at wilt point (m^3water per m^3soil)

θ_{fc}=column-total volumetric soil water content at field capacity (m^3water per m^3soil)

Actual root distribution is not considered during the calculation of soil water stress. When transpirational load is partitioned among individual soil levels, a relative root fraction for each soil layer is calculated as follows

$$rootr_i = rootf_i \frac{\left(1-\frac{\theta_{wp}}{\theta_i}\right)}{\left(1-\frac{\theta_{wp}}{\theta_{fc}}\right)} \tag{5.14}$$

where rootf$_i$ is the actual root density for the layer being considered, and $\theta_i$is the volumetric soil content of that layer. All values of $rootr$ are normalized by dividing by the summation of $rootr$ over all soil levels. This formulation allows an individual soil layer to remove water during transpiration in excess of the amount allowed by the actual root density if the layer holds sufficient water. When volumetric soil water content is equal among layers, water is removed proportional to actual root density. This allows the more realistic response of transpirational load shifting to deep layers when surface layers dry out following rainfall. After an infiltration event, surface layers with

the greater root mass will reacquire the burden of removing water for transpiration.

Photosynthesis is constrained in SiB by high- and low-temperature stress [*Sellers et al.*, 1987; *Collatz et al.*, 1991], but the low-temperature stress did not have a lasting impact; as soon as temperature increased, canopy function was returned to normal levels. A lingering 'frost stress' has been observed [*Vogg et al.*, 1998a, 1998b; *Strand et al.*, 1995; *Hallgren et al.*, 1990] in vegetation that is seasonally exposed to very low temperatures. Frost stress generally refers to biochemical mechanisms vegetation uses to cope with ice formation and dehydration of tissues. *Vogg et al.* [1998a] show that the slowdown in photosynthesis that accompanies these coping mechanisms can last for several days following a cold episode. We have developed a simple approximation of frost stress, which uses a simple relationship between canopy temperature and minimum air temperature in the following manner

$$stress_{frost} = \frac{1}{[1 + exp\,(0.6\,(T_{ref} - T_{min}))]} \tag{5.15}$$

where

$stress_{frost}$=frost stress factor, similar to soil water or temperature stress; a value of 1 implies no stress, 0 implies total shutdown of photosynthesis.

T_{ref}=Reference temperature, 269.15 K

T_{min}=Minimum vegetation temperature

The minimum vegetation temperature is retained as the model moves forward in time, with a relaxation of 4 (degrees) K day^{-1}. This forces an extended period of stress with extreme cold, and disallows brief periods of photosynthetic uptake during warm intervals in winter (in evergreen forests).

Discrimination and fractionation of isotopes during biophysical processes can be a powerful tool for partitioning carbon flux into its component parts. *Ciais et al.* [1995a, 1995b] used δ C measurements to partition global carbon flux into its terrestrial and oceanic fractions. In [*Ciais et al.*, 1995a] a primitive treatment of discrimination of carbon isotopes during photosynthesis was in-

corporated into SiB. With more measurements and greater physical realism in our models, isotopes become a tool to use to further constrain our models and tighten our understanding of surface-atmosphere exchange. Modeled variability of the carbon isotope ratios of CO_2 fluxes between the terrestrial biosphere and the atmosphere can be used to infer the spatial and temporal distribution of carbon sources and sinks *Ciais et al.*, 1995a; *Enting et al.*, 1995; *Francey et al.*, 1995; *Keeling et al.*, 1995; *Joos et al.*, 1998; *Trudinger et al.*, 1999, *Battle et al.*, 2000]. Understanding of the variability inherent to carbon isotope discrimination associated with photosynthesis can also help in interpreting observed δ13C ratios of other plant fractions and fluxes including plant tissues and decomposition products, volatile organic carbon (VOC), exudates, soil litter, humic and fulvic fractions, dissolved organic matter (DOC), and even kerogen and bitumen.

In SiB3, carbon isotope discrimination by C3 plants is modeled as a multistage process involving transport of CO_2 to the chloroplast, followed by fixation with ribulose bisphosphate carboxylase/oxygenase (Rubisco) [*Suits et al.*, 2005]. Net discrimination against ^{13}C is produced by factors affecting rates of photosynthesis and leaf conductance. C3 discrimination is approximately 19 ‰, but can vary a couple of per mil in response to environmental changes such as vapor pressure deficit. The source of assimilated carbon in SiB is the air in the canopy. Since concentrations and isotope ratios of CO_2 of the canopy air space are determined explicitly, the δ^{13}C values of plant carbon will reflect recycling of isotopically depleted respired carbon dioxide and the impact of photosynthesis on carbon isotope ratios in the canopy air. Carbon isotope discrimination by C4 plants is held constant to the value associated with stomatal conductance, 4.4‰. Net discrimination by all plants within a grid cell is largely controlled by the relative contributions of C3 and C4 plants to total photosynthetic rates.

5.3 Numerical Scheme

Here we present the equation set used in version 3.0 of the Simple Biosphere model, SiB3. The fundamental equations are introduced in Sellers (1986) and Sellers et al (1996), and the prognostic canopy air space is outlined in Vidale and Stockli (2004). In this document we'll go into

more detail-starting with the prognostic variables and the equations used to increment them through the numerical technique and the order of operations used to perform the timestepping. The idea here is to show the continuous equations that SiB is based upon and expand the description of the numerical scheme beyond what is normally done in journal articles. However, this description is not comprehensive-there are details that will be ignored, such as adjustment to vapor flux deposition on a cold snow surface or the effect near-surface relative humidity on latent heat flux from the soil. There are numerous details like this in the code, and most of them won't be covered here.

The prognostic variables in SiB represent the condition of the vegetation, air, and soil. The main prognostic variables are:

- Reference level Temperature, T_m
- Reference level water vapor pressure, e_m

(NOTE: The domain of SiB is the ground through the approximate top of the canopy. For numerical stability in incorporating the prognostic canopy airspace, we've had to put a lower limit on canopy depth of 4 meters. What we call the 'reference level' is the atmosphere above the level of the canopy, usually the boundary layer. Reference level variables will come from the lowest model level in a situation where SiB is coupled to a mesoscale model or GCM. In an offline situation, as is described here, the reference level variables will be provided by observations.)

Prognostic variables, continued:

- Canopy air space temperature, T_a
- Canopy air space water vapor pressure, e_a
- Canopy air space CO_2 concentration, $pco2ap$
- Vegetation temperature, T_c
- Vegetation stomatal resistance rst
- Soil temperature, T_s

- Snow temperature, T_{snow}
- Soil liquid water, www_{liq}
- Soil ice water, www_{ice}
- Canopy water interception storage, $capac_1$
- Soil surface water interception storage, $capac_2$ (puddles)

The number of soil layers is user-specified, usually 10. Additionally, up to 5 snow layers can exist: There are prognostic variables for temperature, liquid and ice water for each snow layer, in addition to thickness. The snow and soil treatment in SiB3 is based on CLM (Dai *et al*, 2003). Partial snow cover is problematic for numerical treatments such as SiB; the snow amount never covers all the ground in a gridcell, so in snow-covered situations there are issues with the partitioning of intercepted radiation as well as with heat flux. In a particular grid cell with partial snow cover, it is obvious that the bare (no snow) portion of the top soil layer will have a different temperature (and other state variables) than the snow-covered area. We do not currently treat this sort of sub-grid scale heterogeneity explicitly; our solution is to make the assumption that if snow is present, all incident radiation will be intercepted by the snow-all soil is treated as snow-covered. As the fraction of snowcover increases quickly with snow depth, this is not a *completely* unphysical solution, but we are aware that problems exist in this area.

All prognostic variables are solved in groups of simultaneous equations. The Canopy Air Space (CAS) variables, vegetation (temperature and stomatal resistance) and soil temperature are solved as one group. Precipitation is then added, followed by canopy interception,throughfall, and infiltration. The soil moisture variables are then solved as a group. Phase change in soil water represents a mechanism whereby the previously calculated soil temperature values can be changed.

Presently, we are considering the 'offline' or data-driven version of SiB3-not coupled to a mesoscale atmospheric model or GCM. In the offline case, the prognostic variables T_m and e_m are not effected by the SiB fluxes (since they are prescribed), and have simple representations in the solution matrix.

We'll begin by outlining the continuous equations for the prognostic variables, and describing the fluxes that contribute to their values.

5.3.1 Canopy air space temperature, T_a

$$C_a \frac{dT_a}{dt} = H_c + H_m + H_g + H_s \tag{5.16}$$

Where

$C_a =$ CAS heat capacity

$T_a =$ CAS temperature

$H_c =$ Canopy-CAS sensible heat flux

$H_m =$ boundary layer-CAS sensible heat flux

$H_g =$ ground-CAS sensible heat flux

$H_s =$ snow-CAS sensible heat flux

5.3.2 Canopy air space water vapor mixing ratio, e_a

$$\frac{\rho c_p \Delta z}{\gamma} \frac{de_a}{dt} = \lambda E_c + \lambda E_g + \lambda E_s + \lambda E_m \tag{5.17}$$

where

$\rho =$ air density

$c_p =$ specific heat of air at constant pressure

$\Delta z =$ Canopy Air Space thickness in meters

$\gamma =$ psychrometric constant

$\lambda E_c =$ vegetation-to-CAS water vapor flux

$\lambda E_g =$ ground-to-CAS water vapor flux

$\lambda E_s =$ snow-to-CAS water vapor flux

$\lambda E_m =$ boundary layer-to-CAS water vapor flux

5.3.3 *Vegetation temperature,* T_c

$$C_c \frac{dT_c}{dt} = R_{veg} - H_c - \lambda E_c \tag{5.18}$$

where

$C_c =$ vegetation heat capacity

$R_{veg} =$ net radiation absorbed by vegetation

$H_c =$ vegetation-to-CAS sensible heat flux

$\lambda E_c =$ vegetation-to-CAS latent heat flux

Vegetation-to-CAS latent heat flux is comprised of transpiration and evaporation/condensation from leaf surfaces. R_{veg} contains both thermal IR and solar radiation components.

5.3.4 *Ground temperature,* T_g

$$C_g \frac{dT_g}{dt} = R_{ground} - H_g - \lambda E_g - G \tag{5.19}$$

Where

$C_g =$ ground heat capacity

$R_{ground} =$ net radiation absorbed by ground

$H_g =$ ground-to-CAS sensible heat flux

$\lambda E_g =$ ground-to-CAS latent heat flux

$G =$ ground sensible heat flux

As with canopy latent heat flux, the ground latent heat flux has two components: evaporation/condensation to/from the ground surface, and evaporation/condensation from within the top soil layer.

5.3.5 Soil temperature and soil moisture

SiB3.0 follows CLM (version 2.0, I think) in its treatment of soil and snow. We'll avoid addressing the topic here, as the continuous equations and numerical scheme are outlined in the CLM Technical Manual.

5.3.6 stomatal resistance

SiB uses Farquhar kinetics and the Ball-Berry equation to prognose stomatal resistance (or conductance, if you prefer). Descriptions of these calculations can be found in Sellers *et al* (1986, 1992, 1996) and Sellers (1985, 1987).

5.3.7 Canopy and Ground interception water storage

Interception storage on vegetation and in puddles on the ground are determined at the end of the timestep in SiB. Predetermined storage limits are used, and excess storage can become runoff. The prognostic equations for interception stores are simply the sum of inputs (precipitation) and outputs (runoff, infiltration, evaporation).

5.4 Radiative Scheme

The SiB radiative scheme is explained in detail in the series of SiB papers (Sellers (1985), Sellers et al (1986), Sellers (1987), Sellers et al (1992), and Sellers et al (1996)). The basic idea is that the two-stream approximation (Goudriaan 1977) is used to differentiate between visible and near-IR wavelength intervals, as their broad-band scattering coefficients are quite different. Canopy

penetration and absorbtion are expressed in the standard exponential form, e^{-kL_t}, where k is the extinction coefficient and L_t is leaf area index. The calculations of albedo and radiative transfer are explained in detail in the aforementioned papers, and won't be reproduced here. For this paper, we need to be concerned with longwave radiation, both intercepted and emitted, from the ground surface and the canopy. These terms will be part of the prognostic equations for T_c and T_g, so a little more explanation is warranted. A 'canopy gap fraction' is calculated as $fac1 = 1 - R_{interceped}$, and this factor is used in calculating what fraction of outgoing longwave from the ground is intercepted by the canopy. Similarly, the canopy radiates longwave energy towards the ground and into the atmosphere. We use the Stefan-Boltzmann law

$$I = \varepsilon_{IR}\sigma_{SB}T^4 \tag{5.20}$$

where

I =emitted radiation

ε_{IR} = infrared emissivity

σ_{SB} = Stefan-Boltzmann constant

and its derivative with respect to temperature

$$\frac{dI}{dT} = 4\varepsilon_{IR}\sigma_{SB}T^3 \tag{5.21}$$

or, discretized

$$\Delta I = 4\varepsilon_{IR}\sigma_{SB}T^3(T^{n+1} - T^n) \tag{5.22}$$

In SiB, the net shortwave radiation terms are calculated using the radiative transfer scheme as outlined in the various SiB publications. Change in outgoing and intercepted longwave for canopy and ground are included in the prognostic equations, as will be shown in subsequent sections of this document.

5.5 Canopy Air Space Temperature

Now let's go into more depth. We'll start with Canopy Air Space (CAS) temperature, T_a.

$$C_a \frac{dT_a}{dt} = H_c + H_m + H_g \tag{5.23}$$

or

$$C_a \frac{dT_a}{dt} - H_c - H_m - H_g = 0 \tag{5.24}$$

Where

$C_a =$ CAS heat capacity

$T_a =$ CAS temperature

$H_c =$ Canopy-CAS sensible heat flux

$H_m =$ CAS-boundary layer sensible heat flux

$H_g =$ ground-CAS sensible heat flux

We now define the component sensible heat fluxes, H_c, H_m, H_g as:

$$H_c = \frac{\rho c_p}{r_b}(T_c - T_a) \tag{5.25}$$

$$H_m = \frac{\rho c_p}{r_a}(T_m - T_a) \tag{5.26}$$

$$H_c = \frac{\rho c_p}{r_d}(T_g - T_a) \tag{5.27}$$

Where

$\rho =$ air density

$c_p =$ specific heat of air at constant pressure

$r_a =$ CAS-to-reference level resistance

$r_b =$ leaf surface-to-CAS resistance

$r_d =$ ground-to-CAS resistance

$T_c =$ leaf (vegetation) temperature

$T_g =$ ground surface temperature

$T_m =$ reference level temperature

Following Kalnay and Kanamitsu (1988), we utilize an 'explicit coefficient/implicit temperature' numerical scheme, where the temperatures on the right hand side of the equations exist at timestep 'n+1'. The 'explicit coefficient' part of the equation comes from the fact that the resistance terms (r_a, r_b, r_d) are computed at timestep 'n'. The continuous equations of the component fluxes are discretized as follows:

$$H_c = \frac{\rho c_p}{r_b}({T_c}^{n+1} - {T_a}^{n+1}) \tag{5.28}$$

$$H_m = \frac{\rho c_p}{r_a}({T_m}^{n+1} - {T_a}^{n+1}) \tag{5.29}$$

$$H_g = \frac{\rho c_p}{r_d}({T_g}^{n+1} - {T_a}^{n+1}) \tag{5.30}$$

and the full equation becomes

$$C_a\frac{{T_a}^{n+1} - {T_a}^{n}}{\Delta t} - \frac{\rho c_p}{r_b}({T_c}^{n+1} - {T_a}^{n+1}) - \frac{\rho c_p}{r_a}({T_m}^{n+1} - {T_a}^{n+1}) - \frac{\rho c_p}{r_d}({T_g}^{n+1} - {T_a}^{n+1}) = 0 \tag{5.31}$$

We now define 'timestep n' fluxes for H_c, H_m and H_g as follows

$${H_c}^{n} = \frac{\rho c_p}{r_b}({T_c}^{n} - {T_a}^{n}) \tag{5.32}$$

$${H_m}^{n} = \frac{\rho c_p}{r_a}({T_m}^{n} - {T_a}^{n}) \tag{5.33}$$

$${H_g}^{n} = \frac{\rho c_p}{r_d}({T_g}^{n} - {T_a}^{n}) \tag{5.34}$$

and add them to both sides of (5.31) and the full equation becomes

$$\begin{aligned} C_a\frac{{T_a}^{n+1} - {T_a}^{n}}{\Delta t} - \frac{\rho c_p}{r_b}({T_c}^{n+1} - {T_a}^{n+1}) + \frac{\rho c_p}{r_b}({T_c}^{n} - {T_a}^{n}) - \\ \frac{\rho c_p}{r_a}({T_m}^{n+1} - {T_a}^{n+1}) + \frac{\rho c_p}{r_a}({T_m}^{n} - {T_a}^{n}) - \\ \frac{\rho c_p}{r_d}({T_g}^{n+1} - {T_a}^{n+1}) + \frac{\rho c_p}{r_d}({T_g}^{n} - {T_a}^{n}) = \\ {H_c}^{n} + {H_m}^{n} + {H_g}^{n} \end{aligned} \tag{5.35}$$

For the solution, we want to group the terms around ${T_x}^{n+1} - {T_x}^n$. We will then solve for these 'delta' terms in the solution matrix. Rearranging (5.35), we obtain

$$\begin{aligned}({T_a}^{n+1} - {T_a}^n)(\frac{C_a}{\Delta t} + \frac{\rho c_p}{r_b} + \frac{\rho c_p}{r_a}) - ({T_c}^{n+1} - {T_c}^n)(\frac{\rho c_p}{r_b}) - \\ ({T_m}^{n+1} - {T_m}^n)(\frac{\rho c_p}{r_a}) - ({T_g}^{n+1} - {T_g}^n)(\frac{\rho c_p}{r_d}) = \\ {H_c}^n + {H_m}^n + {H_g}^n \end{aligned} \tag{5.36}$$

Keeping in mind that we are considering the 'no snow' case here, so there will be 15 prognostic variables solved for in this particular matrix:

1. $T_m =$ reference level temperature

2. $e_m =$ reference level water vapor mixing ratio

3. $T_a =$ Canopy Air Space temperature

4. $e_a =$ Canopy Air Space water vapor mixing ratio

5. $T_c =$ leaf (vegetation) temperature

6. $T_g =$ ground surface layer temperature

$7 - 15$. $T_i =$ deep soil layer temperatures, $(i = 2, 10)$

In the situation where snow is present, there will be from one to five extra snow temperature layers. Snow/soil liquid water is currently treated in a separate matrix equation. Therefore, we will be solving a $15x15$ matrix to update these particular prognostic variables. We will designate the right hand side of (5.36) as F_{T_a}, the part of the equation containing the timestep n terms. The terms for CAS temperature T_a will then be:

1. $T_m = -\frac{\rho c_p}{r_a}$

2. $e_m = 0$

3. $T_a = \frac{C_a}{\Delta t} + \frac{\rho c_p}{r_b} + \frac{\rho c_p}{r_a}$

4. $e_a = 0$

5. $T_c = -\frac{\rho c_p}{r_b}$

6. $T_g = -\frac{\rho c_p}{r_d}$

$7 - 15.\ T_i = 0$

$F_{T_a} = {H_c}^n + {H_m}^n + {H_g}^n$

In the snow case, the solution will not be much different. Partial snowcover is a difficult problem, and for the moment we punt on the solution. What we do in SiB3 is to say that if there is *any* snow, then the ground is treated as *completely* covered by the energy budget equations. We do not partition radiation incident on the surface between bare- and snow-covered fractions; all radiation is intercepted by the snow-covered surface. While potentially unrealistic, this technique has provided reasonable results to date.

5.6 Canopy Air Space Water Vapor Pressure

Now let's look at e_a, CAS water vapor pressure. The continuous equation is as follows:

$$\frac{\rho c_p \Delta z}{\gamma} \frac{de_a}{dt} = \lambda E_c + \lambda E_g + \lambda E_m \tag{5.37}$$

where

$\Delta z =$ Canopy Air Space thickness in meters

$\gamma =$ psychrometric constant

The evaporation term λE_m represents the water vapor flux between the CAS and the boundary layer, and is dependent only upon the resistance (r_a) between the two layers, as well as the vapor gradient. The other two terms $(\lambda E_c, \lambda E_g)$ have multiple components. the vapor flux between the vegetation and the CAS (λE_c) is a result of transpirational vapor flux as well as evaporation of water stored on the leaves themselves (i.e. dew, accumulated rain). It is assumed that there will be no

transpiration from a wet leaf surface. Evaporation of surface storage (puddles) as well as evaporation from within the top soil layer are combined into ground-to-CAS water vapor flux(λE_g). The continuous equations for these three components are as follows:

$$\lambda E_m = \frac{\rho c_p}{\gamma r_a}(e_m - e_a) \tag{5.38}$$

$$\lambda E_c = \frac{\rho c_p}{\gamma}\Big(\frac{wc}{r_b} + \frac{(1-wc)}{r_{can}}\Big)(e^*(T_c) - e_a) \tag{5.39}$$

$$\lambda E_g = \frac{\rho c_p}{\gamma}\Big(\frac{wg}{r_d} + \frac{(1-wg)}{r_{soil}}\Big)(e^*(T_g) - e_a) \tag{5.40}$$

Following what was done for T_a, we define the component vapor fluxes as follows:

$$\lambda E_m = \frac{\rho c_p}{\gamma r_a}({e_m}^{n+1} - {e_a}^{n+1}) \tag{5.41}$$

$$\lambda E_c = \frac{\rho c_p}{\gamma}\Big(\frac{wc}{r_b} + \frac{(1-wc)}{r_{can}}\Big)(e^*({T_c}^{n+1}) - {e_a}^{n+1}) \tag{5.42}$$

$$\lambda E_g = \frac{\rho c_p}{\gamma}\Big(\frac{wg}{r_d} + \frac{(1-wg)}{r_{soil}}\Big)(e^*({T_g}^{n+1}) - {e_a}^{n+1}) \tag{5.43}$$

To calculate the saturation vapor pressure (e^*) terms at timestep $(n+1)$, we take the derivative of the Clausius-Clapyron equation at temperature T_x^n and assume the following:

$$e^*(T^{n+1}) = e^*(T^n) + \frac{de^*(T)}{dT}(T^{n+1} - T^n) \tag{5.44}$$

Now equations (5.42), (5.43) become

$$\lambda E_c = \frac{\rho c_p}{\gamma}\Big(\frac{wc}{r_b} + \frac{(1-wc)}{r_{can}}\Big)\Big(e^*({T_c}^n) + \frac{de^*(T_c)}{dT_c}({T_c}^{n+1} - {T_c}^n) - {e_a}^{n+1}\Big) \tag{5.45}$$

$$\lambda E_g = \frac{\rho c_p}{\gamma}\Big(\frac{wg}{r_d} + \frac{(1-wg)}{r_{soil}}\Big)\Big(e^*({T_g}^n) + \frac{de^*(T_g)}{dT_g}({T_g}^{n+1} - {T_g}^n) - {e_a}^{n+1}\Big) \tag{5.46}$$

Substituting (5.41),(5.45),and (5.46) back into (5.37) yields

$$\frac{\rho c_p \Delta z}{\gamma}\frac{({e_a}^{n+1}-{e_a}^{n})}{\Delta t} = \frac{\rho c_p}{\gamma r_a}({e_m}^{n+1}-{e_a}^{n+1}) + \frac{\rho c_p}{\gamma}\Big(\frac{wc}{r_b}+\frac{(1-wc)}{r_{can}}\Big)\Big(e^*({T_c}^n)+\frac{de^*(T_c)}{dT_c}({T_c}^{n+1}-{T_c}^n)-{e_a}^{n+1}\Big) + \frac{\rho c_p}{\gamma}\Big(\frac{wg}{r_d}+\frac{(1-wg)}{r_{soil}}\Big)\Big(e^*({T_g}^n)+\frac{de^*(T_g)}{dT_g}({T_g}^{n+1}-{T_g}^n)-{e_a}^{n+1}\Big) \quad (5.47)$$

Add $\lambda {E_m}^n$, $\lambda {E_c}^n$ and $\lambda {E_g}^n$ to both sides, rearrange and cancel some terms to obtain

$$({e_a}^{n+1}-{e_a}^{n})\Big(\frac{\rho c_p \Delta z}{\gamma \Delta t}+\frac{\rho c_p}{\gamma r_a}+\frac{\rho c_p}{\gamma}\Big(\frac{wc}{r_b}+\frac{(1-wc)}{r_{can}}\Big)+\frac{\rho c_p}{\gamma}\Big(\frac{wg}{r_d}+\frac{(1-wg)}{r_{soil}}\Big)\Big) - ({e_m}^{n+1}-{e_m}^{n})\frac{\rho c_p}{\gamma r_a} - ({T_c}^{n+1}-{T_c}^{n})\frac{de^*(T_c)}{dT_c}\Big(\frac{\rho c_p}{\gamma}\Big(\frac{wc}{r_b}+\frac{(1-wc)}{r_{can}}\Big)- ({T_g}^{n+1}-{T_g}^{n})\frac{de^*(T_g)}{dT_g}\Big(\frac{\rho c_p}{\gamma}\Big(\frac{wg}{r_d}+\frac{(1-wg)}{r_{soil}}\Big) = \lambda {E_m}^n+\lambda {E_c}^n+\lambda {E_g}^n \quad (5.48)$$

If we look at the e_a equation term-by-term as was done for T_a, the values are these:

1. $T_m = 0$
2. $e_m = -\frac{\rho c_p}{\gamma r_a}$
3. $T_a = 0$
4. $e_a = \frac{\rho c_p \Delta z}{\gamma \Delta t}+\frac{\rho c_p}{\gamma r_a}+\frac{\rho c_p}{\gamma}\Big(\frac{wc}{r_b}+\frac{(1-wc)}{r_{can}}\Big)+\frac{\rho c_p}{\gamma}\Big(\frac{wg}{r_d}+\frac{(1-wg)}{r_{soil}}\Big)$
5. $T_c = -\frac{de^*(T_c)}{dT_c}\Big(\frac{\rho c_p}{\gamma}\Big(\frac{wc}{r_b}+\frac{(1-wc)}{r_{can}}\Big)$
6. $T_g = -\frac{de^*(T_g)}{dT_g}\Big(\frac{\rho c_p}{\gamma}\Big(\frac{wg}{r_d}+\frac{(1-wg)}{r_{soil}}\Big)$

$7-15.\ T_i = 0$

$F_{e_a} = \lambda {E_m}^n+\lambda {E_c}^n+\lambda {E_g}^n$

5.7 Vegetation Temperature

Vegetation (leaf) temperature is a balance between absorbed radiation and latent and sensible heat fluxes. Stomatal resistance determines potential evapotranspiration, and therefore the Bowen Ratio of the fluxes from the leaf to the CAS. From the Introduction, we have the continuous equation as follows:

$$C_c \frac{dT_c}{dt} = R_{veg} - H_c - \lambda E_c \tag{5.49}$$

We can represent the sensible heat flux between the vegetation and the CAS as

$$H_c = \frac{\rho c_p}{r_b}(T_c - T_a) \tag{5.50}$$

and the latent heat flux-which contains terms for both evaporation of interception storage and transpiration-as

$$\lambda E_c = \frac{\rho c_p}{\gamma}\Big(\frac{wc}{r_b} + \frac{(1-wc)}{r_{canopy}}\Big)\Big(e^*(T_c) - e_a\Big) \tag{5.51}$$

where

$wc =$ wet fraction of the canopy

$r_{canopy} =$total canopy resistance ($r_b + r_{stomatal}$)

Specifying (5.50) and (5.51) at timestep $n+1$ and substituting back into (5.49) yields

$$C_c \frac{{T_c}^{n+1} - {T_c}^{n}}{dt} + \frac{\rho c_p}{r_b}({T_c}^{n+1} - {T_a}^{n+1}) + \frac{\rho c_p}{\gamma}\Big(\frac{wc}{r_b} + \frac{(1-wc)}{r_{canopy}}\Big)\Big(e^*({T_c}^{n+1}) - {e_a}^{n+1}\Big) = R_{veg} \tag{5.52}$$

Add ${H_c}^n$ and $\lambda {E_c}^n$ to both sides, expand the $e^*({T_c}^{n+1})$ terms and rearrange to obtain

$$(T_c{}^{n+1} - T_c{}^n)\Big(\frac{C_c}{\Delta t} + \frac{\rho c_p}{r_b} + \frac{de^*(T_c)}{dTc}\big(\frac{\rho c_p}{\gamma}\big(\frac{wc}{r_b} + \frac{(1-wc)}{r_{canopy}}\big) + \frac{\rho c_p}{\gamma r_b}\big)\Big)$$
$$- (T_a{}^{n+1} - T_a{}^n)\frac{\rho c_p}{r_b}$$
$$- (e_a{}^{n+1} - e_a{}^n)\big(\frac{\rho c_p}{\gamma}\big(\frac{wc}{r_b} + \frac{(1-wc)}{r_{canopy}}\big) + \frac{\rho c_p}{\gamma r_b}\big)$$
$$= R_{veg} - H_c{}^n - \lambda E_c{}^n \quad (5.53)$$

We'll now address the R_{veg} term. The basic idea of the radiative scheme is outlined in Section 2; For purposes of the radiative scheme we partition radiation into absorbed atmospheric radiation (shortwave and longwave), absorbed longwave emitted from the ground, and outgoing longwave emitted from the vegetation itself. For the ground and canopy longwave terms, we'll be using the $fac1$ term defined in Section 2 to describe the 'canopy hole' or fraction of canopy closure. Expanding the R_{veg} term, we can say

$$R_{veg} = R_{atmospheric} - LW_{veg} + LW_{ground} \quad (5.54)$$

The $R_{atmospheric}$ term is calculated to exist at timestep n, while the two longwave terms are defined at timestep $n+1$ and can be discretized as follows:

$$LW_{veg} = 2fac1(4\varepsilon_{IR}\sigma_{SB}T_c{}^3(T_c{}^{n+1} - T_c{}^n)) \quad (5.55)$$

and

$$LW_{ground} = fac1(4\varepsilon_{IR}\sigma_{SB}T_g{}^3(T_g{}^{n+1} - T_g{}^n)) \quad (5.56)$$

Where (5.55) is multiplied by two to account for longwave radiation exiting the canopy in both upward and downward directions. Equation (5.53) now becomes

$$(T_c{}^{n+1} - T_c{}^n)\Big(\frac{C_c}{\Delta t} + \frac{\rho c_p}{r_b} + \frac{de^*(T_c)}{dTc}\big(\frac{\rho c_p}{\gamma}(\frac{wc}{r_b} + \frac{(1-wc)}{r_{canopy}})\big) + 2fac1(4\varepsilon_{IR}\sigma_{SB}T_c{}^3)\Big)$$
$$- (T_a{}^{n+1} - T_a{}^n)\frac{\rho c_p}{r_b}$$
$$- (e_a{}^{n+1} - e_a{}^n)\big(\frac{\rho c_p}{\gamma}(\frac{wc}{r_b} + \frac{(1-wc)}{r_{canopy}})\big)$$
$$- (T_g{}^{n+1} - T_g{}^n)4fac1\varepsilon_{IR}\sigma_{SB}T_g{}^3$$
$$= R_{atmospheric} - H_c{}^n - \lambda E_c{}^n \quad (5.57)$$

So the matrix terms for T_c are

1. $T_m = 0$

2. $e_m = 0$

3. $T_a = -\frac{\rho c_p}{r_b}$

4. $e_a = -\frac{\rho c_p}{\gamma}(\frac{wc}{r_b} + \frac{(1-wc)}{r_{canopy}})$

5. $T_c = \frac{C_c}{\Delta t} + \frac{\rho c_p}{r_b} + \frac{de^*(T_c)}{dTc}\big(\frac{\rho c_p}{\gamma}(\frac{wc}{r_b} + \frac{(1-wc)}{r_{canopy}})\big) + 2fac1(4\varepsilon_{IR}\sigma_{SB}T_c{}^3)$

6. $T_g = -4fac1\varepsilon_{IR}\sigma_{SB}T_g{}^3$

$7 - 15$. $T_i = 0$

$F_{T_c} = R_{atmospheric} - H_c{}^n - \lambda E_c{}^n$

5.8 Ground Surface Temperature

This can be either the top soil surface, or, as mentioned before, the top snow surface when snow layers are present. For convenience, the bare soil case will be shown here. The continuous equation is

$$C_g\frac{dT_g}{dt} = R_{ground} - H_g - \lambda E_g - G \quad (5.58)$$

The sensible heat component of the flux can be represented as

$$H_g = \frac{\rho c_p}{r_d}(T_g - T_a) \tag{5.59}$$

As was the case with vegetation, the latent flux from the ground surface has two components: evaporation from within the top soil layer, and evaporation of surface interception storage (puddles). We can express the latent flux as

$$\lambda E_g = \frac{\rho c_p}{\gamma}\left(\frac{wg}{r_d} + \frac{(1-wg)}{r_{soil}}\right)(e^*(T_g) - e_a) \tag{5.60}$$

Ground heat flux (G) in (5.58) merely represents flux between the surface layer and the layer below. SiB3 has adopted the CLM numerical scheme for soil heat flux, and it will not be described in detail in this document. Briefly, the heat flux across ain interior soil layer interface is

$$F_j = \lambda(z_{h,j})\frac{T_{j+1} - T_j}{z_{j+1} - z_j} \tag{5.61}$$

where

$F_j =$ heat flux from layer j to layer $j+1$

$\lambda(z_{h,j}) =$ thermal conductivity at layer interface

$z_{j+1}, z_j =$ node depths of layers $n+1$, n

Radiation is broken into components in a manner consistent with what was done for vegetation. The amount of atmospheric radiation (shortwave and longwave) that is absorbed by the surface is a function of $(1 - fac1)$, where $fac1$ is the fraction of closure of the canopy. Additional longwave components are downwelling longwave from the vegetation intercepted by the surface, and upwelling longwave from the surface itself. We can express the net radiation of the surface as

$$R_{ground} = R_{atmospheric} + LW_{veg} - LW_{ground} \tag{5.62}$$

where

$$LW_{veg} = fac1(4\varepsilon_{IR}\sigma_{SB}{T_c}^3({T_c}^{n+1} - {T_c}^n)) \tag{5.63}$$

and

$$LW_{ground} = (4\varepsilon_{IR}\sigma_{SB}{T_g}^3({T_g}^{n+1} - {T_g}^n)) \tag{5.64}$$

We can now discretize the soil surface temperature equation as

$$\begin{aligned}\frac{C_g}{\Delta t}(T_g^{n+1} - T_g^n) + \frac{\rho c_p}{r_d}(T_g^{n+1} - T_a^{n+1}) + \frac{\rho c_p}{\gamma}\big(\frac{wg}{r_d} + \frac{(1-wg)}{r_{soil}}\big)(e^*(T_g^{n+1}) - e_a^{n+1}) \\ + (4\varepsilon_{IR}\sigma_{SB}{T_g}^3({T_g}^{n+1} - {T_g}^n)) - fac1(4\varepsilon_{IR}\sigma_{SB}{T_c}^3({T_c}^{n+1} - {T_c}^n)) \\ + \frac{\lambda(z_{h,j})}{z_{j+1} - z_j}(T_{soil2}^{n+1} - T_g^{n+1}) = R_{atmospheric}\end{aligned} \tag{5.65}$$

To gather terms into the 'delta' form used in the previous prognostic equations, we will subtract latent and sensible heat flux at timestep n ($H_g^n, \lambda E_g^n$) from both sides and expand $e^*(T_g^{n+1})$. Additionally, the ground heat flux term from timestep n (G^n)

$$G^n = \frac{\lambda(z_{h,j})}{z_{j+1} - z_j}(T_{soil2}^n - T_g^n) \tag{5.66}$$

must be added to both sides, and rearranged to obtain

$$\begin{aligned}-(T_a^{n+1} - T_a^n)\frac{\rho c_p}{r_d} - (e_a^{n+1} - e_a^n)\Big(\frac{\rho c_p}{\gamma}\big(\frac{wg}{r_d} + \frac{(1-wg)}{r_{soil}}\big)\Big) \\ - ({T_c}^{n+1} - {T_c}^n)4\varepsilon_{IR}\sigma_{SB}{T_c}^3 fac1 \\ + (T_g^{n+1} - T_g^n)\Big(\frac{C_g}{\Delta t} + \frac{\rho c_p}{r_d} + 4\varepsilon_{IR}\sigma_{SB}{T_g}^3 + \frac{de^*(T_g)}{dT_g}\big(\frac{\rho c_p}{\gamma}\big(\frac{wg}{r_d} + \frac{(1-wg)}{r_{soil}}\big)\big) \\ + \frac{\lambda(z_{h,j})}{z_{j+1} - z_j}\Big) = R_{atmospheric} - H_g^n - \lambda E_g^n + G^n\end{aligned} \tag{5.67}$$

So the matrix terms for T_g are

1. $T_m = 0$

2. $e_m = 0$

3. $T_a = -\frac{\rho c_p}{r_d}$

4. $e_a = -\frac{\rho c_p}{\gamma}\left(\frac{wg}{r_d} + \frac{(1-wg)}{r_{soil}}\right)$

5. $T_c = -4\varepsilon_{IR}\sigma_{SB}{T_c}^3 fac1$

6. $T_g = \frac{C_g}{\Delta t} + \frac{\rho c_p}{r_d} + 4\varepsilon_{IR}\sigma_{SB}{T_g}^3 + \frac{de^*(T_g)}{dT_g}\left(\frac{\rho c_p}{\gamma}\left(\frac{wg}{r_d} + \frac{(1-wg)}{r_{soil}}\right)\right) + \frac{\lambda(z_{h,j})}{z_{j+1}-z_j}$

7. $T_2 = \frac{\lambda(z_{h,j})}{z_{j+1}-z_j}$

$8-15.\ T_i = 0$

$F_{T_g} = R_{atmospheric} - H_g^n - \lambda E_g^n + G^n$

5.9 Internal Soil Layers

As previously mentioned, SiB3 follows CLM in its treatment of soil and snow. Therefore, the numerical method won't be examined in detail here. This applies to both soil temperature and soil moisture.

5.10 Matrix Solution

This gives the general impression of how the development of the timestep matrix progresses. We've shown the development of the prognostic variables T_a and e_a, T_c, soil surface temperature T_g, and deep soil temperatures (T_{soil}). Reference level temperature and water vapor mixing ratio (T_m, e_m), will have matrix coefficients of 1.0 when the model is run in 'offline' mode, that is when meteorogical data is used to force the SiB code. When coupled to an atmospheric model, the coefficients will be different. We are currently working with this coupling, as it has changed with the incorporation of the prognostic canopy airspace.

Soil moisture is treated in its own matrix, and is not solved in the main matrix with the other prognostic variables. This separation is intentional, and is done to simplify the calculation(s). Precipitation is added to the SiB3 vegetation following the timestepping of the canopy prognostic variables, interception/throughfall is calculated, and the soil moisture is timestepped following the determination of amount of precipitation intercepted by the ground. While it may be possible to incorporate the precipitation and soil moisture calculations into the 'main' solution matrix, there are a number of complicating factors that make separation desirable, including

- Calculation of interception store amount on vegetation and surface. The energy budget takes the presence of interception storage (water on leaves, puddles on ground) into account, but restricting partition of sensible/latent heat by available depth of storage is not done until after most prognostic variables have been updated in the 'main' matrix. This calculation would become significantly more complex if it were subsumed into the main timestepping matrix along with precipitation interception.

- Water liquid and ice amounts are treated explicitly in SiB3 soil and snow layers. Currently, we calculate phase change after temperatures have been timestepped. Calculating solid and liquid amount, their temperatures, and phase change collectively would be a prodigious task indeed. The process is simplified signifcantly by breaking the calculations into sequential parts.

The augmented matrix for solving the SiB prognostic variables is shown below. We've chosen the simple (no snow) case for illustration; The number of rows and columns will increase by 1 to 5 (based on number of layers) when snow is present.

$$\begin{pmatrix}
T_m & 0 & 0 & 0 & 0 & 0 & 0 & 0 & 0 & 0 & 0 & 0 & 0 & 0 & 0 & 0 \\
0 & e_m & 0 & 0 & 0 & 0 & 0 & 0 & 0 & 0 & 0 & 0 & 0 & 0 & 0 & 0 \\
T_m & 0 & T_a & 0 & T_c & T_g & 0 & 0 & 0 & 0 & 0 & 0 & 0 & 0 & 0 & F_{T_a} \\
0 & e_m & 0 & e_a & T_c & T_g & 0 & 0 & 0 & 0 & 0 & 0 & 0 & 0 & 0 & F_{e_a} \\
0 & 0 & T_a & e_a & T_c & T_g & 0 & 0 & 0 & 0 & 0 & 0 & 0 & 0 & 0 & F_{T_c} \\
0 & 0 & T_a & e_a & T_c & T_g & T_{s01} & 0 & 0 & 0 & 0 & 0 & 0 & 0 & 0 & F_{T_g} \\
0 & 0 & 0 & 0 & 0 & T_g & T_{s02} & T_{s03} & 0 & 0 & 0 & 0 & 0 & 0 & 0 & F_{T_{s02}} \\
0 & 0 & 0 & 0 & 0 & 0 & T_{s02} & T_{s03} & T_{s04} & 0 & 0 & 0 & 0 & 0 & 0 & F_{T_{s03}} \\
0 & 0 & 0 & 0 & 0 & 0 & 0 & T_{s03} & T_{s04} & T_{s05} & 0 & 0 & 0 & 0 & 0 & F_{T_{s04}} \\
0 & 0 & 0 & 0 & 0 & 0 & 0 & 0 & T_{s04} & T_{s05} & T_{s06} & 0 & 0 & 0 & 0 & F_{T_{s05}} \\
0 & 0 & 0 & 0 & 0 & 0 & 0 & 0 & 0 & T_{s05} & T_{s06} & T_{s07} & 0 & 0 & 0 & F_{T_{s06}} \\
0 & 0 & 0 & 0 & 0 & 0 & 0 & 0 & 0 & 0 & T_{s06} & T_{s07} & T_{s08} & 0 & 0 & F_{T_{s07}} \\
0 & 0 & 0 & 0 & 0 & 0 & 0 & 0 & 0 & 0 & 0 & T_{s07} & T_{s08} & T_{s09} & 0 & F_{T_{s08}} \\
0 & 0 & 0 & 0 & 0 & 0 & 0 & 0 & 0 & 0 & 0 & 0 & T_{s08} & T_{s09} & T_{s10} & F_{T_{s09}} \\
0 & 0 & 0 & 0 & 0 & 0 & 0 & 0 & 0 & 0 & 0 & 0 & 0 & T_{s09} & T_{s10} & F_{T_{s10}}
\end{pmatrix}$$

This matrix is currently solved using a freely available software package routine (LAPACK, subroutine dgesv) by LU decomposition with partial pivoting and row exchanges. The solution of this matrix comprises a significant share of SiB3 computing time, so development of more efficient matrix solving techniques is a priority. We have indications that this is an area where efficiency can be increased significantly.

5.11 SiB3 Order of Operations

The following list shows the sequence of operations used in SiB3. This is a rough sketch, not an exhaustive listing. The calculations and their order are:

(1) Albedos via two-stream approximation. Follows Sellers *et al* (1985), appendix A.

(2) Absorption of radiation by surface.

(3) Total radiative balance of canopy, ground and snow.

(4) Initialize model state: includes

- heat capacity and thermal conductivity for canopy and soil/snow
- wetness fractions of leaf and ground surface
- saturation vapor pressures and derivatives of vegetation and ground surface
- soil moisture stress
- soil evaporation resistance

(5) Resistances;

- aerodynamic
- soil-to-CAS
- leaf surface-to-CAS

(6) Determine respiration; follows Denning *et al* (1996)

(7) Canopy conductance and photosynthesis

(8) Partial derivatives of longwave fluxes

(9) Partial derivatives and matrix components of vapor fluxes

(10) Partial derivatives and matrix componenst of sensible heat fluxes

(11) solve main prognostic variable solution matrix

(12) adjust interception stores and energy fluxes

(13) distribute transpiration load among root profile

(14) phase change in soil/snow layers

(15) add precipitation to canopy; determine interception/throughfall

(16) precipitation to surface; infiltration into snow/soil

(17) soil moisture solution matrix; setup and solution

(18) runoff; overland and subsurface

(19) snow layer compaction

(20) snow layer combination/subdivision

(21) check energy/moisture balance

Soil and snow follow CLM, while the photosynthesis follows the traditional SiB methodology with a multiple-physiology (multi-phys) capability built in. Multi-phys allows for multiple physiological types (usually C3/C4, but other capabilities exist) to coexist on the same soil column, and to exchange carbon with the same canopy air. This is important for isotopic calculations.

5.12 List of Symbols

5.12.1 Prognostic Variables

$T_m =$ reference level temperature

$e_m =$ reference level water vapor pressure

$T_a =$ CAS temperature

$e_a =$ CAS water vapor pressure

$T_c =$ leaf (vegetation) temperature

$T_g =$ ground surface temperature

$T_{soil_i} =$ soil temperature, subsurface layers

5.12.2 Energy Fluxes

$H_c =$ Canopy-CAS sensible heat flux

$H_m =$ CAS-boundary layer sensible heat flux

H_g = ground-CAS sensible heat flux

H_s = snow-CAS sensible heat flux

λE_c = vegetation-to-CAS water vapor flux

λE_g = ground-to-CAS water vapor flux

λE_s = snow-to-CAS water vapor flux

λE_m = CAS-to-reference level water vapor flux

5.12.3 Resistance

r_a = CAS-to-reference level resistance

r_b = leaf surface-to-CAS resistance

r_d = ground-to-CAS resistance

$r_{stomatal}$ = stomatal resistance

r_{canopy} =total canopy resistance ($r_b + r_{stomatal}$)

5.12.4 Radiation

$R_{atmospheric}$ = absorbed atmospheric radiation

R_{veg} = net radiation absorbed by vegetation

R_{ground} = net radiation absorbed by ground

I =emitted radiation

ε_{IR} = infrared emissivity

σ_{SB} = Stefan-Boltzmann constant

$fac1$ = canopy closure fraction

5.12.5 Miscellaneous

$C_a =$ CAS heat capacity

$C_c =$ vegetation heat capacity

$C_g =$ ground heat capacity

$\rho =$ air density

$\Delta z =$ Canopy Air Space thickness in meters

$\gamma =$ psychrometric constant

$c_p =$ specific heat of air at constant pressure

$wc =$ wet fraction of the canopy

$wg =$ wet fraction of the ground

BIBLIOGRAPHY

Ackerly, D.D. W.W. Thomas, C.A.C Ferreira, J.R. Pirani, 1989, The forest-=cerrado transition zone in souther Amazonia-results of the 1985 Projeto Flora Amazonica expedition to Mato Grosso. *Brittonia*, *41*(2), 113-128.

Adler, R.F., G.J. Huffman, A. Chang, R. Ferraro, P. Xie, J. Janowiak, B. Rudolf, U. Schneider, S. Curtis, D. Bolvin, A. Gruber, J. Susskind, P. Arkin, and E. Nelkin (2003), The Version 2 Global Precipitation Climatology Project (GPCP) Monthly Precipitation Analysis (1979-Present). *J. Hydrometeor.*, *4*,1147-1167.

Andreae M.O., P. Artaxo, C. Brando, F.E. Carswell, P. Ciccioli, A.L. da Costa, A.D. Culf, J.L. Esteves, J.H.C. Gash, J. Grace, P. Kabat, J. Lelieveld, Y. Malhi, A.O. Manzi, F.X. Meixner, A.D. Nobre, C. Nobre, M.d.L.P. Ruivo, M.A. Silva-Dias, P. Stefani, R. Valentini, J. von Jouanne, M.J. Waterloo (2002),Biogeochemical cycling of carbon, water, energy, trace gases, and aerosols in Amazonia: The LBA-EUSTACH experiments, *J. Geophys. Res.-Atmos.*, *107* (D20): Art. No. 8066.

Aragão, L.E.O.C., Y. Malhi, R.M. Roman-Cuesta, S. Saatchi, L.O. Anderson, Y.E. Shimabukuro, 2007, Spatial patterns and fire response of recent Amazonian droughts. *Geophys. Res. Let.*, *34*, L07701, doi:10.1029/2006GL028946.

Aranibar, J.N., J.A. Berry, W.J. Riley, D.E. Patakis, B.E. Law, J.R. Ehleringer (2006), Combining Meteorology, Eddy Fluxes, Isotope Measurements, and Modeling to Understand Environmental Controls of Carbon Isotope Discrimination at the Canopy Scale. *Glob. Change Biol.*, *12*, 710-730.

Araujo, A.C., A.D. Nobre, B. Kruijt, J.A. Elbers, R. Dallarosa, P. Stefani, C. von Randow, A.O.Manzi, A.D. Culf, J¿H.C. Gash, R. Velentini, P. Kabat, 2002, Comparative measurements of carbon dioxide fluxes from two nearby towers in a central Amazonian rainforest: The Manaus LBA site. *J. Geophys. Res.*, *107*(D20), 8090, doi:10.1029/2001JD000676.

Avissar, R., P.L. Silva Dias, M.A.F. Silva Dias, C. Nobre (2002), The Large-Scale Biosphere-Atmosphere Experiment in Amazonia (LBA): Insights and future research needs. *J. Geophys. Res.*, *107*(D20),8086,doi:10.1029/2002/JD002704.

Avissar, R., Werth, D. (2004) Global Hydroclimatological Teleconnections Resulting from Tropical Deforestation, *J. Hydrometeor.*, *6*, 134-145.

Bacastow, R.B., 1976, Modulation of atmospheric carbon dioxide by the Southern Oscillation. *Nature*, *261*(5), 116-118.

Baker, D.F., R.M. Law, K.R. Gurney, P. Rayner, P. Peylin, A.S. Denning, P Bousquet, L. Bruhwiler, Y.-H. Chen, P. Ciais, I.Y. Fung, M. Heimann, J. John, T. Maki, S. Maksyutov, K. Masarie. M. Prather, B. Pak, I. Taguchi and Z. Zhu, 2006. TransCom 3 inversion intercomparison: Impact of transport model errors on the interannual variability of regions CO2 fluxes, 1988-2003. *Global Biogeochem. Cy.*, **20**, GB1002, doi: 10.1029/2004GB002439.

Baker, I.T., A.S. Denning, N. Hanan, L. Prihodko, P.-L. Vidale, K. Davis and P. Bakwin (2003), Simulated and observed fluxes of sensible and latent heat and CO_2 at the WLEF-TV Tower using SiB2.5. *Glob. Change Biol.*, *9*, 1262-1277.

Baker, I.T., A.S. Denning, L. Prihodko, K. Schaefer, J.A. Berry, G.J. Collatz, N.S. Suits, R. Stöckli, A. Philpott, O. Leonard (2007), Global Net Ecosystem Exchange (NEE) of CO_2, Available on-line [http://www.daac.ornl.gov] from Oak Ridge National Laboratory Distributed Active Archive Center, Oak Ridge, Tennessee, U.S.A.

Baker, I.T., L. Prihodko, A.S. Denning, M. Goulden, S. Millller and H. da Rocha, 2008. Seasonal drought stress in the Amazon: Reconciling models and observations. *J. Geophys. Res.*, **113**, G00B01, doi:10.1029/2007JG000644.

Baker, I.T., R. Stöckli, A.S. Denning, 2010, North American gross primary productivity: regional characterization and interannual variability. *Tellus*, *62B*, 533-549, doi:10.1111/j.1600-0889.2010.00492.x.

Baker, I.T., H.R. da Rocha, N. Restrepo-Coupe, R. Stöckli, L.S. Borma, O.M. Cabral, A.O. Manzi, A.D. Nobre, S.C. Wofsy, S.R. Saleska, M.L. Goulden, S.D. Miller, F.L. Cardoso, A.S. Denning, 2011, Surface ecophysiological behavior across vegetation and moisture gradients in Amazonia. *J. Geophys. Res.*, in review.

[] Battle, M. M.L Bender, P.P. Tans, J.W.C. White, J.T. Ellis, T. Conway, R.J. Francey, 2000, Global carbon sinks and their variability inferred from atmospheric O-2 and delta C-13. *Science*, *287*(5462), 2467-2470.

Betts, R.A., P.M. Cox, M. Collins, P.P. Harris, C. Huntingford, C.D. Jones, 2004, The role of ecosystem-atmosphere interactions in simulated Amazonian precipitation decrease and forest dieback under global climate warming. *Theor. Appl. Climatol.*, *78*(1-3), 157-175.

Borma, L.S., H.R. da Rocha, O.M. Cabral, C. von Randow, E. Collicchio, D. Kurzatkowski, F.J. Brugger, H. Freitas, R. Tannus, L. Oliveira, C.D. Rennó, P. Artaxo, 2009, Atmosphere and hydrological controls of the evaportransopiratoin over a floodplain forest in the Bananal Island region, Amazonia. *J. Geophys. Res.*, *114*, G01003, doi:10.1029/2007JG000641.

Bosquet, P., P. Peylin, P. Ciais, C. Le Quere, P. Friedlingstein, P.P. Tans (2000), Regional Changes in Carbon Dioxide Fluxes of Land and Oceans Since 1980. *Science*, *290*, 1342-1346, 17 November 2000.

Brando, P.M., S.J. Goetz, A. BAccini, D.C. Nepstad, P.S.A. Beck, M.C. Christman, 2010, Seasonal and interannual variability of climate and vegetation indices across the Amazon. *P. Nat. Acad. Sci. USA*, *107*(33), 14685-14690, doi:10.1037/pnas.0908741107.

Bretherton, C.S., M. Widmann, V.P. Dymnikov, J.M. Wallace and I.Bladé, 1998. The effective number of spatial degrees of freedom of a time-varying field. *J. Clim.*, **12**, 1990-2009.

Brown, M.E., J. Pinzon and C.J. Tucker, 2004. New vegetation index dataset available to monitor global change. *Eos Trans.*, **85**:565, 2004.

Canadell, J., R.B. Jackson, J.R. Ehleringer, H.A. Mooney, O.E. Sala, E.D. Schulze, 1996, Maximum rooting depth of vegetation types at the global scale. *Oecologia, 108*(4), 583-595.

Carvalho, L.M.V., C. Jones, B. Liebmann, 2004, The South Atlantic Convergence Zone: Intensity, form persistence, and relationships with intraseasonal to interannual activity and extreme rainfall. *J. Clim.*, *17*(1), 88-108.

Cattanio, J.H., E.A. Davidson, D.C. Nepstad, L.V. Verchot, I.L. Ackerman, 2002, Unexpected results of a pilot throughfall exclusion experiment on soil emissions of CO_2, CH_4, N_2O and NO in eastern Amazonia. *Biol. Fert. Soils*, *36*(2), 102-108.

Choudhury, B., 1983, Simulating the effects of weather variables and soil-water potential on a corn canopy temperature. *Agr. Meteor.*, *29*(3), 169-182.

Ciais, P., P.P. Tans, J.W.C. White, M. Trolier, R.J. Francey, J.A. Berry, D.R. Randall, P.J. Sellers, J.G. Collatz, D.S. Schimel, 1995a, Partitioning of ocean and land uptake of CO_2 as inferred by δ^{13}C measurements from the NOAA climate monitoring and diagnostics laboratory global air sampling network. *J. Geophys. Res.*, *100*(D3), 5051-5070.

Ciais, P., P.P. Tans, M. Trolier, J.W.C. White, R.J. Francey, 1995b, A large northern-hemisphere terrestrial CO_2 sink indicated by the $^{13}C/^{12}C$ ratio of atmospheric CO_2. *Science*, *269*(5227), 1098-1102.

Clapp, R.B. and Hornberger, G.M., 1978, Empirical equations for some soil hydraulic properties. *Water. Resour. Res.*, *14*(4), 601-604.

Coelho, C.A.S., C.B. Uvo, T. Ambrizzi, 2002, Exploring the impacts of the tropical Pacific SST on the precipitation patterns over South America during ENSO periods. *Theor. Appl. Climatol.*, *71*, 185-197.

Colello, G.D., C.Grivet, P.J. Sellers and J.A. Berry, 1998. Modelig of energy, water and CO_2 flux in a temperate grassland ecosystem with SiB3: May-October 1987. *J. Atmos.Sci.*, **55**, 1141-1169.

Collatz, G.J., J.T. Ball, C. Grivet, J.A. Berry (1991), Physiological and Environmental Regulation of Stomatal Conductance, Photosynthesis and Transpiration: A Model that Includes a Laminar Boundary Layer. *Agr. Forest Meteor.*, *54*, 107-136.

Collatz, G.J., M. Ribas-Carbo, J.A. Berry (1992), Coupled Photosynthesis-Stomatal Conductance Model for Leaves of C4 Plants. *Aust. J. Plant Physiol.*, *19*(5), 519-538.

Corbin, K.D., A.S. Denning, L. Lu, J.-W. Wang and I.T. Baker, 2008. Possible representation errors in inversions of satellite CO_2 retrievals. *J. Geophys. Res.*, **113**, D02301, doi:10.1029/2007JD008716.

Costa M.H. and J.A. Foley, 1998. A comparison of precipitation datasets for the Amazon basin. *Geophys. Res. Let.*, **25**(2), 155-158.

Costa, M.H. and J.A. Foley, 1999, Trends in the hydrologic cycle of the Amazon basin. *J. Geophys. Res.*, *104*(D12), 14189-14198.

Cowling, S.A., R.A. Betts, P.M. Cox, V.J. Ettwein, C.D. Jones, M.A. Maslin, S.A. spall, 2004, Contrasting simulated past and future responses of the Amazonian forest to atmospheric change. *Philos. T. R. Soc. B., 359*(1443): 539-547.

Cox, P.M., R.A. Betts,, C.D. Jones,, S.A. Spall,,I.J. Totterdell, (2000),Acceleration of Global Warming Due to Carbon-Cycle Feedbacks in a Coupled Climate Model, *Nature, 408*, 9 November, 184-187.

Cox, P.M., R.A. Betts, M. Collins, P.P. Harris, C. Huntingford, C.D. Jones, 2004, Amazonian forest dieback under climate-carbon cycle projections for the 21st century. *Theor. Appl. Climatol., 78*(1-3), 137-156.

Dai, Y., X. Zeng, R.E. Dickinson, I. Baker, G. Bonan, M. Bosilovich, S. Denning, P. Dirmeyer, P. Houser, G. Niu, K. Oleson, A. Schlosser and Z.-L. Yang (2003), The common land model (CLM). *B. Am. Meteorol. Soc., 84*, 1013-1023.

Dai, Y., R.E. Dickinson, Y-P. Wang (2004), A Two-Big-Leaf Model for Canopy Temperaure, Photosynthesis, and Stomatal Conductance. *J. Climate*, *17*, 2281-2299.

da Rocha, H.R., H.C. Freitas, R. Rosolem, R. Juarez, R.N. Tannus, M.A. Ligo, O.M.R. Cabral, M.A.F. Silva Dias, 2002, Measurements of CO_2 exchange over a woodland savanna (Cerrado Sensu strictu) in southeast Brazil. *Biota Neotropica, 2*(1).

da Rocha H.R., M.L. Goulden, S.D. Miller, M.C. Menton, L.D.V.O. Pinto, H.C. de Frietas, A.M. E Silva Figueira (2004), Seasonality of Water and Heat Fluxes over a Tropical Forest in Eastern Amazonia. *Ecol. Appl., 14*(4) Supplement, S22-S32.

da Rocha, H.R., A.O. Manzi, O.M. Cabral, S.D. Miller, M.L. Goulden, S.R. Saleska, N.R. Coupe, S.C. Wofsy, L.S. Borma, P. Artaxo, G. Vourlitis, J.S. Noguiera, F.L. Cardoso, A.D. Nobre, B. Kruijt, H.C. Frietas, C. von Randow, R.G. Aguiar, J.F. Maia, 2009, Patterns of water and heat flux across a biome gradient from tropical forest to savanna in Brazil. *J. Geophys. Res., 114*, G00B12, doi:10.1029/2007JG000640.

Dawson, T.E., 1993, Hydraulic lift and water-use by plants-implications for water-balance, performance, and plant-plant interactions. *Oecologia, 95*(4), 565-574.

Dawson, T.E., 1996, Determining water use by trees and forests from isotopic, energy balance and transpiration analysis: The roles of tree size and hydraulic lift. *Tree. Physiol., 16*(1-2), 263-272,

DeFries, R.S. and J.R.G. Townshend, 1994. NDVI-derived land cover classification at a global scale. *Int. J. Remote Sens.*, **15**(17), 3567-3586.

de Souza, E.B., and Ambrizzi, T., 2002, ENSO impacts on the South American rainfall during 1980s: Hadley and Walker circulation. *atmosfera, 15*, 105-120.

Denning, A.S., G.J. Collatz, C. Zhang, D.A. Randall, J.A. Berry, P.J. Sellers, G.D. Colello, D.A. Dazlich (1996), Simulations of Terrestrial Carbon Metabolism and Atmospheric CO_2in a General Circulation Model. Part 1: Surface Carbon Fluxes. *Tellus B , 48*B, 521-542.

Denning, A.S., M. Nicholls, L. Prihodko, I. Baker, P.L. Vidale, K. Davis, P. Bakwin, 2003, Simiulated variations in atmospheric CO_2 over a Wisconsin forest using a coupled ecosystem-atmosphere model. *Glob. Change Biol., 9*(9), 1241-1250.

de Pury, D.G.G., G.D. Farquhar (1997), Simple Scaling of Photosynthesis from Leaves to Canopies Without the Errors of Big-Leaf Models. *Plant Cell Environ.*, *20*, 537-557.

Dias, M.A.F.S. Dias, P.L.S., M. Longo, D.R. Fitzjarrald, A.S. Denning, 2004, River breeze circulation in eastern Amazonia: Observations and modeling results. *Theor. Appl. Climatol.*, *78*(1-3), 111-121.

Eiten, G., 1972, Cerrado vegetation of Brazil. *Bot. Rev.*, *38*(2), 201-.

Eltahir. E. and Bras, R.L., 1994, Precipitation recycling in the Amazon Basin. *Q. J. Roy. Meteor. Soc.*, *120*(518A), 861-880.

Enfield, D.B., A.M. Mestas-Nuñez, D.A. Mayer, L. Cid-Serrano, 1999, How ubiquitous is the dipole relationship in tropical Atlantic sea surface temperatures? *J. Geophys. Res.*, *104*(C4), 7841-7848.

Enting, I.G., C.M. Trudinger, R.J. Francey, 1995, A synthesis inversion of the concentration and δ^{13}C of atmospheric CO_2. *Tellus*, *47*(1-2), 35-52.

Eugster, W., Siegrist, F. (2000), The Influence of Nocturnal CO_2Advection on CO_2 Flux Measurements. *Basic Appl Ecol.*, *1*, 177-188.

Farquhar, G.D., S. von Caemmerer, J.A. Berry (1980), A Biochemical Model of Photosynthetic CO_2 Assimilation in Leaves of C3 Species. *Planta*, *149*, 78-90.

Foken, T., F. Wimmer, M. Mauder, C. Thomas, C. Liebethal, 2006, Some aspects of the energy balance closure problem. *Atmos. Chem. Phys.*, *6*, 4395-4402.

Foley, J.A., A. Botta, M.T. Coe, 2002, El Niñ0-Southern Oscillation and the climate, ecosystems and rivers of Amazonia. *Glob. Biogeochem. Cy.*, *16*(4), 1132, doi:10.1029/2002/GB001872.

Francey, R.J., P.P. Tans, C.E. Allison, I.G. Enting, J.W.C. White, M. Trolier, 1995, Changes in oceanic and terrestrial carbon uptake since 1982. *Nature*, *373*(6512), 326-330.

Franks, S.W., K.J. Beven, P.F. Quinn, I.R. Wright (1997), On the Sensitivity of Soil-Vegetation-Atmosphere Transfer (SVAT) Schemes: Equifinality and the Problem of Robust Calibration. *Agr. Forest Meteor.*, *86*, 63-75.

Friedlingstein, P.F., L. Bopp,P. Ciais, J-L Dufresne,L. Fairhead, H. LeTreut, P. Monfray, J. Orr (2001), Positive Feedback Between Future Climate Change and the Carbon Cycle, *Geophys. Res. Lett.*, *28*(8), 1543-1546.

Friedlingstein, P.F., P. Cox, R. Betts, L. Bopp, W. von Bloh, V. Brovkin, P. Cadule, S. Doney, M. Eby. I. Fung, G. Bala, J. John, C. Jones, F. Joos, T. Kato, M. Kawamiya, W. Knoff, K. Lindsay, H.D. Matthews, T. Raddatz, P. Rayner, C. Reick, E. Roeckner, K.-G. Schnitzler, R. Schnur, K. Strassmann, A.J. Weaver, C. Yoshikawa, N. Zeng, (2006), Climate-carbon cycle feedback analysis: Results from the C^4MIP model intercomparison, *J. Clim.*, *19*, 3337-3353.

Fu, R., B. Zhu, R.E. Dickinson, 1999, How do atmosphere and land surface influence seasonal changes of convection in the tropical amazon? *J. Clim.*, *12*(5), 1306-1321.

Fu, R. and Li. W., 2004, The influence of the land surface on the transition from dry to wet season in Amazonia. *Theor. Appl. Climatol.*, *78*, 97-110, doi:10.1007/s00704-004-0046-7.

Gifford, R.M., 2003, Plant respiration in productivity models. conceptualism, representation and issues for global terrestrial carbon-cycle research. *Funct. Plant Biol.*, *30*(2), 171-186.

Goudriaan, J., 1977: Crop Micrometeorology: A Simulation Study. Wageningen Center for Agricultural Publishing and Documentation, 249pp.

Goulden, M.L., S.D. Miller, H.R. da Rocha, M.C. Menton, H.C. de Freitas, A.M. E Silva Figueira, C.A.D. de Sousa (2004), Diel and Seasonal Patterns of Tropical Forest CO_2 Exchange. *Ecol. Appl.*, *14*(4) Supplement, S42-S54.

Gu, L., D. Baldocchi, S.B. Verma, T.A. Black, T. Vesala, E.M. Falge and P.R. Dowty, 2002. Advantages of diffuse radiation for terrestrial ecosystem productivity. *J. Geophys. Res.*, **107**(D6), doi: 10.1029/2001JD001242.

Gurney, K.R., R.M. Law, A.S. Denning, P.J. Rayner, D. Baker, P. Bousquet, L. Bruhwiler, Y-H. Chen, P. Ciais, S. Fan,.Y. Fung, M. Gloor, M. Heimann, K. Higuchi, J. John, T. Maki, S. Maksyutov, K.Masarie, P. Peylin, M. Prather, B.C. Pak, J. Randerson, J. Sarmiento, S. Taguchi, T. Takahasihi, C-W. Yuen (2002), Towards robust regional estimates of CO_2 sources and sinks using atmospheric transport models. *Nature*, *415*, 07 February 2002, 626-629.

Gurney, K.R., D. Baker, P. Rayner and A.S. Denning, 2008. Interannual variations in continental-scale net carbon exchange and sensitivity to observing networks estimated from atmospheric CO_2 inversions for the period 1980 to 2005. *Glob. Biogeochem. Cyc.*, **22**(3), doi:10.1029/2007GB003082..

Hallgren, J.E., T. Lundmark, M. Strand, 1990, Photosynthesis of Scots Pine in the field after night frosts during summer. *Plant Physiol. Bioch.*, *28*(4), 437-445.

Hanan, N.P., J.A. Berry, S.B. Verma, E.A. Walter-Shea, A.E. Suyker, G.G. Burba, A.S. Denning (2005), Testing a model of CO_2, water and energy exchange in Great Plains tallgrass prairie and wheat ecosystems. *Agr. Forest Meteor.*, *131*, 162-179.

Harper, A.B., A.S. Denning, I.T. Baker, M.D. Branson, L. Prihodko, D.A. Randall, 2010, Role of deep soil moisture in modulating climate in the Amazon. *Geophys. Res. Lett.*, *37*, L05802, doi:10.1029/2009GL042302.

Hogberg, P., A. Nordgren, N. Buchmann, A.F.S. Taylor, A. Ekblad, M.N. Hogberg, G. Nyberg, M. Ottosson-Lofvenius, D.J. Read, 2001, Large-scale forest girdling shows that current photosynthesis drives soil respiration. *Nature*, *411*(6839), 789-792.

Hollinger, D.Y., Richardson, A.D., 2005, Uncertainty in eddy covariance measurements and its application to physiological models. *Tree Physiol.*, *25*(7), 873-885.

Horel, J.D., A.N. Hahmann, J.E. Geisler, 1989, An investigation of the annual cycle of convective activity over the tropical Americas. *J. Clim.*, *2*(11), 1388-1403.

Houghton, R.A., D.S. Skole, C.A. Nobre, J.A. Hackler, K.T. Lawrence, W.H. Chomentowski, (2000), Annual Fluxes of Carbon from Deforestation and Regrowth in the Brazillian Amazon, *Nature*, *403*, 20 January, 301-304.

Houghton, R.A., K.T. Lawrence, J.L. Hackler, S. Brown (2001), The Spatial Distribution of Forest Biomass in the Brazilian Amazon: A Comparison of Estimates. *Glob. Change Biol.*, 7, 731-746.

Huete, A.R., K. Didan, Y.E. Shimabukuro, P. Ratana, S.R. Salexska, L.R. Hutyra, W. Yang, R.R. Nemani, R. Myneni (2006), Amazon Rainforests Green-up with Sunlight in Dry Season. *Geophys. Res. Lett.*, *33*, L06405, doi:10.1029/2005GL025583.

Huntingford, C., P.P. Harris, N. Gedney, P.M. Cox, R.A. Betts, J.A. Marengo, J.H.C. Gash, 2004: Using a GCM analogue model to investigate the potential for Amazonian forest dieback. *Theor. Appl. Climatol.*, *78*(1-3): 177-185.

Huntingford, C., R.A. Fisher, L. Mercado, B.B.B. Booth, S. Sitch, P.P. Harris, P.M. Cox, C.D. Jones, R.A. Betts, Y. Malhi, G.R. Harris, M. Collins, P. Moorcroft, 2008: Towards quantifying uncertainty in predictions of Amazon dieback. *Philos. T. R. Soc. B.*, *363*(1498): 1857-1864.

Hutyra, L.R., J.W. Munger, S.R. Saleska, E. Gottleib, B.C. Daube, A.L. Dunn, D.F. Amaral, P.B. de Camargo, S.C. Wofsy, 2007, Seasonal controls on the exchange of carbon and water in an Amazonian rain forest. *J. Geophys. Res.*, *112*(G4), G04099, doi:10.1029/2007JG000573.

Ichii, K., H. Hashimoto, M. A. White, C. Potter, L.R. Hutyra, A.R. Huete, R.B. Myneni, R. R. Nemani (2007), Constraining Rooting Depths in Tropical Rainforests Using Satellite Data and Ecosystem Modeling for Accurate Simulation of Gross Primary Production Seasonality. *Glob. Change Biol.*, *13*, 67-77, doi:10.1111/j.1365-2486.2006.01277.x

IPCC (2007), Climate Change 2007. *The Physical Science Basis. Contribution of Working Group I to the Fourth Assessment Report of the Intergovernmental Panel on Climate Change* [Solomon, S., D. Qin, M. Manning, Z. Chen, M. Marquis, K.B. Averyt, M. Tignor and H.L. Miller (eds.)]. Cambridge University Press, Cambridge, United Kingdom and New York, USA, 996 pp.

Jackson, R.B., J. Canadell, J.R. Ehleringer, H.A. Mooney, O.E. Sala, E.D. Schulze (1996), A global Analysis of root distributions for terrestrial biomes. *Oecologia*, *108*, 389-411.

Jipp, P.H., D.C. Nepstad, D.K. Cassel, C.R. de Carvalho (1998), Deep Soil Moisture Storage and Transpiration in Forests and Pastures of Seasonally-Dry Amazonia. *Climatic Change*, *39*, 395-412.

Jones, C.D., M. Collins, P.M. Cox, S.A. Spall, 2001, The carbon cycle response to ENSO: A coupled climate-carbon cycle model study. *J. Clim.*, *14*(11), 4113-4129.

Joos, F., and Bruno, M., 1998. Long-term variability of the terrestrial and oceanic carbon sinks and the budgets of the carbon isotopes C-13 and C-14. *Glob. Biogeochem. Cy.*, *12*(2), 277-295.

Jordan, R., 1991, A one-dimensional temperature model for a snow cover. Technical documentation for SNTHERM.89. *Special Report, U.S. Army Corps of Engineers*, No. 91-16.

Kalnay, E. And Kanamitsu, M., 1988: Time Schemes for Strongly Nonlinear Damping Equations. Monthly Weather Review, 116(10), 1945-1958.

Kalnay, E., Kanamitsu, M., Kistler, R., Collins, W., Deaven, D., Gandin, L., Iredell, M., Saha, S., White, G., Woollen, J., Zhu, Y, Cheliah, M., Ebisuzaki, W., Higgins, W., Janowiak, J., Mo, K.C., Ropelewski, C., Wang, J., Leetmaa, A., Reynolds, R., Jenne, R. and Joseph, D., 1996. The NCEP/NCAR 40-year reanalysis project. *Bull. Am. Met. Soc.*, **77**(3),437-471.

Kanamitsu, M., W. Ebisuzaki, J. Woollen, S.-K. Yang, J.J. Hnilo, M. Fiorino and G.L. Potter, 2002: NCEP-DOE AMIP-II Reanalysis (R-2). *B. Am. Meterol. Soc.*, **83**(11), 1631-1643.

Keeling, C.D., T.P. Whorf, M. Whalen and J.van der Plicht, 1995. Interannual extremes in the rate of rise of atmospheric carbon dioxide since 1980. *Nature*, **375**, 666-670.

Keller, M., A. Alencar, G.P. Asner, B. Braswell, M. Bustamante, E. Davidson, T. Feldpausch, E. Fernandes, M. Goulden, P. Kabat, B. Kruijt, F. Luizao, S. Miller, D. Markewitz, A.D. Nobre, C.A. Nobre, N.P. Filho, H da Rocha, P. Silva Dias, C von Randow, G.L. Vourlitis (2004), Ecological Research in the Large-Scale Biosphere-Atmosphere Experiment in Amazonia: Early Results. *Ecol. Appl.*, *14*(4) Supplement, S3-S16.

Kindermann, J., G. Würth, G.H. Kohlmaier, 1996, Interannual variation of carbon exchange fluxes in terrestrial ecosystems. *Glob. Biogeochem. Cy.*, *10*(4), 737-755.

Kleidon, A., Heimann, M. (1999), Deep-rooted Vegetation, Amazonian Deforestation and Climate: Results from a Modelling Study, Global Ecol. *Biogeogr.*, *8*(5), 397-405.

Lee, J-E., R.S. Olivieira, T.E. Dawson, I. Fung (2005), Root Functioning Modifies Seasonal Climate, P. Natl. Acad. *Science*, *102*(49), 17576-17581, 6 December 2005.

Lee, X. (1998), On Micrometeorological Observations of Surface-Air Exchange over Tall Vegetation. *Agr. Forest Meteor.*, *91*, 39-49.

Lenters, J.D. and K.H. Cook, 1997, On the origin of the Bolivian high and related circulation features of the South American climate. *J. Atmos. Sci.*, *54*(5), 656-667.

Li, W. and Fu. R., 2004, Transition of the large-scale atmospheric and land surface conditions from the dry to the wet season over Amazonia as diagnosed by the ECMWF re-analysis. *J. Clim.*, *17*(7), 2637-2651.

Li, W. and R. Fu, 2006, Influence of cold air intrusions on the wet season onset over Amazonia. *J. Clim.*, *19*(2), 257-275.

Li, W., R. Fu, R.E. Dickinson, 2006, Rainfall and its seasonality over the Amazon in teh 21st century as assessed by the coupled models for the IPCC AR4. *J. Geophys. Res.*, *111*, D02111, doi:10.1029/2005JD006355.

Los, S.O., G.J. Collatz, P.J. Sellers, C.M. Malmstrom, N.H. Pollack, R.S. DeFries, L. Bounoua, M.T. Parris, C.J. Tucker, D.A. Dazlich (2000), A Global 9-Year Biophysical Land Surface Dataset from NOAA AVHRR Data. *J. Hydrometeor.*, *1*, 183-199.

Los, S.O., G.J. Collatz, L. Bounoua, P.J.Sellers, C.J. Tucker, 2001, Global anterannual variations in sea surface temperature and land surface vegetation, air temperature and precipitation. *J. Clim.*, *14*(7), 1535-1549.

Lu, L.X., A.S. Denning, M.A. da Silva-Dias, P. da Silva-Dias, M. Longo, S.R. Freitas, S. Saatchi, 2005, Mesosscale circulations and atmospheric CO_2 variations in the Tapajos region, Para, Brazil. *J. Geophys. Res.*, *110*(D21), D21101, doi:10.1029/2004JD005757.

Magrin, G., C. Gay Garcia, D. Cruz Choque, J.C. Gimnez, A.R. Moreno, G.J. Nagy, C. Nobre, A. Villamizar (2007), Latin America. *Climate Change 2007: Impacts, Adaptation and Vulnerability. Contribution of Working Group II to the Fourth Assessment Report of the Intergovernmental Panel on Climate Change*, M.L. Parry, O.F. Canziani, J.P. Palutikof, P.J. van der Linden and C.E. Hanson, Eds. Cambridge University Press, Cambridge, UK, 581-615.

Mahrt, L. (1998), Flux Sampling Errors for Aircraft and Towers. *J. Atmos. Ocean. Tech.*, *15*(2), 416-429.

Malhado, A.C.M., M.H. Costa, F.Z. Lima, K.C. Portilho, D.N. Figueiredo, 2009, Seasonal leaf dynamics in an Amazonian tropical forest. *Forest Ecol. Manag.*, *258*(7), 1161-1165.

Marengo, J.A., Nobre, C.A. (2001), *General Characteristics and Variability of Climate in the Amazon Basin and its Links to the Global Climate System, in The Biogeochemistry of the Amazon Basin*, eds. M.E. McClain, R.L. Victoria, J.E. Richey, Oxford University Press, Oxford.

Markewitz, D. S. Devine, E.A. Davidson, P. Brando, D.C. Nepstad, 2010, Soil moisture depletion under simulated drought in the Amazon: Impacts on deep root uptake. *New Phytol.*, *187*(3), 592-607.

Miller, S.D., M.L. Goulden,M.C. Menton,H.R. da Rocha, H.C. de Freitas,A.M.E.S. Figueira,C.A.D. de Sousa (2004), Biometric and Micrometeorological Measurements of Tropical Forest Carbon Balance, *Ecol. Appl.*,*14*(4) Supplement, S114-S126.

Moron, V., S. Bigot, P. Roucou, 1995, Rainfall variability in subequatorial America and Africa and relationships with the main sea-surface temperature modes (1951-1990). *Int. J. Climatol.*, *15*, 1297-1322.

Myneni, R.B., W. Yang, R.R. Nemani, A.R. Huete, R.E. Dickinson, Y. Knyazikhin, K. Didan, R. Fu, R.I.N. Juarez, S.S. Saatchi, H. Hashimoto, K. Ichii, N.V. Shabanov, B. Tan, P. Ratana, J.L. Privette, J.T. Morisette, E.F. Vermote, D.P. Roy, R.E. Wolfe, M.A. Friedl, S.W. Running, P. Votava, N. El-Saleous, S. Devadiga, Y. su, V.V. Salomonson, 2007, Large seasonal swings in leaf area of Amazon rainforests. *P. Natl. Acad. Sci. USA*, *104*(12), 4820-4823.

Nepstad, D.C, C.R. de Carvlho, E.A. Davidson, P.H. Jipp, P.A. Lefebvre, G.H. Negreiros, E.D. da Silva, T.A. Stone, S.E. Trumbore, S. Vieira (1994), The Role of Deep Roots in the Hydrological And Carbon Cycles of Amazonian Forest and Pastures. *Nature*, *372*, 666-669, 15 December 1994.

Nepstad, D.C., P. Moutinho, M.B. Dias, E. Davidson, G. Cardinot, D. Markewitz,R. Figueiredo, N. Vianna, J. Chambers, D. Ray, J.B. Guerreiros, P. Lefebvre, L. Sternberg, M. Moreira, L. Barros, F.Y. Ishida, I. Tohlver, E. Belk, K. Kalif, K. Schwalbe, 2002, The effects of partial throughfall exclusion on canopy processes, aboveground production, and biogeochemistry of an Amazon forest. *J. Geophys. Res.*, *107*(D20), 8085, doi:10.1029/2001JD000360.

Nepstad, D.C., I.M. Tohlver, D. Ray, P. Moutinho, G. Carcinot, 2007, Mortality of large trees and lianas following experimental drought in an Amazon forest. *Ecology*, *88*(9), 2259-2269.

Nepstad, D.C., C.M. Stickler, B. Soares-Filho, F. Merry, 2008, Interactions among Amazon land use, forests and climate: prospects for a near-term forest tipping point. *Phil. T. R. Soc. B.*, *363*(1498), 1737-1746.

Nicholls, M.E., A.S. Denning, Prihodko, L., P.L. Vidale, I. Baker, K. Davis, P. Bakwin, 2004, A multiple-scale simulatin of variations in atmospheric carbon dioxide using a coupled biosphere-atmosphere model. *J. Geophys. Res.*, *109*(D18), D18117, doi:10.1029/2003JD004482.

Nijssen, B., G.M. O'Donnell, D.P. Lettenmaier, 2001, Predicting the discharge of global rivers. *J. Clim.*, *14*(8), 3307-3323.

Niyogi, D., H.-I. Chang, V.K. Saxena, T. Holt, K. Alapaty, F. Booker, F. Chen, K.J. Davis, B. Holben, T. Matsui, T. Meyers, W.C. Oechel, R.A. Pielke Sr., R. Wells, K. Wilson, Y. Xue, 2004, Direct observations of the effects of aerosol loading on net ecosystem CO_2 exchanges over different landscapes. *Geophys. Res. Let.*, *31*, L20506, doi:10.1029/2004GL020915.

Nobre, C.A., Sellers, P.J., Shukla, J. (1991), Amazonian Deforestation and Regional Climate Change, *J. Climate*, *4*, 957-988.

Oeschger, H., U. Seigenthaler, U. Schotterer and A. Gugelman, 1975. A box diffusion model to study the carbon dioxide exchange in nature. *Tellus*, **17**(2), 168-192.

Oliviera, R.S., T.E. Dawson, S.S.O. Burgess, D.C. Nepstad (2005), Hydraulic Redistribution in There Amazonian Trees. *Oecologia, 145*, 354-363.

Peylin, P., P. Bousquet, C. Le Quére, S. Sitch, P. Friedlingstein, G. McKinley, N. Gruber, P. Rayner, P. Ciais, 2005, Multiple constraints on regional CO_2 flux variations over land and oceans. *Glob. Biogeochem. Cy.*, *19*, GB1011, doi:10.1029/2003GB002214.

Phillips, O.L., L.E.O.C. Aragão, S.L. Lewis, J.B. Fisher, J. Lloyd, G. López-González, Y. Mallhi, A. Monteagudo, J. Peacock, C.A. Quesada, G. van der Heijden, S. Almeida, I. Amaral, L. Arroyo, G. Aymard, T.R. Baker, O. Bánki, L. Blanc, D. Bonal, P. Brando, J. Chave, A.C.A. de Oliveria, N.D. Cardozo, C.I. Czimczik, T. R. Feldpausch, M.A. Freitas, E. Gloor, N. Higuchi, E. Jiminéz, G. Lloyd, P. Meir, C. Mendoza, A. Morel, D.A. Neill, D. Nepstad, S. Patiño, M.C. Peñuela, A. Prieto, R. Ramírez, M Schwarz, J. Silva, M Sllveira, A.S. Thoma, H ter Steege, J. Stropp, R. Aásquez, P. Zelazowski, E.A. Dávila, S. Andelman, A. ANdrade, K.-J. Chao, T.Erwind, A.Di Fiore, E. Honorio C., H. Keeling, T.J. Killeen, W.F. Laurance, A. Peña Cruz, N.C.A. Pitman, P.N. Vargas, R. Ramírez-Angulo, A. Rudas, R. Salamão, N. Silva, J. Terborgh, A. Torres-Lezama, 2009, Drought sensitivity of the Amazon forest, *Science*, *323*, 1344-1347.

Pinzon, J., M.E. Brown and C.J. Tucker, 2006. Satellite time series correction of orbital drift artifacts using empirical mode decomposition. In: *Applications of Empirical Mode Decomposition*, Chapter 10, Part II, Editor: Nordon Huang.

Potter, C., S. Klooster, V. Brooks, 1999, Interannual variability in terrestrial net primary production: Exploration of trends and controls on regional to global scales. *Ecosystems*, *2*, 36-48.

Potter, C., S. Klooster, C.R. de Carvalho, V.B. Genovese, A. Torregrosa, J. Dungan, M. Bobo, J. Coughlan, 2001, Modeling seasonal andn interannual variability in ecosystem carbon cycleing for the Brazilian Amazon region. *J. Geophys. Res.*, *106*(D10), 10423-10446.

Potter, C., S. Klooster, R. Myneni, V. Genovese, P.-N. Tan, V. Kumar, 2003, Conteinteal-scale comparisons of terrestrial carbon sinkes estimated from satellite datea and ecosystem modeling, 1982-1998. j*Global Planet. Change*, *39*, 201-213.

Potter, C., S. Klooster, M. Steinbach, P.-N. Tan, V. Kumar, S. Shekhar, C.R. de Carvalho, 2004, Understanding global teleconnections of climae to regional model estimates of Amazon ecosystem carbon fluxes. *Glob. Change Biol.*, *10*, 693-703, doi:10.1111/j.1529-8817.2003.00752.x.

Potter, C., S. Klooster, P. Tan, M. Steinbach, V. Kumar, V. Genovese, 2005, Variability in terrestrial carbon sinks over two decades. Part III: South America, Africa, and Asia. *Earth Interact.*, *9*, Paper No. 29.

Qian, H., R. Joseph, N. Zeng, 2008, Response of the terrestrial carbon cycle to the El Niño-Southern Oscillation. *Tellus, 60B*, 537-550.

Raich, J.W., E.B. Rastetter, J.M. Melilllo, D.W. Kicklighter, P.A. Steudler, B.J. Peterson, A.L. Grace, B. Moore III, C.J. Vorosmarty (1991), Potential Net Primary Productivity in South America: Application of a Global Model. *Ecol. Appl.*, *1*(4), 399-429.

Randall, D.A., D.A. Dazlich, C. Zhang, A.S. Denning, P.J. Sellers, C.J. Tucker, L. Bounoua, J.A. Berry, G.J. Collatz, C.B. Field, S.O. Los, C.O. Justice, I. Fung (1996), A Revised Land Surface Parameterization (SiB2) for GCMs. Part III: The Greening of the Colorado State University General Circulation Model. *J. Climate, 9*(4), 738-763.

Randerson, J.T., G.R. van der Werf, G.J. Collatz, L. Giglio, C.J. Still, P. Kasibhatla, J.B. Miller, J.W.C. White, R.S. DeFries, E.S. Kasischeke, 2005, Fire emissions from C3 and C4 vegetation and their influence on interannual variability of atmospheric CO_2 and δCO_2-^{13}C. *Glob. Biogeochem. Cy.*. *19*(2), GB2019, doi:10.1029/2004GB002366.

Rasmusson, E.M., and T.H. Carpenter, 1982. Variations in tropical sea surface temperature and surface wind fields associate with the southern oscillation/El Niño. *Mon. Wea. Rev.*, **110**, 354-384.

Rayner, P.J. and Law, R.M., 1999, The relationship between tropical CO_2 fluxes and the El Niño-Southern Oscillation. *Geophys. Res. Let*, *26*(4), 493-496.

Restrepo-Coupe, N., S.R. Saleska, and coauthors, 2011a, Observed Carbon Flux in South America. *J. Geophys. Res.*, in review.

Restrepo-Coupe, N., S.R. Saleska, and coathors, 2011b, Longwave determination in low-latitude tropical forest. *J. Geophys. Res.*, in review.

Ricciuto, D. and coathors, 2011. Comparison of tower-based and reanalysed meteorological drivers. Paper in preparation.

Rödenbeck, C., S. Houweling, M. Gloor and M. Heimann, 2003. CO_2 flux history 1982-2001 inferred from atmospheric data using a global inversion of atmospheric transport. *Atmos. Chem. Phys.*, **3**, 1919-1964.

Romero-Saltos, H., L.S.L. Sternberg, M.Z. Moreira, D.C. Nepstad (2005), Rainfall Exclusion in an Eastern Amazonian Forest Alters Soil Water Movement and Depth of Water Uptake. *Am. J. Bot.*, *92*(3),443-455.

Ronchail, J., G. Cochonneau, M. Molinier, J.-L. Guyot, A.G.de Miranda Chaves, V. Guimarães. E. de Oliveira, 2002, Interannual rainfall variability in the Amazon Basin and sea-surface temperatures in the equatorial Pacific and the tropical Atlantic Oceans. *Int. J. Climatol.*, *22*, 1663-1686, doi:10.1002/joc.815.

Ropelewski, C.F. and Halpert, M.S., 1987, Global and regional scale precipitation patterns associated with the El Niño/Southern Oscillation. *Mon. Weather Rev.*, *115*(8), 1606-1626.

Ryel, R.J., M.M. Caldwell, C.K. Yoder, D. Or, A.J. Leffler (2002), Hydraulic Redistribution in a Stand of Artemisia tridentata: Evaluation of Benefits to Transpiration Assessed with a Simulation Model. *Oecologia, 130*, 173-184.

Salati, E., A. Dallollio, E. Matsui, J.R. Gat, 1979, Recycling of water in the Amazon-Basin-Isotopic Study. *Water Resour. Res.*, *15*(5), 1250-1258.

Salati, E., Vose, P.B. (1984), Amazon Basin-A System in Equilibrium. *Science*, *225*(4658), 129-138.

Saleska, S.R., S.D. Miller, D.M. Matross, M.L. Goulden, S.C. Wofsy, H.R. da Rocha, P.B de Camargo, P. Crill, B.C. Dauge, H.C. de Frietas, L.R. Hutyra, M. Keller, V. Kirchoff, M. Menton, J.W. Munger, E.H. Pyle, A.H. Rice, H. Silva (2003), Carbon in Amazon Forests: Unexpected Seasonal Fluxes and Disturbance-Induced Losses. *Science*, *302*, 1554-1557, 28 November 2003.

Saleska, S.R., K. Didan, A.R. Huete, H.R. da Rocha (2007), Amazon Forests Green-Up During 2005 Drought. *Science*, *318*(5850), 612. (10.1126/science.1146663)

Samanta, A. S. Ganguly, H. Hashimoto, S. Devadiga, E. Vermote, Y. Knyazikhin, R. R. Nemani, R.B. Myneni, 2010, Amazon forest did not green-up during the 2005 drought. *Geophys. Res. Let.*, *37*, L05401, doi:10.1029/2009GL042154.

Sato, N. P.J. Sellers, D.A. Randall, E.K. Schneider, J. Shukla, J.L. Kinter, Y.T. Hou, E. Albertazzi, 1989, Effects of implementing the Siimple Biophere Model in a General Circulation Model. *J. Atmos. Sci.*, *46*(18), 2757-2782.

Schaefer, K., G.J. Collatz, P. Tans, A.S. Denning, I. Baker, J. Berry, L. Prihodko, N. Suits and A. Philpott, 2008. The combined Simple Biosphere/Carnegie-Ames-Stanford Approach (SiBCASA) terrestrial carbon cycle model. *J. Geophys. Res.*,**113**, G03034, doi:10.1029/2007JG000603.

Schaefer, K., A.S. Denning, N. Suits, J. Kaduk, I. Baker, S. Los and L. Prihodko, 2002. Effect of climate on interannual variability of terrestrial CO_2 fluxes. *Glob. Biogeochem. Cyc.*, **16**(4), 1102, doi: 10.1029/2002GB001928.

Schaefer, K., A.S. Denning, O. Leonard, 2004, The winter Arctic Oscillation and the timing of snowmelt in Europe. *Geophys. Res. Let.*, *31*(22), L22205, doi:10.1029/2004GL021035.

Schaefer, K., A.S. Denning, O. Leonard, 2005, The winter Arctic Oscillation, the timing of spring, and carbon fluxes in the Northern Hemisphere. *Glob. Biogeochem. Cy.*, *19*(3), GB3017, doi:10.1029/2004GB002336.

Schwalm, C.R., C.A. Williams, K. Schaefer, I. Baker, G.J. Collatz, C. Rödenbeck, 2011. Does terrestrial drought explain global atmospheric CO_2 flux anomalies induced by El Niño? *Biogeosciences*, in review.

Sellers, P.J. (1985), Canopy Reflectance, Photosynthesis and Transpiration. *Int. J. Remote Sens.*, *6*(8), 1335-1372.

Sellers, P.J., Y. Mintz, Y.C. Sud, A. Dalcher (1986), A Simple Biosphere Model (SiB) for Use within General Circulation Models. *J. Atmos. Sci.*, *43*(6), 505-531.

Sellers, P.J., 1987, Canopy reflectance, photosynthesis, and Transpiration. 2. The role of biophysics in the linearity of the interdependence. *Remote Sens. Environ.*, *21*(2), 143-183.

Sellers, P.J., W.J. Shuttleworth, J.L. Dorman, A. Dalcher, J.M. Roberts, 1989, Calibrating the Simple Biosphere Model for Amazonian tropical forest using field and remote-sensing data. 1. Average calibration with field data. *J. Appl. Meteor.*, *28*(8), 727-759.

Sellers, P.J., J.A. Berry, G.J. Collatz, C.B. Field, F.G. Hall (1992), Canopy Reflectance, Photosynthesis, and Transpiration. III. A Reanalysis Using Improved Leaf Models and a New Canopy Integration Scheme. *Remote Sens. Environ.*, *42*, 1878-216.

Sellers, P.J. D.A. Randall, G.J. Collatz, J.A. Berry, C.B. Field, D.A. Dazlich, C. Zhang, G.D. Colello, L. Bounoua (1996a), A Revised Land Surface Parameterization (SiB2) for Atmospheric GCMs. Part I: Model Formulation. *J. Climate, 9*(4), 676-705.

Sellers, P.J. S.O. Los, C.J. Tucker, C.O. Justice, D.A. Dazlich, G.J. Collatz, D.A. Randall (1996b), A Revised Land Surface Parameterization (SiB2) for Atmospheric GCMs. Part II: The Generation of Global Fields of Terrestrial Biophysical Parameters from Satellite Data. *J. Climate*, *9*(4), 706-737.

Sellers, P.J., R.E. Dickinson, D.A. Randall, A.K. Betts, F.G. Hall, J.A. Berry, G.J. Collatz, A.S. Denning, H.A. Mooney, C.A. Nobre, N. Sato, C.B. Field and A. Henderson-Sellers, 1997. Modeling the exchanges of energy, water, and carbon between continents and the atmosphere. *Science*, **275**, 502-509.

Sellers, P.J., M.J. Fennessy, R.E. Dickinson, 2007, A numerical approach to calculating soil wetness and evapotranspiration over large grid areas. *J. Geophys. Res.*, *112*(D18), D18106, doi:10.1029/2007JD008781.

Silver, W.L., J. Neff, M. McGroddy, E. Veldkamp, M. Keller, R. Cosme (2000), Effects of Soil Temperature on Belowground Carbon and Nutrient Storage in a Lowland Amazonian Forest Ecosystem, *Ecosystems*, *3*, 193-209.

Solomon, S., G.-K. Plattner, R. Knitti and P. Friedlingstein, 2009, Irreversible climate change due to carbon dioxide emissions. *P. Nat. Acad. Sci. USA*, *106*(6), doi:10.1073/pnas.0812721106.

Stephens, B.B., K.R. Gurney, P.P. Tans, C. Sweeney, W. Peters, L. Bruhwiler, P. Ciais, M. Ramonet, P. Bousquet, T. Nakazawa, S. Aoki, T. Machida, G. Inoue, N. Vinnichenko, J. Lloyd, A. Jordin, M. Heimann, O. Shibistova,R.L. Langenfelds, L.P. Steele, R.J. Francey, A.S. Denning (2007), Weak Northern and Strong Tropical Land Carbon Uptake from Vertical Profiles of Atmospheric CO_2, *Science*, *316*, 22 June, 1732-1735.

Stöckli, R. T. Rutishauser, D. Dragoni, J. O'Keefe, P.E. Thornton, M. Jolly, L. Lu, A.S. Denning, 2008, Remote sensing data assimilation for a prognostic phenology model. *J. Geophys. Res.*, *113*(G4), G04021, doi:10.1029/2008JG000781.

Strand, M., Lundmark, T., 1995, Recovery of photosynthesis in 1-year-old needles of unfertilized and fertilized Norway Spruce (Picea-Abies(L) Karst) during spring. *Tree Physiol.*, *15*(3), 151-158.

Suits, N.S., A.S. Denning, J.A. Berry, C.J. Still, J. Kaduk, J.B. Miller, I.T. Baker, 2005, Simulation of carbon isotope discriiminatin of teh terrestrial biosphere. *Glob. Biogeochem. Cy.*, *19*(1), GB1017, doi:10.1029/2003GB002141.

Taylor, K.E. (2001), Summarizing Multiple Aspects of Model Performance in a Single Diagram. *J. Geophys. Res.*, *106*(D7), 7183-7192.

Tian, H., J.M. Melillo, K.W. Kickligher, A.D. McGuire, J.V.K. Helfrich III, B. Moore II, C.J. Vörösmarty, 1998, Effect of interannual climate variability on carbon storage in Amazonian ecosystems. *Nature*, *396*, 664-667.

Trenberth, K.E., 1999, Atmospheric moisture recycling: Role of advection and local evaporation. *J. Clim.*, *12*(5), 1368-1381.

Trudinger, C.M., I.G. Enting, R.J. Francey, D.M. Etheridge, R.J. Raynor, 1999, Long-term variability in the global carbon cycle inferred from a high-precision CO_2 and $\delta^{13}C$ ice-core record. *Tellus*, *51*(2), 233-248.

Tucker, C.J., J.E. Pinzon, M.E. Brown, D.A. Slayback, E.W. Pak, R. Mahoney, E.F. Vermote, N. El Saleous (2005), An Extended AVHRR 8-km NDVI dataset compatible with MODIS and SPOT vegetation NDVI Data, *Int. J. Remote Sens.*, *26*(20), 4485-4498.

Twine, T.E., W.P. Kustas, J.M. Norman, D.R. Cook, P.R. Houser, T.P. Meyers, J.H. Prueger, P.J. Starks, M.L. Wesely (2000), Correcting Eddy-Covariance Flux Underestimates over a Grassland. *Agr. Forest Meteor.*, *103*, 279-300.

van der Ent, R.J., H.H.G. Savenjie, B. Schaefli, S.C. Steele-Dunn, 2010, Origin and fate of atmospheric moisture over continents. *Water Resour. Res.*, *46*, doi:10.1029/2010/WR009127.

van der Werf, G.R., J.T. Randerson, J. Collatz, L. Giglio, 2003, Carbon emissions from fires in tropical and subtropical ecosystems. *Global Change Biol.*, *9*, 547-562.

Vidale, P.L., Stöckli, R. (2003), Prognostic canopy air solutions for land surface exchanges. *Theor. Appl. Climatol.*, *80*, 245-257.

Vogg, G. R. Heim, J. Hansen, C. Shafer, E. Beck, 1998a, Frost hardening and photosynthetic performance of Scots Pine (pinus sylvestrus L.) needles. I. Seasonal changes in photosynthetic apparatus and its function. *Planta*, *204*(2), 193-200.

Vogg, G., R. Heim, B. Gotschy, E. Beck, J. Hansen, 1998b, Frost hardening and photosynthetic performance of Scots Pine (pinus sylvestrus L.) needles. II. Seasonal changes in the fluidity of thylakoid membranes. *Planta*, *204*(2), 201-206.

von Randow, C., A.O. Manzi, B. Kruijt, P.J. de Oliveira, F.B. Zanchi, R.L. Silva, M.G. Hodnett, J.H.C. Gash, J.A. Elbers, M.J. Waterloo, F.L. Cardoso, P. Kabat, 2004. Comparative measurements and seasonal variations in energy and carbon exchange over forest and pasture in South West Amazonia. *Theor. Appl. Climatol.*, *78*, 5-26.

von Randow, C., B. Kruijt, A.A.M. Holtslag, M.B.L.Oliveira, 2008, Exploring eddy-covariance and large-aperture scintillometer measurements in an Amazonian rain forest. *Ag. Forest. Meteor.*, *148*(4), 680-690.

Vourlitis, G.L., N. Priante, M.M.S. Hayashi, J.D. Nogueira, F.T. Caseiro, J.H. Campelo, 2001, Seasonal variations in the net ecosystem CO_2 exchange of a mature Amazonian transitional tropical forest (cerradão). *Funct. Ecol.*, *15*(3), 388-395.

Vourlitis, G.L., N. Priante, M.M.S. Hayashi, J.D. Nogueira, F.T. Caseiro, J.H. Campelo, 2002, Seasonal variations in the evapotranspiration of a transitional tropical forest of Mato Grosso, Brazil. *Water Resour. Res.*, *38*(6), Art. No. 1094, doi:10.1029/2000WR000122.

Vourlitis, G.L., N. Priante, M.M.S. Hayashi, J.D. Nogueira, F. Raiter, W. Hoegel, J.H. Campelo, 2004, Effects of meteorological variations on the CO_2 exchange of a Brazilian transitional tropical forest. *Ecol. Appl.*, *14*(4), S89-S100.

Vourlitis, G.L., J.D. Nogueira, N.P. Filho, W. Hoeger, F. Raiter, M.S. Biudes, J.C. Arruda, V.B. Capistrano, J.L. Brito de Faria, F.A. Almeida, 2005, The sensitivity of diel CO_2 and H_2 vapor exchange of a tropical transitional forest to seasonal variation in meteorology and water availability. *Earth Interact.*, *9*, Art. No. 27.

Vourlitis, G.L., J.D. Noguiera, F.A. Lobo, K.M. Sendall, S.R. Paulo, C.A.A. Dias, O.B. Pinto Jr., N.L.R. Andrade, 2008, Energy balance and canopy conductance of a tripical semideciduous forest of the southern Amazon Basin. *Water Resour. Res.*, *44*(3), W03412, doi:10.1029/2006WR005526.

Wang, J.W., A.S. Denning, L. Lu, I.T. Baker, K.D. Corbin, K.J. Davis, 2007, Observations and simulations of synoptic, regional, and local variations in atmospheric CO_2. *J. Geophys. Res.*, *112*(D4), D0418, doi:10.1029/2006JD007410.

Wang, Y-P., R. Leuning (1998), A Two-Leaf Model for Canopy Conductance, Photosynthesis and Partitioning of Available Energy I: Model Description and Comparison with a Multi-Layered Model. *Agr. Forest Meteor.*, *91*, 89-111.

Waring, R.H., Schlesinger, W.H., 1985, *Forest Ecosystems: Concepts and Management*, Academic Press, Inc.

Wilson, K., A. Goldstein, E. Falge, M. Aubinet, D. Baldocchi, P. Berbigier, C. Bernhofer, R. Ceulemans, H. Dolman, C. Field, A. Grelle, A. Ibrom, B.E. Law, A. Kowalski, T. Meyers, J. Moncrieff, R. Monson, W. Oechel,. J. Tenhunen, R. Valentini, S. Verma (2002), Energy Balance Closure at FLUXNET Sites. *Agr. Forest Meteor.*, *113*, 223-243.

Wolter, K. and M.S. Timlin, 1993. Monitoring ENSO in COADS with a seasonally adjusted principal component index. Proc. of the 17th Climate Diagnostics Workshop, Norman, OK, NOAA/NMC/CAC, NSSL, Oklahoma Clim. Survey, CIMMS and the School of Meteor., Univ. of Oklahoma, 52-57.

Wolter, K. and M. S. Timlin, 1998. Measuring the strength of ENSO events - how does 1997/98 rank? *Weather*, **53**, 315-324.

Yoon, J.-H., Zeng, N., 2010, An Atlantic influence on Amazon rainfall. *Clim. Dyn.*, *34*, 249-264, doi:10.1007/s00382-009-0551-6.

Zeng, N., 1999, Seasonal cycle and interannual variability in the Amazon hydrologic cycle. *J. Geophys. Res.*, *104*(D8), 9097-9106.

Zeng, N. Mariotti, A., Wetzel, P. (2005), Terrestrial Mechanisms of Interannual CO_2 Variability, *Global Biogeochem. Cy.*, *19*, GB1016 doi:10.1029/2004GB002273

Zeng, N., J.-H. Yoon, J.A. Marengo, A. Subramaniam, C.A. Nobre, A. Mariotti, J.D. Neelin, 2008, Causes and impacts of the 2005 Amazon drought. *Environ. Res. Lett.*, *3*, 014002, doi:10.1088/1748-9326/3/1/014002.

Zhang, K., J.S. Kimball, M. Zhao, W.C. Oechel, J. Cassano and S.W. Running, 2007: Sensitivity of pan-Arctic terrestrial net primary productivity simulations to daily surface meteorology from NCEP-NCAR and ERA-40 reanalyses.*J. Geophys. Res.*,**112**, G01011, doi:10.1029/2006JG000249.

Zhao, M. and S.W. Running, 2006: Sensitivity of Moderate Resolution Imaging Spectroradiometer (MODIS) terrestrial primary production to the accuracy of meteorological reanalyses. *J. Geophys. Res.*,**112**, G01002, doi:10.1029/2004JG000004.